UNIVERSITY OF CALIFORNIA, SAN DIEGO

Bio-inspired fluidic lens for biomedical applications

A dissertation submitted in partial satisfaction of

the requirements for the degree Doctor of Philosophy

in

Electrical Engineering (Photonics)

by

Shang-Feng (Frank) Tsai

Committee in charge:

Professor Yu-Hwa Lo, Chair
Professor Sadik Esener
Professor Truong Nguyen
Professor Deli Wang
Professor John Watson

2010

The dissertation of Shang-Feng (Frank) Tsai is approved, and it is acceptable in quality and form for publication on microfilm and electronically:

_____

_____

_____

_____

_____

Chair

University of California, San Diego

2010

Dedication

This dissertation is dedicated to my family.

Table of Contents

List of Figures

List of Tables

Acknowledgements

I would like to thank my advisor, Prof. Yu-Hwa Lo, for his support and faith in me. My original background was very different from his research field, but he believed in me that I can make contributions to this new field. Research-wise, he has helped me identified the difference between scientific research and engineering. But most importantly, I ran into several low-downs in life and in research during my PhD studies. He didn't give up on me easily and helped me to continue move on in life. I am very grateful to have him as my advisor during my PhD studies as he has helped me tremendously in my growth in this very important time of my life. I also thank the other members of dissertation committee, Prof. Sadik Esener, Prof. John Watson, Prof. Truong Nguyen, and Prof. Deli Wang. They contributed not only to the direction of this work but also to my development as a scientist and engineer.

I am also indebted to all of the colleagues and graduate students I have learned from and worked with. I would like to start with the members of Lo group: Sung Hwan Cho, Jessica Godin, Victor Lien, Nicole Justis, Deiyin Zhang, Wen Qiao, Kai Zhao, Randy Chen, Ashkan Arianpour, Shawn Meade, Eugene Berdichevsky, Vyacheslav Gomon. Aside from being great collaborators in getting research done, they were also the people who helped me survived through several of the low-downs during research. Furthermore, the topic covered in my research is very vast, and it is difficult to accomplish by one person alone. Many of the contribution are a collective contribution from several people, and I would like to acknowledge them for their close collaboration with me to get things to work. Furthermore, I would like to thank the people who

worked closely with me to improve the technology of bio-inspired fluidic lens. In Rhevision, I must thank Bob Vasko, Jeff Vasko, and Nam-Hyong Kim. In Calit2, I have to thank Daniel Johnson, Cuong Vu, Laura Wolszon, Donald Kimball, Doug Palmer. In Nano3, I need to thank Ryan Anderson, Bernd Fruhberger, Larry Grissom, and Maribel Montero. In UCSD medical school, I have to thank Prof. Santiago Horgan, Prof. Mark Talamini, Prof. Yoav Mintz, Dr. Kari Thompson, Dr. Adam Spivak, and Cameron Francis. It is their help from the medical side and in the surgery room that makes my dissertation work complete. And finally, there are several UCSD fellow graduate students that I have to thank, Jack Tzeng, Dayu Teng, and Ian Lien.

Last but not the least; I owe my motivation and appreciation to my parents, Suhar and Ronlon, and to the rest of my family, particularly Shiau-Wan and Sam. It goes without saying that I could not have done much of anything without their support and love. They provided me the reason of keep going.

Chapter 2 or portion thereof has been published in ***Proceesings of SPIE*, vol. 7061, 70610N (2008)**. Chapter 3 or portion thereof has been published in ***Optics Letters*, Vol 33, Iss. 3, pp. 291-293 (2009)**. Chapter 4 or portion thereof has been published in ***Proceesings of SPIE*, vol. 7061, 70610N (2008)**. Chapter 4 or portion thereof has also been submitted for publication in the following manuscript: Frank S. Tsai, Daniel Johnson, Cameron S. Francis, Sung Hwan Cho, Wen Qiao, Ashkan Arianpour, Yu-Hwa Lo, “Fluidic lens laparoscopic zoom camera for minimally invasive surgery.”

Vita

June, 1999	Bachelor of Science in Electronic Engineering National Chiao Tung University, Hsinchu, Taiwan
1999 – 2001	Graduate Student Researcher Department of Electronics National Chiao Tung University, Hsinchu, Taiwan
June, 2001	Master of Science in Electronics National Chiao Tung University, Hsinchu, Taiwan
2001 – 2005	Engineer Industrial Technology Research Institute, Hsinchu, Taiwan
2005 – 2009	Gradute Student Researcher Department of Electrical and Computer Engineering University of California, San Diego
March, 2010	Doctor of Philosophy in Electrical and Computer Engineering University of California, San Diego

Publications

1. **Frank S. Tsai**, Daniel Johnson, Sung Hwan Cho, Wen Qiao, Ashkan Arianpour, Cameron Francis, and Yu-Hwa Lo, "Fluidic lens laparoscopic zoom camera for minimally invasive surgery," submitted to ***IEEE Photonics Technology Letters***.

2. Chun-Hao Chen, Sung Hwan Cho, **Frank S. Tsai**, Ahmet Erten, and Yu-Hwa Lo, "Microfluidic cell sorter with integrated piezoelectric actuator," ***Biomedical Microdevices***, DOI10.1007, Aug. 2009.

3. Wen Qiao, Daniel Johnson, **Frank S. Tsai**, Sung Hwan Cho, Huimin Yan, and Yu-Hwa Lo, "Bio-Inspired Accommodating Fluidic Intraocular Lens," to appear in ***Optics Letters***.

4. Sung Hwan Cho, **Frank S. Tsai**, Wen Qiao, Nam-Hyong Kim, and Yu-Hwa Lo, "Fabrication of Aspherical Polymer Lenses Using Tunable Liquid-Filled Mold," ***Optics***

Letters, Vol. 34, Issue 5, pp. 605~607, Feb. 2009.

5. Wen Qiao, **Frank S. Tsai**, Sung Hwan Cho, Huimin Yan, and Yu-Hwa Lo, "Fluidic intraocular lens with a large accommodation range," ***IEEE Photonics Technology Letters***, Vol. 21, Iss. 5, pp. 304~306, March 2009.

6. Jessica Godin, Chun-Hao Chen, Sung Hwan Cho, Wen Qiao, **Frank S. Tsai**, Yu-Hwa Lo, "Microfluidics and photonics for Bio-System-on-a-Chip: A review of advancements in technology towards a microfluidic flow cytometry chip" ***Journal of Biophotonics***, Vol. 1, Iss. 5, pp. 355~376, Jun. 2008. (***review*** paper).

7. **Frank S. Tsai**, Sung Hwan Cho, Yu-Hwa Lo, Bob Vasko, and Jeff Vasko, "Miniaturized Universal Imaging Device Using Fluidic Lens," ***Optics Letters***, Vol. 33, Iss. 3, pp. 291~293, Feb. 2008.

8. Chun-Hao Chen, **Frank Tsai**, Victor Lien, Nicole Justis, and Yu-Hwa Lo, "Scattering-Based Cytometric Detection Using Integrated Arrayed Waveguides with Microfluidics," ***IEEE Photonics Technology Letters***, Volume 19, Issue 6, pp. 441~443, March 2007.

9. Maria C. Yuang, Steven S. W. Lee, Po L. Tien, J. Shih, Yu-Min Lin, **Frank Tsai**, and Alice Chen, "Optical Coarse Packet Switched IP-over-WDM Network (OPSINET): Technologies and Experiments," ***IEEE Journal on Selected Areas in Communications,*** Vol. 24, No. 8, August 2006.

10. **Frank S. Tsai**, Daniel Johnson, Sung Hwan Cho, Wen Qiao, Ashkan Arianpour, and Yu-Hwa Lo, "Bio-inspired fluidic lens enhanced surgical camera for MIS," ***IEEE EMBC***, Minneapolils, MN, Sep. 2009.

11. Wen Qiao, Daniel Johnson, **Frank S. Tsai**, Sung Hwan Cho, and Yu-Hwa Lo, "An Accommodating Fluidic Intraocular Lens Design and Process," ***IEEE EMBC***, Minneapolils, MN, Sep. 2009.

12. Sung Hwan Cho, Chun H. Chen, **Frank S. Tsai**, and Yu-Hwa Lo, "Automated Real-time sorting with high throughput microfabricated fluorescence-activated cell sorter," ***IEEE EMBC***, Minneapolils, MN, Sep. 2009.

13. M. Gross, H. Zhang, **S.-F. Tsai**, P. Wen, S. Esener, A. Husain, "Active Optical Backplane/Extenders for Military Systems," ***Government Microcircuit Applications & Critical Technology Conference***, Orlando, FL, March 2009.

14. Sung Hwan Cho, Jessica Godin, Chun Hao Chen, **Frank S. Tsai**, Yu-Hwa Lo, "Microfluidic Photonic Integrated Circuits," ***SPIE APOC***, Oct. 2008. ***(invited)***

15. Wen Qiao, **Frank S. Tsai**, Sung Hwan Cho, Huimin Yan, Yu-Hwa Lo, "Tunable Fluidic Intraocular Lens in Human Eye Model," ***OSA Frontiers in Optics*****,** OSA Technical Digest (CD), Optical Society of America, 2008.

16. Sung Hwan Cho, **Frank S. Tsai**, Wen Qiao, Nam-Hyong Kim, and Yu-Hwa Lo, "Fabrication of Polymer Lenses Using Liquid-Filled Mold," ***Proceedings in UKC 2008***, San Diego, CA, USA, Aug. 14-17, 2008.

17. **Frank S. Tsai**, Sung Hwan Cho, Wen Qiao, Nam-Hyong Kim, and Yu-Hwa Lo, "Miniaturized Universal Imaging Device Using Bio-inspired Fluidic Lens," **SPIE O+P**, San Diego, Aug. 2008. ***(invited)***.

18. Sung Hwan Cho, **Frank S. Tsai**, Bob Vasko, Jeff Vasko, and Yu-Hwa Lo, "Fluid-Filled Tunable Mold for Polymer Lenses," **CLEO/QELS**, San Jose, CA, USA, May 2008.

19. **Frank S. Tsai**, Sung Hwan Cho, Yu-Hwa Lo, Bob Vasko, and Jeff Vasko, "Miniature Unified Imaging Device Using Fluidic Lenses," ***IEEE LEOS***, Lake Buena Vista, FL, USA, pp. 455 – 456, Oct. 2007.

20. Chun H. Chen, **Frank Tsai**, and Yu-Hwa Lo, "High-Sensitivity scattering-based detection under symmetrical arrayed-waveguide platform," ***IEEE LEOS***, Montreal, Quebec, Canada, July 2006.

21. Maria C. Yuang, Po L. Tien, J. Shih, Steven S. W. Lee, Yu-Min Lin, **Frank Tsai**, and Alice Chen, "Optical Coarse Packet Switched IP-over-WDM Network (OPSINET): Technologies and Experiments," ***SPIE APOC***, Beijing, China, Nov. 2004.

22. Maria C. Yuang, Po-Lung Tien, Julin Shih, Steven S. Lee, Alice Chen, Yu-Min Lin, and **Frank Tsai** , "QoS Contention Control for Optical Coarse Packet Switched IP-over-WDM Networks," ***COIN/ACOFT 2003***, Melbourne, Australia, pp. 217-220, July 2003.

23. **Frank S. Tsai** and Chen-Yi Lee, "A Novel Single-bit Input All Digital Synchronizer and Demodulator Baseband Processor for Fast Frequency Hopping System," ***Proc. IEEE Int. Symp. on Circuits and Systems (ISCAS-2001)***, Sydney, Australia, vol. 4, pp. 132-135, May 2001.

ABSTRACT OF THE DISSERTATION

Bio-inspired fluidic lens for biomedical applications

by

Shang-Feng (Frank) Tsai

Doctor of Philosophy in Electrical Engineering (Photonics)

University of California, San Diego, 2010

Professor Yu-Hwa Lo, Chair

My research interests and experiences have focused on bio-inspired fluidic lens, which is a lens that can change its curvature just like the crystalline lens of the human eye. The curvature tuning capability allows for a theoretical limit of 300 diopters of tuning without having any moving lenses. With this key feature, the lens can be made very small but yet has a tremendous amount of tuning capability. This is very different from traditional optical lenses, which are made out of rigid material where the curvature cannot change. Hence, the only way for traditional optical systems to change its power is by changing the location of the lenses. This forces the traditional optics to be much

larger, much longer, and much bigger with limited functionality. With bio-inspired fluidic lenses, the lenses are much smaller and compact with more optical function.

My main contribution is in developing the fabrication process for the fluidic lens and the optical design techniques that will improve the image quality. With only one single fluidic lens, I designed a miniature optical system that can function as a regular camera, micro-mode camera, or even a microscope. With two fluidic lenses, I designed a miniature optical zoom camera that has very large optical zoom (17 mm total track and >4X optical zoom). The working distance can be as short as 2 cm, which is difficult to design with traditional lens technology. The unique functions of the optical systems are made possible with the unique function of bio-inspired fluidic zoom lens.

Finally, the unique technology of this optical device has particular interest in biomedical applications, such as minimally invasive surgery, retinal camera, etc. Several functions of biomedical applications are demonstrated. Most importantly, a demonstration gallbladder removal surgery was performed solely relying on the images acquires with the miniature zoom lens developed with fluidic lenses.

Chapter 1

Introduction and background

Technology is constantly bringing smaller, cheaper, and more powerful tools to the society. Take the semiconductor technology for instance. The supercomputer of the past is a roomful of vacuum tubes. It is now replaced by a simple chip which has millions of transistors. This has made possible personal computing tools as in iPods, laptops, cell phones, etc. Growing with the semiconductor technology is the cost down and the proliferation of CMOS sensors. With the cost down of CMOS sensors,

miniaturized imaging systems are distributed everywhere. We see miniature imagers in web cameras, laptops, cell phones, iPods, etc. However, the sensor only solves one part of the problem – it only detects light. An image has to be formed on the sensor first. And the only way to form an image is to place an optical lens in front of the CMOS sensor.

Although the trend is slower in improvement, the optical lens technology is also following the same trend as transistors in becoming smaller, cheaper and more powerful. Early optical lenses were made out of glass and had a spherical profile. Through several decades, fabrication technology improved and aspherical lenses and different glass materials are available. This allows for great improvement in image quality and reduction in lens size. Recent advancements include inclusion of diffractive optics to reduce size, as seen in Canon imager, and the advancement of plastic lenses. It is also because of plastic lens technology that enabled the wide distribution of miniature imaging systems. However, there is something missing in these imagers. The technology is small, but it doesn't have much of a focusing range. The web camera cannot image something that is written on the paper very clearly. It cannot take close up images. And the only way for cell phones to zoom is through digital zoom. The image quality is greatly compromised when performing digital zoom.

The challenge is how can we can continue the trend in miniaturization, but still provide high functionality. When comparing the function of the cell phone camera to the human eye, we quickly notice that our eye has much better functionality than those miniature cameras. The reason is that we can easily see far and see close. Realizing

that there is something that can be learned from Nature, we studied animal eyes to develop a new optical device that can provide function beyond traditional lens technology. With this new device, I will demonstrate in my dissertation a unified miniaturized imager where a small imager can function as a regular camera and then turn into a microscope without having any moving optical parts. The second functionality that I will demonstrate is that with this technology, the world's shortest zoom camera with the largest zoom can be designed and achieved. What's more this camera can also see far and close. Most importantly, this unseen functionality is demonstrated in the surgical room with cholecystomy procedure.

1.1 From Nature to new optical lens technology

As mentioned earlier, animal eye provides function that is beyond what is feasible with human made technology. This is because animal eyes have been tested and improved through millions of years of evolution. Initially, it was just the simple epithelial cells that have the capability to detect photons. Over time, the light detection function eventually evolved to eyes that form high resolution images with high sensitivity. The animal eyes have utilized several different types of image forming mechanisms. Some squids have a pin-hole eye, some fish have fixed spherical lens, some other fish have multiple lenses, and most mammals have a single lens with the ability of changing its curvature for accommodation (i.e. auto-focusing).

Regardless of the mechanism, one feature about the animal eye is that they are usually very small, compact, but has a tremendous capability in terms of tuning power, which allows for amazing amount of functionality. Take our own eyes for instance. Our eyes are very small, when compared to several man made optics, but we can easily see far and see close. In drastic contrast, the optics in human-made imaging systems is far more complicated and bulkier than animal eyes for similar or sometimes less functionality.

Why is it that the eyes from the animal kingdom can be so small and yet provides much more function than man-made optics?

The most important difference in optics between animal eyes and human-made optics is that the former achieves focusing by change of lens shape but the latter is done by varying the distances between fixed-shaped lenses. By changing the curvature of the lens, animals can have a wide tuning range in an extremely compact design. As an example, a young person can achieve a tuning range of 14 diopters, producing a focal range from around 8 cm to infinity. In fact, cormorants have a tuning range as wide as 50 diopters while the size and weight of eye is only one tenths or even one hundredths of a human-made system. This indicates that changing curvature is an effective and economic way to change the focal length of the optical system.

To strengthen our case, we can take an even closer look at the accommodation mechanism of the human eye, the ciliary muscles change the curvature of the human crystalline lens. To achieve an accommodation range of 10 dioptres (corresponding to a

focal range from 10 cm to infinity) the ciliary muscles exerts less than 8 grams of force and a moves about 0.1mm, we are not aware of any human-made systems capable of the same performance with such limited force and travel.

The concept that the lens can change its curvature translates to the capability of a lens to change its power without moving its positioning. Since lens that can change its power can save space and provide advanced optical function, the core of this thesis is about how to make bio-inspired fluidic lens and how to utilize them in optical systems to provide high quality image. But before those topics are considered, a basic study on the possible approaches to making a lens that can change its power without changing its position is needed. In this introduction chapter, we will look at some of the physical phenomenons used by different researchers worldwide to develop lenses that can changes its power.

1.2 Different power tuning lens design

Basically, a lens is an optical component that bends the direction of the rays in a fashion that an image can be formed. In traditional man-made optics, there are two general classes of lenses: index of refraction gradient and lens curvature. These two classes are also utilized in power tuning lenses. Over the past decade, there have been numerous studies on fluidic lenses using the above two mechanisms. The key driver behind these research are advanced materials, processing technology, and better understanding the physics involving micro-fluidics. A brief discussion of various fluidic lenses is given next.

While we study the different types of mechanisms for tunable fluidic lens, it is important to keep in mind that the ultimate goal of the fluidic lens is to provide large tuning capability to the fluidic lens. So, the key parameters while studying different types and forms of the fluidic lens is (1) scalability; (2) tuning capability; (3) thermal and mechanical stability.

1.2.1 Graded-index fluidic lens

Index gradient lenses refocus the straying rays back into the center to form an image. This mechanism is used in fiber endoscopes, which is a type of relay system. The key enabling material for this type of fluidic lens is liquid crystal (LC).

The liquid crystal molecule is either elongated (rodlike) or flat (disklike) [1]. Because of its long molecular structure, liquid crystal exhibits a birefringent behavior that the incoming light with different polarization experiences a different index of refraction change. The index of refraction that is exhibited on the incoming light can be controlled by controlling the orientation of the LC molecule. In short, the liquid crystal molecules are oriented in a way such that a radially index gradient is created in the system, thus creating lensing effect [2].

The method to create radial index gradient with liquid crystal is a rich research topic. One approach to create the radial index gradient is by designing the electric field. To do so, electrodes are cleverly placed at special positions and applied with controlled voltages such that an axially symmetrical inhomogeneous electric field is created in the LC layer [3]. This can be done by sectioning the electrodes and applying different

voltages [4-6] or by placing curved glasses into the fluidic lens to change the spacing between the electrodes [7-9]. Yet another approach to create the radial index gradient is by mixing liquid crystals with polymers. When the polymers polymerizes, it will lock the liquid crystals in its original orientation, keeping it from moving when electric field is applied. This causes the lens to have a varying index of refraction throughout the entire lens and create the lensing effect. [10-12]

There are several applications for the liquid crystal fluidic lens. For instance, it has been applied to micro-lenses [13, 14], confocal microscopy [15], and disc storage systems [16, 17] .

The main challenge with liquid crystal fluidic lens is in the fabrication as well as the tuning range. Without wide tuning range, advanced biomedical applications cannot be achieved.

1.2.2 Curvature tunable fluidic lens

Different from fluidic lens that changes its index or refraction gradient, the other major type of fluidic lens tunes its curvature. Different physical mechanisms can be

used to tune the curvature of a lens. We will discuss some that has been studied by researchers world-wide.

One of the first techniques to be applied was electro-wetting effect, which is the change of contact angle of a liquid droplet on a surface by an applying voltage to that sruface. The basic reason is because water is a polar molecule, and by changing the voltage of a surface, or wall, water molecules will like to get closer or further away from the surface. The physics of electro-wetting can be characterized by the Lippman-Young equation: $\cos(\theta) = \cos(\theta_0) + \frac{\varepsilon\varepsilon_0}{2\gamma_{LG}d}V^2$, where θ is the contact angle, θ_0 is the initial contact angle with zero voltage applied, ε is the dielectric constant of the dielectric layer, ε_0 is the permittivity of vacuum, γ_{LG} is the interfacial energy between the droplet and the ambient, d is the thickness of the dielectric layer, and V is the voltage applied between the substrate and the droplet. By changing the contact angle of the droplet, the curvature of the lens changes [18-23].

Another physical phenomenon that can be used to tune the curvature of the lens is dielectrophoresis. A dielectric molecule experiences a net force in an electrical flux gradient. Although a dielectric molecule has no polarization in it, it nevertheless creates small small amount of polarization under electric field. If the electric flux concentration on the 2 sides of the molecule is different, the molecule will be pulled towards the side with more flux concentration. One key problem in this approach is in finding the right dielectric material. Some materials that have been explored include liquid crystals [24]

and silicone oils [25, 26]. By manipulating the electric field with specifically designed and patterned electrodes, the dielectric liquid can change its curvature.

Other approaches of curvature changing fluidic lens includes utilizing the surface tension of the lens create the curvature. The main limitation of this is mechanical stability.

Among many different types of fluidic lenses, we believe the most attractive design is to use an optically clear elastic membrane to constrain the fluid in a lens chamber. The structure of the fluidic lens is shown in Figure 2.4. The lens power is determined by the lens curvature and the refractive index difference between air and the optical fluid. The deformable elastic membrane is used to constrain the optical fluid and to produce the desired lens profile under a pressure difference between the lens chamber and the ambient. When optical fluid is injected into the lens chamber to create a positive pressure, the elastomer membrane produces a convex shape for a positive lens. Conversely, when optical fluid is withdrawn from the lens chamber into a reservoir, a negative pressure is formed to produce a concave lens. Such design offers flexibilities and characteristics (i.e. tuning power) matched by no other fluidic lenses. As long as the fluid does not interact with the elastomer membrane, one has the freedom to select the optical fluid of desired index and dispersion properties for optimal system performance. Another merit of the design is that the lens profile is determined solely by the mechanical properties of the membrane, independent of the lens fluid. Hence, one can engineer the lens profile by adjusting the processing and material structure of the membrane. Different lens configurations, including plano-convex, bi-convex, plano-

concave, bi-concave, positive meniscus, negative meniscus, etc. have been demonstrated [27]. Various lens actuation mechanisms have been investigated, including piezoelectric actuator, thermal actuator [28], pneumatic actuation [29], aperture size actuation [30, 31], electromagnetic actuator [32], fibrous actuator [33], pH-responsive hydrogel actuation [34] etc.

Although there are several different mechanisms to make fluidic lenses, there are several fundamental properties that we need to consider before choosing the type of bio-inspired fluidic lens device to use. The considerations are (1) tuning range, (2) scalability, and (3) mechanical and thermal stability.

Tuning range determines the function and the performance of the optical system. A small tuning range yields a limited focal range for auto-focusing system, and creates great difficulties for compact optical zoom systems. Scalability refers to the size of lens diameter a technology can create. Typically, with larger aperture, it is possible to capture more light, thus allowing for a faster system. Finally, to live up to the expectation of being a paradigm-shifting solution in the field of optics, fluidic lens needs to be mechanically robust, thermally stable, and low cost to manufacture.

We have found that fluid-filled, elastomer-membrane lenses perform well in all the above areas. Such fluidic lenses can produce a record high tuning range of 200 dioptres, can change the lens type between convex and concave structures, can scale to a relatively large clear aperture of over 10 mm, and have superb mechanical robustness and reliability.

1.3 Conclusion

Since membrane-based bio-inspired fluidic lens is the best fluidic lens, I will focus on this fluidic lens technology in the remaining part of this dissertation. The unique functionality (i.e. ultra-wide tuning range), the small size, and the image quality achievable with this type of fluidic lens promises many important applications in biomedical fields. There are several potential applications such as minimally invasive surgery, dermatology, denstistry, laryngoscopy, retinal diagnosis, intraocular lens, digital pathology, etc. We focus on demonstrating one important application, the minimally invasive surgery, in this dissertation.

In chapter 2, I will discuss cover the device aspect to make this powerful bio-inspired fluidic lens. The fabrication technology that enables good image quality will be discussed. Then I will discuss the details on the analysis of lens profile.

In chapter 3, I will discuss the integration of fixed lens and fluidic lens that can integrate into a high quality imaging system. This optical system is a miniaturized unified imager that can turn into a camera and a microscope. The fabrication of the fluidic lens is reviewed and the optical system design process in Code V is also covered. Images from the optical system are also shown to demonstrate the functionality and image quality.

In chapter 4, I will cover the the design and testing of bio-inspired fluidic zoom lens for minimally invasive surgery. The design and fabrication of the bio-inspired

fluidic zoom lens will be covered. Then experimental to demonstrate the image quality, functionality will be shown in engineering lab and surgical lab.

Finally, chapter 5 will document a successful gallbladder removal surgery was performed with bio-inspired fluidic zoom lens. The camera was developed in collaboration with Calit2, and it is called Surgicam.

References

[1] A. Yariv and P. Yeh, Photonics -- Optical Electronics in Modern Communications. New York: Oxford University Press, 2007.

[2] K. Iizuka, Elements of Photonics, vol. I: Wiley-Interscience.

[3] S. Sato, "Applications of Liquid Crystals to Variable-Focusing Lenses," Optical Review, vol. 6, pp. 471-485, 1999.

[4] M. Ye, B. Wang, and S. Sato, "Liquid-Crystal Lens with a Focal Length that is Variable in a Wide Range," Applied Optics, vol. 43, pp. 6407-6412, 2004.

[5] M. Ye, B. Wang, and S. Sato, "Liquid crystal lens with focus movable in focal plane," Optics Communications, vol. 259, pp. 710-722, 2006.

[6] B. Wang, M. Ye, and S. Sato, "Liquid Crystal Lens With Focal Length Variable From Negative to Positive Values," Photonics Technology Letters, IEEE, vol. 18, pp. 79-81, 2006.

[7] H. Ren and S. T. Wu, "Adaptive liquid crystal lens with large focal length tunability," Optics Express, vol. 14, pp. 11292-11298, 2006.

[8] Y. H. Fan, H. Ren, X. Liang, H. Wang, and S. T. Wu, "Liquid crystal microlens arrays with switchable positive and negative focal lengths," IEEE/OSA Journal of Display Technology, vol. 1, pp. 151-156, 2005.

[9] B. Wang, M. Ye, and S. Sato, "Lens of Electrically Controllable Focal Length Made by a Glass Lens and Liquid-Crystal Layers," Applied Optics, vol. 43, pp. 3420-3425, 2004.

[10] V. V. Presnyakov and T. V. Galstian, "Electrically tunable polymer stabilized liquid-crystal lens," Journal of Applied Physics, vol. 97, pp. 103101, 2005.

[11] V. Presnyakov and T. Galstian, "Polymer-stabilized liquid crystal lens for electro-optical zoom," Proceedings of SPIE, vol. 5577, pp. 861, 2004.

[12] V. Presnyakov, K. Asatryan, T. Galstian, and A. Tork, "Polymer-stabilized liquid crystal for tunable microlens applications," Optics Express, vol. 10, pp. 865-870, 2002.

[13] H. Ren, Y. H. Fan, S. Gauza, and S.-T. Wu, "Tunable microlens arrays using polymer network liquid crystal," Optics Communications, vol. 230, pp. 267-271, 2004.

[14] L. G. Commander, S. E. Day, and D. R. Selviah, "Variable focal length microlenses," Optics Communications, vol. 177, pp. 157-170, 2000.

[15] A. M. R. L. Yang, E. M. McCabe, L. A. Dunbar, and T. Scharf, , "Confocal microscopy using variable-focal-length microlenses and an optical fiber bundle," Applied Optics, vol. 44, pp. 5928-5936, 2005.

[16] J. Knittel, H. Richter, M. Hain, S. Somalingam, and T. Tschudi, "Liquid crystal lens for spherical aberration compensation in a Blu-ray disc system," Science, Measurement and Technology, IEE Proceedings-, vol. 152, pp. 15-18, 2005.

[17] M. Hain, R. Gl 鐨 kner, S. Bhattacharya, D. Dias, S. Stankovic, and T. Tschudi, "Fast switching liquid crystal lenses for a dual focus digital versatile disc pickup," Optics Communications, vol. 188, pp. 291-299, 2001.

[18] B. Berge and J. Peseux, "Variable focal lens controlled by an external voltage: An application of electrowetting," The European Physical Journal E-Soft Matter, vol. 3, pp. 159-163, 2000.

[19] S. Kuiper and B. H. W. Hendriks, "Variable-focus liquid lens for miniature cameras," Applied Physics Letters, vol. 85, pp. 1128-1130, 2004.

[20] J. Park, C.-X. Liu, and J.-W. Choi, "A Planar Liquid Lens Design Based on Electrowetting," presented at Sensors, 2007 IEEE, 2007.

[21] F. Krogmann, R. Shaik, W. Monch, and H. Zappe, "Repositionable liquid micro-lenses with variable focal length," Micro Electro Mechanical Systems, 2007. MEMS. IEEE 20th International Conference on, pp. 707-710, 2007.

[22] S. Grilli, L. Miccio, V. Vespini, A. Finizio, S. De Nicola, and P. Ferraro, "Liquid micro-lens array activated by selective electrowetting on lithium niobate substrates," Optics Express, vol. 16, pp. 8084-8093, 2008.

[23] "http://www.varioptic.com/en/index.php."

[24] C. C. Cheng, C. A. Chang, and J. A. Yeh, "Variable focus dielectric liquid droplet lens," Optics Express, vol. 14, pp. 4101-4106, 2006.

[25] C. C. Cheng and J. A. Yeh, "Dielectrically actuated liquid lens," Optics Express, vol. 15, pp. 7140-7145, 2007.

[26] H. Ren and S. T. Wu, "Tunable-focus liquid microlens array using dielectrophoretic effect," Optics Express, vol. 16, pp. 2646-2652, 2008.

[27] D. Zhang, N. Justis, and L. Y.-H., "Fluidic adaptive lens of transformable lens type," Applied Physics Letters, vol. 84, pp. 4194-4196, 2004.

[28] W. Wang and J. Fang, "Design, fabrication and testing of a micromachined integrated tunable microlens," J. Micromech. Microeng, vol. 16, pp. 1221-1226, 2006.

[29] K. Campbell, Y. Fainman, and A. Groisman, "Pneumatically actuated adaptive lenses with millisecond response time," Applied Physics Letters, vol. 91, pp. 171111, 2007.

[30] H. Ren and S. T. Wu, "Variable-focus liquid lens by changing aperture," Applied Physics Letters, vol. 86, pp. 211107, 2005.

[31] H. Ren, D. Fox, P. A. Anderson, B. Wu, and S. T. Wu, "Tunable-focus liquid lens controlled using a servo motor," Optics Express, vol. 14, pp. 8031-8036, 2006.

[32] S. W. Lee and S. S. Lee, "Focal tunable liquid lens integrated with an electromagnetic actuator," Applied Physics Letters, vol. 90, pp. 121129, 2007.

[33] R. Kuwano, M. Y., T. Tokunaga, and Y. Otani, "Liquid pressure varifocus lens using a fibrous actuator," Proc. of SPIE, vol. 6374, pp. 1-4, 2006.

[34] L. Dong and H. Jiang, "pH-adaptive microlenses using pinned liquid-liquid interfaces actuated by pH-responsive hydrogel," Applied Physics Letters, vol. 89, 2006.

Chapter 2

Fabrication and analysis of bio-inspired fluidic lens

In this chapter, we will cover the device issues for bio-inspired fluidic lens. The first part of this chapter, we will discuss the device that we selected to use as well as the detailed modeling of the device to understand better about it.

The second part of the chapter, we will then discuss the fabrication details of the fluidic lens. Fabrication technique proves to be a very important enabling factor for better image quality. Finally, in the last section, we discuss some of our attempts in

characterizing the physical property of the device through finite element analysis software as well as hardware measurements.

2.1 Fluidic lens structure and operation

The basic structure of a membrane-based fluidic lens is shown in Figure 2.1. The optically clear elastic membrane is used to seal the optical fluid chamber. High index of refraction fluid is used to fill the fluid chamber.

The way this fluidic lens work is by applying pressure to the fluid. When positive pressure is applied to inject fluid into the chamber, the elastomer membrane produces a convex shape for a positive lens. Conversely, when negative pressure is applied to the chamber, the optical fluid is withdrawn into a reservoir and a concave lens is formed.

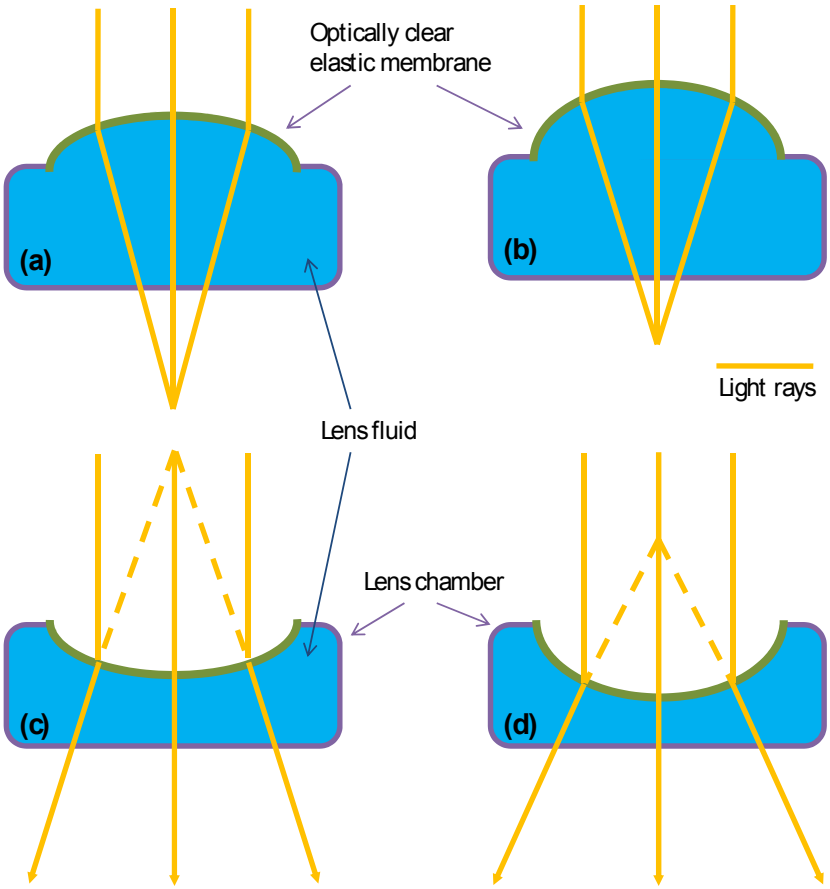

Figure 2.1 Basic fluidic lens structure and function

One major feature of this type of fluidic lens has to do with the fact that the surface profile of the lens is determined by the membrane, and the optical property of the lens is determined by the optical fluid. This provides 2 extra degrees of freedom for fluidic lens device design. Designers can choose different fluids and different membranes to fit their need.

2.2 Fabricating bio-inspired fluidic lens

Fabrication technology improvement is a major contributor to image quality. The fabrication step can be roughly separated into 3 major steps. The first step is membrane preparation. The second step is device assembly and the final step is fluid fill. There are 2 key fabrication techniques that contributed to the yield and the performance of the device: (1) pre-stretch, which improves the image quality, and (2) vacuum filling, which reduces the amount of residual bubbles in the process. To enable pre-stretch technology, a new processing approach that we developed is the oxide-coating technology. Basically, oxide is sputtered onto the aluminum layer as an adhesion layer to facilitate bonding. We will cover the key steps here. However, since the assembly of each fluidic lens is slightly different for different applications, we will focus on introducing the

2.2.1 Making the membrane

Making the fluidic lens membrane is one of the main key technology enabling better image quality. First, an optically clear elastic membrane is prepared by mixing prepolymer Gelest 1.41, a type of polydimethylsiloxane (PDMS), at 1:1 ratio and spincoating it onto a silicon wafer coated with Chlorotrimethylsilane. Then the entire wafer is baked in a 65 degree oven overnight.

To define the circularity of fluidic lens, an anodized aluminum ring is first carefully machined. One side of the aluminum ring is polished with 1 um alumina powder until the ring has near mirror quality surface. A 50 to 100 nm SiO2 thin film is

then sputtered onto the polished side. This SiO2 layer serves as an adhesion layer for aluminum to PDMS.

To handle the membrane, a PDMS membrane holder made out of Sylgard 174 was bonded to the membrane by first exposing both the holder and the membrane to ozone in an UV-ozone cleaner for 3 minutes each. The membrane holder and the membrane are attached and placed in 80° C oven overnight to facilitate bonding.

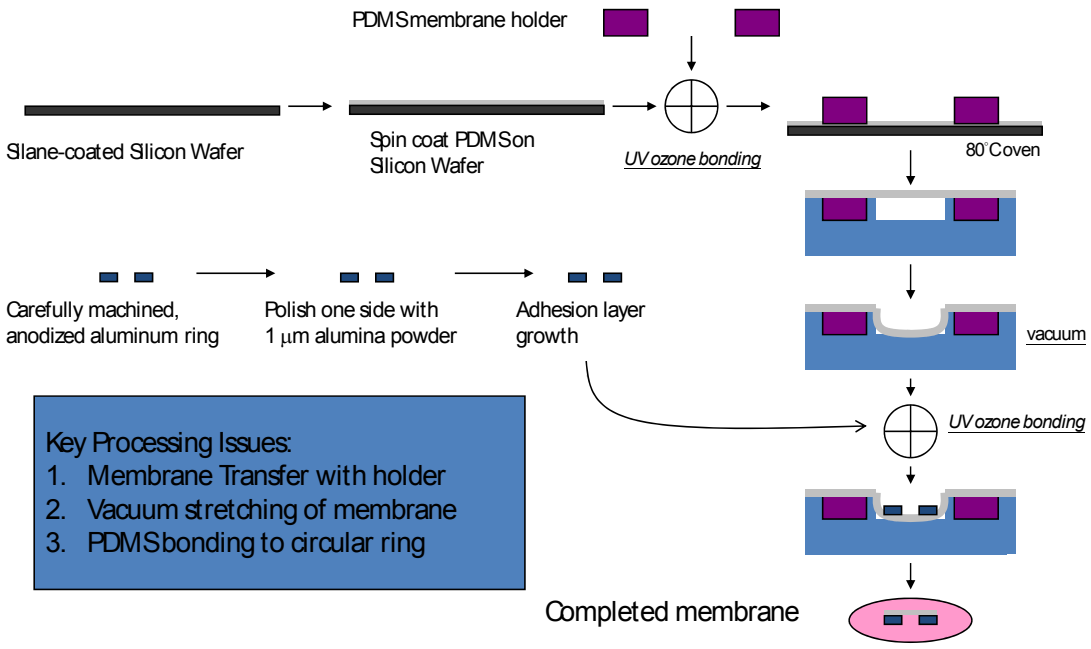

Figure 2.2 Membrane preparation process.

The final phase for preparing the membrane is to mount the membrane to the aluminum ring. To ensure that the membrane is really flat, a small vacuum cup is used to pre-stretch the membrane. Stretching the membrane by a vacuum cup ensures that the stretch on the membrane is rotationally symmetric. Vacuum is slowly applied onto

the vacuum cup to stretch the membrane evenly. The slow application of vacuum is very important because when the membrane is quickly stretched, the bubbles will be trapped between the membrane and the bottom of the cup.

The amount of stretch on the membrane is controlled by the height of the cup and is monitored with a pressure meter. The pre-sputtered Al-ring is aligned to the center of the cup and bonded to the membrane. Without prestretch, the membrane becomes floppy when the fluidic lens is operating with the lens nearly flat, compromising image quality. The typical pre-stretch pressure that we have placed into the membrane is around 0.05~0.08 PSI.

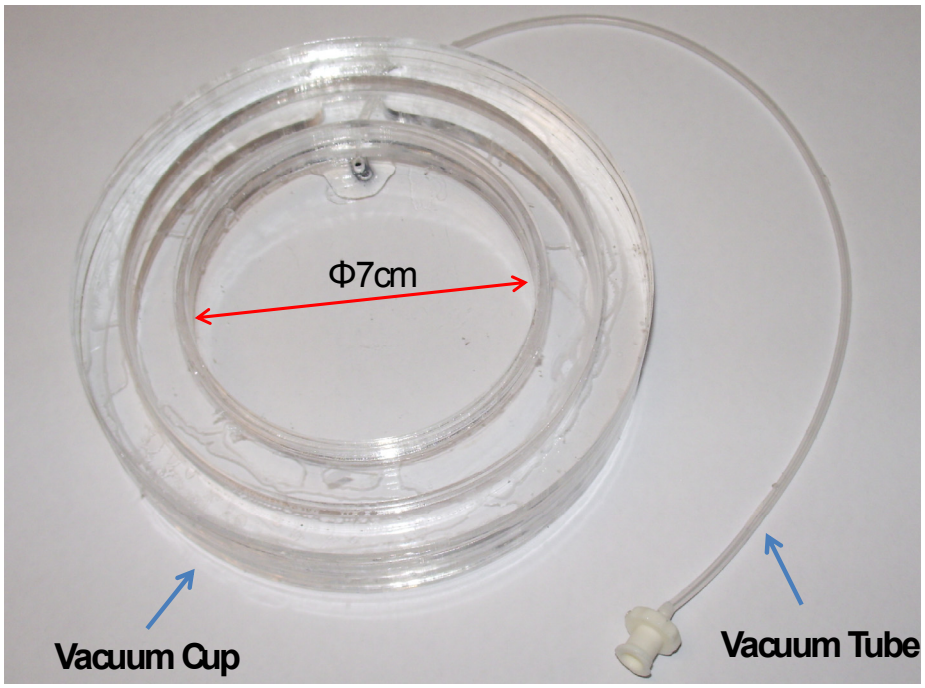

Figure 2.3 Photograph of the vacuum cup designed for prestretch.

There are a few key vacuum cup design issues: (1) larger inner diameter reduce irrotational symmetry; (2) soft pdms bottom to ensure stable bonding – cleaning to avoid too much dust attraction; (3) pre-stretch pressure roughly 0.05~0.08 PSI.

2.2.2 Assembly

The next step after preparation of membrane holder is assembly. Because the assembly of each lens varies greatly due to different materials, it is difficult to document in a general form. The assembly of each lens is documented in each individual chapter.

All PDMS bonding is done by first exposing PDMS surface to ozone in a UV ozone chamber for 3 minutes to activate the surface and then placing the contacted device in an 85 degree oven for several hours to facilitate bonding. After UV ozone treatment, PDMS surface stays activated for more than 40 minutes. Thus, enabling advanced manipulation, such as vacuuming and alignment, after the treatment.

2.2.3 Vacuum filling of optical fluid

The second key technology for fabricating high image quality fluidic lens is the vacuum filling process. With vacuum filling, we are able to fill the lens chamber with very small amount of air bubbles, ensuring the yield of each fabrication.

The entire vacuum filling process comprises of three basic steps shown in Figure 2.4. The first step is the initial step where the entire system is constructed and placed inside the dessicator. At this point, the pressure inside the fluid chamber and the pressure inside the chamber is equivalent.

The second step is the vacuum step. Vacuum pump is turned on to pump air out of the dessicator. Because the pressure inside the fluid chamber is higher than the internal pressure of the dessicator, the air will push itself outside of the chamber. During this process, bubbles are formed and pulled out of the tubing.

The final step is the fill step. This is the point where the vacuum is turned off and the air is slowly released back into the dessicator. This will cause the pressure inside the dessicator to slowly return to air pressure. During the vacuum phase, air is removed from the inside of the fluidic lens chamber, therefore, there is less gas molecules. Under regular air pressure, the same amount of air molecule will take up less space. In other words, the fluid will be pushed into the fluid chamber and fill up the fluidic lens.

The above section documents the 3 basic steps to vacuum filling. In actual operation, the process may be repeated a couple of times. With each iteration, the bubbles will become smaller and smaller. Also, the final iteration usually involves a very slow release of air back into the dessicator. The dessicator is often left over night for a very slow air refill. Whether the slow air release helps in reducing the bubble in the fluid chamber is uncertain, but is carried out each time for all fabricated lens.

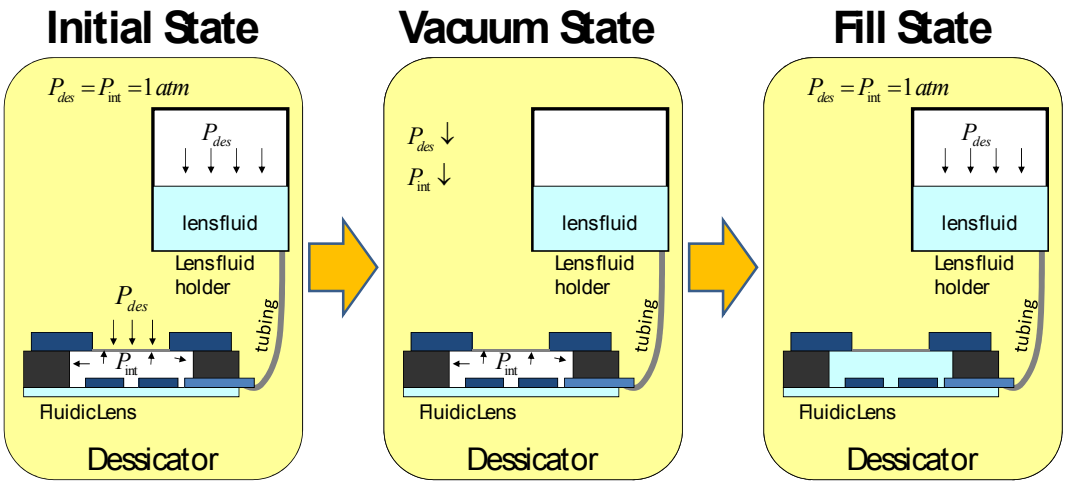

Figure 2.4 The three basic steps of vacuum filling.

2.3 Analysis of bio-inspired fluidic lens surface profile

The optical property of a lens is basically determined by its surface profile and the optical properties of the material. The feature with membrane-based fluidic lens is that the surface profile is determined by the mechanical properties of the membrane and the optical property is determined by the fluid selected. This section, we focus on the study of the surface profile of fluidic lens.

2.3.1 Surface profile modeling

Before we begin our studies, we make the first assumption that the fluidic lens surface profile is basically rotationally symmetric. If there are no fabrication tolerances, the pressure of the fluid is almost the same, thus the first assumption is a logical one. Under the assumption that the surface profile is rotationally symmetric, there is no need

for complicated Zernike polynomials. The surface can be described with odd polynomials, as shown in eq. (1).

$$z = \frac{c \cdot r^2}{1 + \sqrt{1 - (k+1)c^2 r^2}} + A_3 \cdot r^3 + A_4 \cdot r^4 + A_5 \cdot r^5 + \cdots \quad (1)$$

where c is radius of curvature at the vertex of the lens, r is the distance from the center of the lens, and k is the conic constant.

A typical simplification of the above equation is the elliptical equation where only two parameters are involved. Curvature is the reciprocal of the radius at the vertex of the lens and conic constant specifies the nature of the elliptical equation, being elliptical, parabolic, or hyperbolic.

When the conic constant (k) is zero, the equation describes a spherical lens. When k = -1, the shape is a parabola. When k > 0, the shape is an oblate ellipsoid. The shape difference has mechanical and optical implications. Mechanically, when k > 0, more fluid is needed to create the same curvature than a spherical lens (k=0). Conversely, when k < 0, less fluid is needed to achieve the same curvature. Since curvature, in a first-order approximation, determines the lens power, the sign and value of conic factor means different requirements for the actuators that have to move a certain amount of fluid into and out of the lens chamber to vary the focal length. Optically, different conic factor means different geometric aberrations. Hence, the value of conic factor affects how the optical system is designed, and the ability of controlling the conic factor is important to achieve optimal system performance.

2.3.2 Elasticity theory and COMSOL modeling

Since the surface profile is completely determined from the mechanical properties of the elastic membrane, we simulated the effect of the elastic membrane under pressure from the fluid to extract the lens profile in software.

First, the elastic membrane is modeled using the COMSOL Multiphysics simulation software. The analysis is done by solving partial differential equations (PDEs) using the finite element method (FEM).

In setting up the software, one needs to determine the mechanical property for PDMS. The most suitable mechanical model for rubbers where PDMS belongs to is the hyperelastic model where the stress-strain relation is specified by a strain-energy density function [1]. The strain-energy function (W) is a function of the deformation gradient tensor (e.g. $W_{hyp} = W(\mathbf{F})$, where $\mathbf{F}$ is the deformation gradient tensor). For isotropic material, the strain-energy function becomes a function of the principal invariants of the right Cauchy-Green deformation tensor, e.g. $W_{hyp} = W(I_1, I_2, I_3)$ [2, 3]. The right Cauchy-Green Deformation tensor is defined as $\mathbf{C} = \mathbf{F}^T\mathbf{F}$ and the principal invariants are $I_1 = trace(\mathbf{C})$, $I_2 = \frac{1}{2}\{trace((\mathbf{C}))^2 - trace(\mathbf{C}^2)\}$, and $I_3 = \det(\mathbf{C})$. We use Mooney-Rivlin constitutive equations to model the incompressible isotropic elastomer (i.e. PDMS). The strain energy function is defined in COMSOL as follows:

$$W_{hyp} = C_{10}(\bar{I}_1 - 3) + C_{01}(\bar{I}_2 - 3) + \frac{1}{2}K(J_{el} - 1)^2 \tag{2}$$

where C_{10}, C_{01}, and K are material properties for PDMS membrane. $\bar{I}_1 = I_1 \cdot J^{-2/3}$ and $\bar{I}_2 = I_2 \cdot J^{-4/3}$, where I_1 and I_2 are the first and second invariant of the left Cauchy-Green tensor and J is the determinate of the deformation gradient tensor, $J = \det(\mathbf{F})$. $J_{el} = \frac{J}{(1+\varepsilon_{th})^3}$ where ε_{th} is thermal strain. Basically, J describes the volume change and J_{el} is the elastic part of volume change. Note that $\bar{I}_1$ and $\bar{I}_2$ remain constant under volume change.

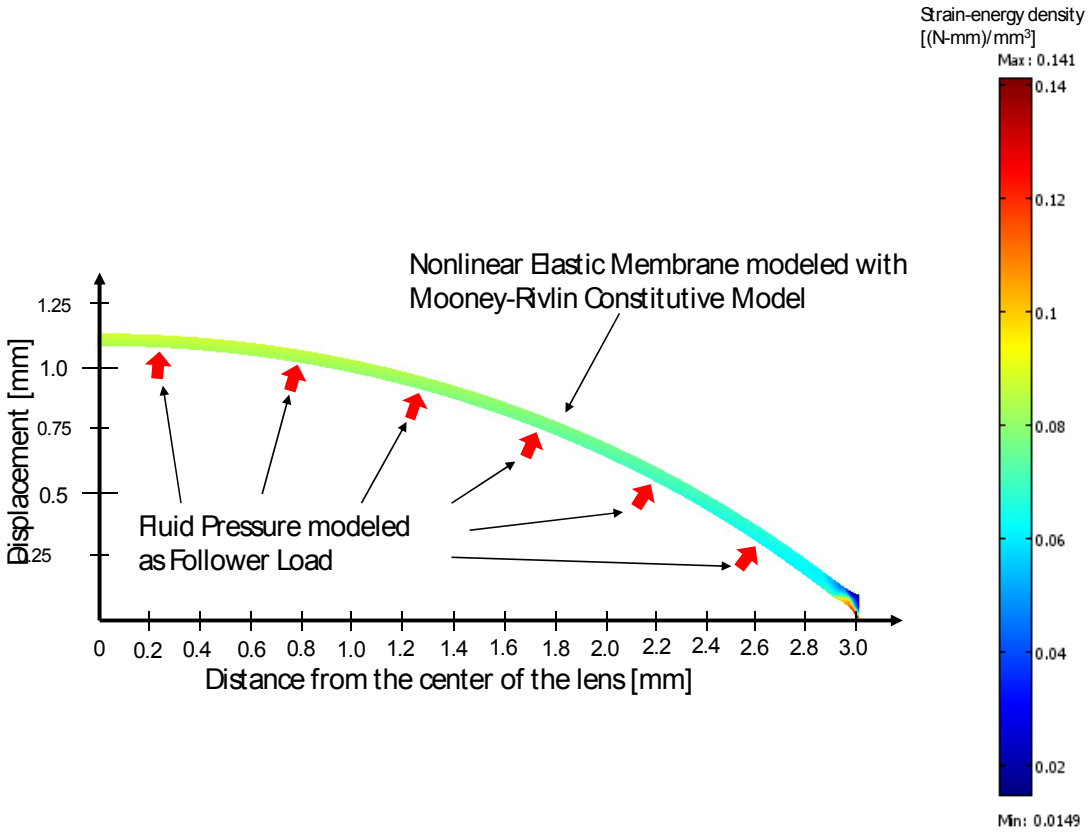

Figure 2.5 Example modeling of the elastic membrane under fluid pressure in COMSOL. The fluid pressure is modeled as follower load and the membrane material property is modeled with Mooney-Rivlin constitutive model.

One major improvement in membrane processing is the application of pre-stretch where the membrane is in tensile stress before being bonded to the Al ring. Pre-stretch of the membrane not only prevents wrinkling at low lens power (nearly flat surface) but also greatly suppresses the effect of gravity. In addition, adjusting the amount of pre-stretch allows us to adjust the value of conic factor [4]. The effect of pre-stretch is simulated in COMSOL by pre-pulling the membrane apart from its initial rested state.

2.3.3 Curvature fitting in Matlab

Once the simulation is completed, we developed proprietary curvature fitting software in Matlab to analyze the lens profile. The overall procedure is shown in Figure 2.6. Basically, the FEM software is set up based on the description in the earlier section. The simulated results are than dumped into Matlab to perform curvature fitting with the curve fitting tool. We first assume that the elliptical equation is sufficient to model the lens profile, so we fitted the simulated profile into the elliptical equation. The software that we developed generated fitting results as well as the fitting errors.

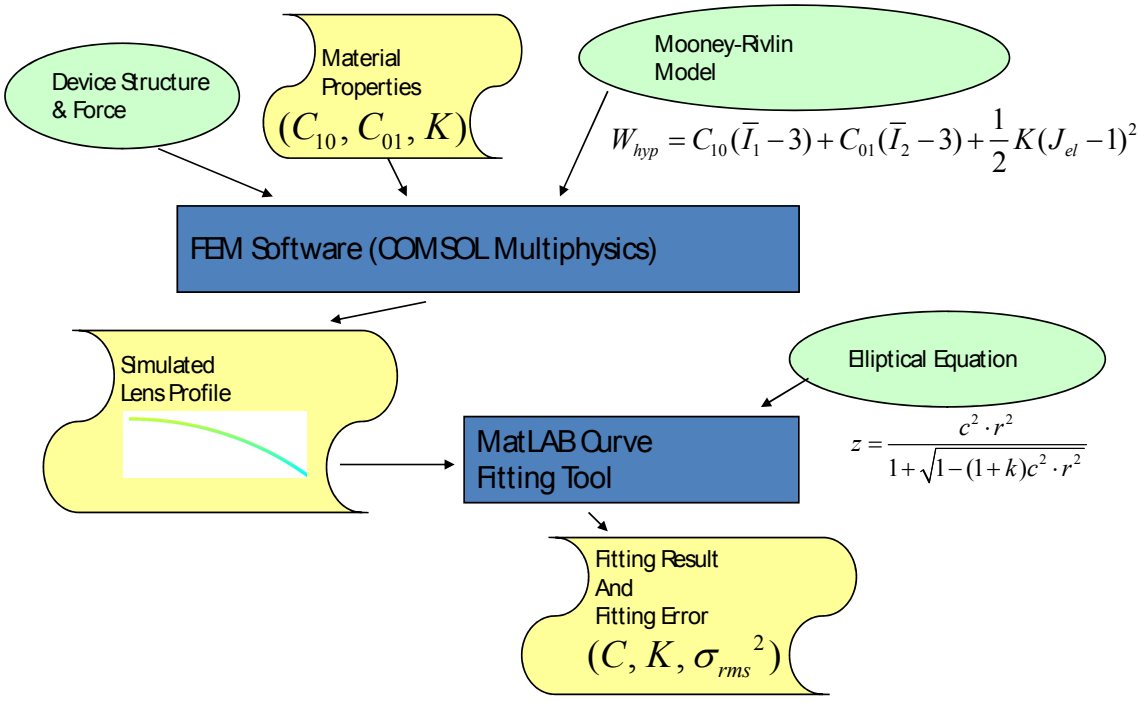

Figure 2.6 Fluidic lens surface profile software analysis procedure.

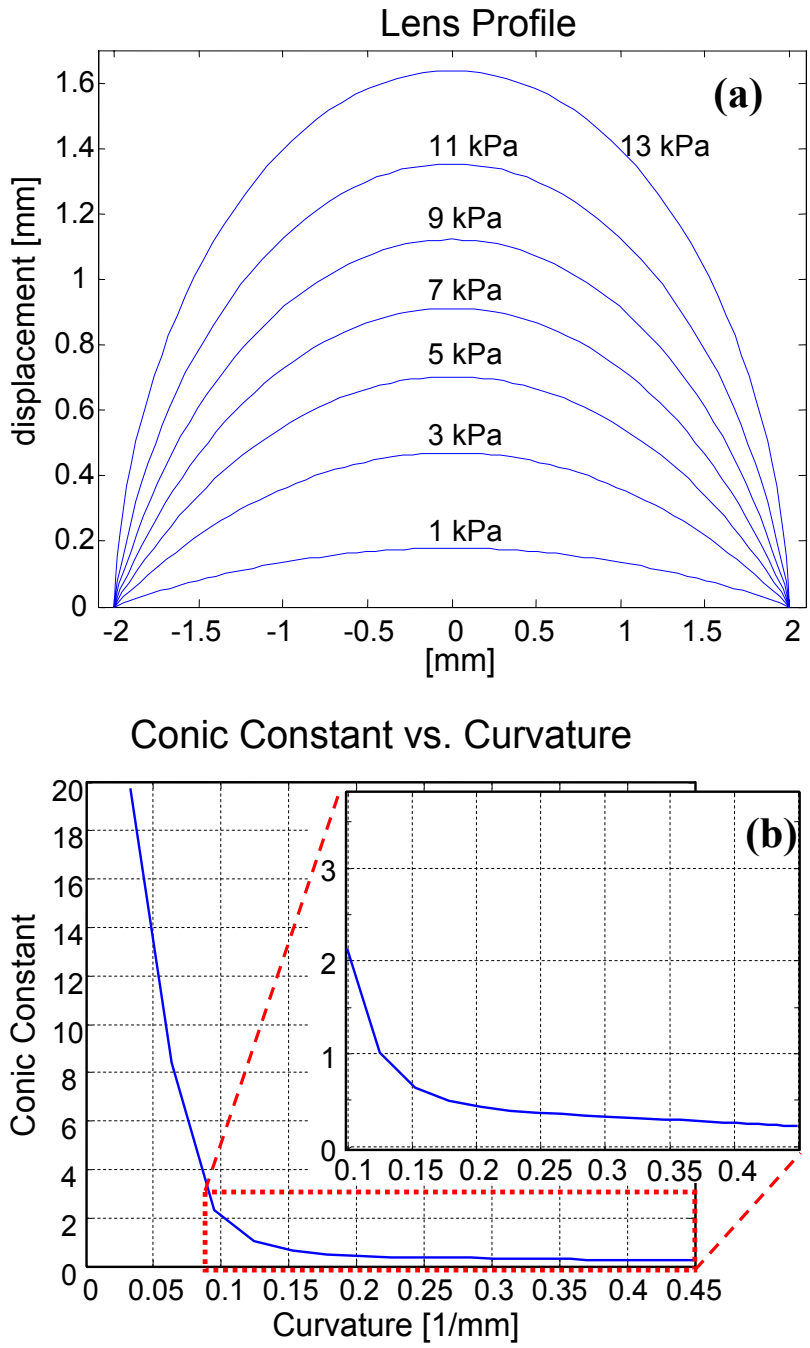

Figure 2.7 (a) Simulated profile of a 4-mm diameter fluidic lens under different chamber pressure. (b) Relationship between radius of curvature and conic constant after fitting the lens profile to an elliptical equation. Positive conic constant suggests that the fluidic

lens has an oblate ellipsoid profile. Note that, in practice, conic factor becomes important when the lens has a significant curvature (> 0.1 mm for the current device).

2.3.4 Error analysis of the curvature fitting

After the fitting is completed, it is important to analyze the error of the fitting to determine if the original assumption that the profile can be fitted into elliptical equation is accurate.

To better understand the problem, we separate the problem into 2 problems. The first is to look at the absolute error of a fitting. One example is shown in Fig. 2.8. The result shows that the sag error is with 50 nm, which is less than $\lambda/10$.

The second part of the study, we studied the error of several fitting resulting from different fluid pressure and different membrane thickness, which can be controlled by spinning rate during the coating process. Since the parameters are different, we need to simplify the error description into simpler terms. We used RMS sag error as a comparison for the quality of the fit. The result is shown in Fig. 2.9. The RMS sag error for all cases are $< \lambda/10$.

With all the errors very low, we conclude that elliptical equation is a good model to describe surface profile.

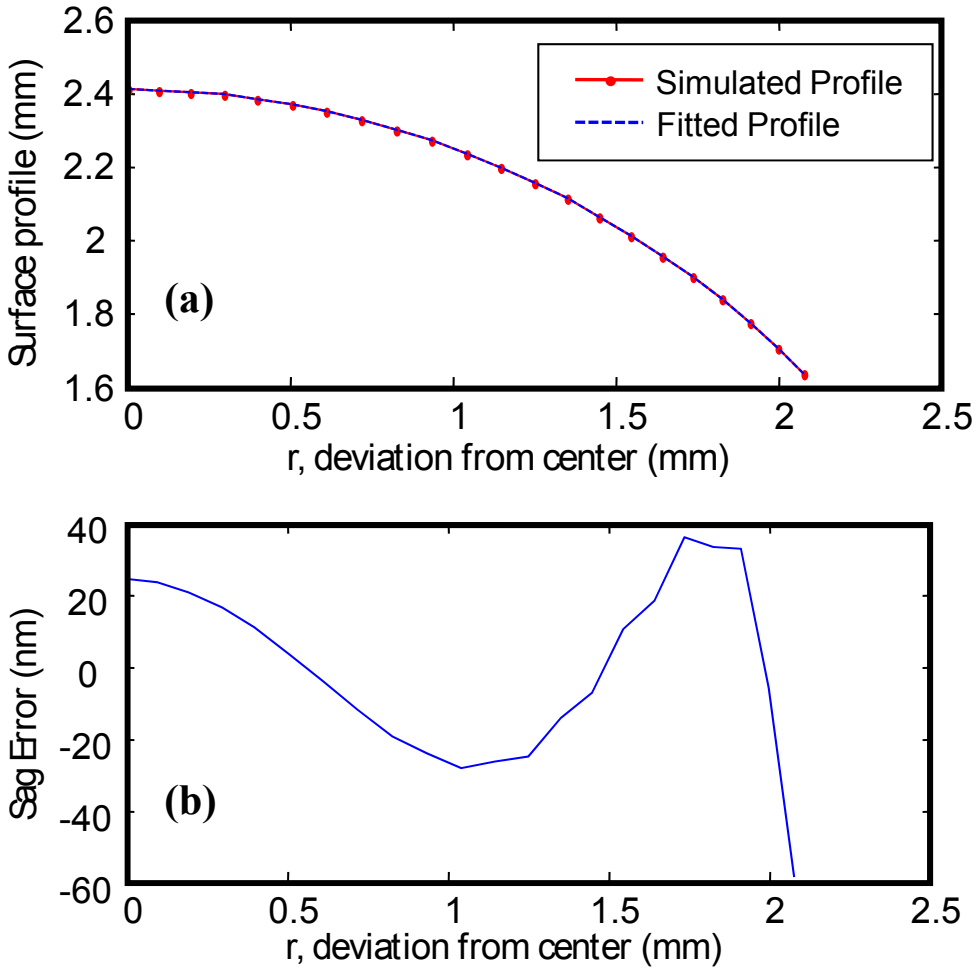

Figure 2.8 (a) over-lay of simulated profile vs. fitted profile based on elliptical equation.

(2) the difference between the 2 profiles, or sag error in nm.

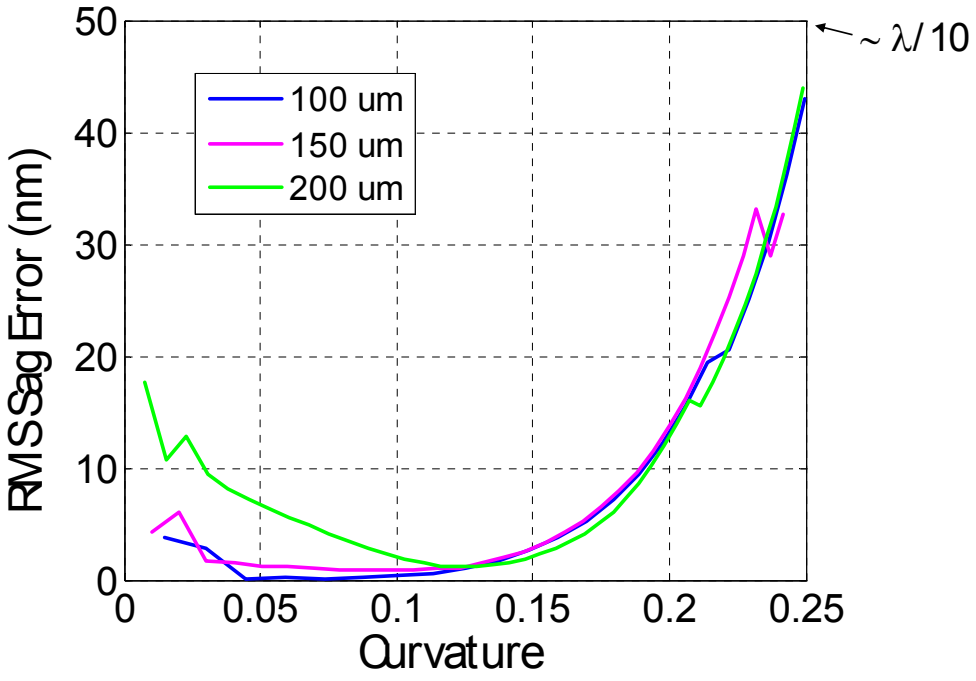

Figure 2.9 RMS sag error under different curvature and different membrane thickness. The difference in curvature is caused by different fluid pressure.

2.3.5 Hardware testing and experiments

Upon finishing analysis of the software, analysis needs to be done on the actual hardware to verify the accuracy of the modeling.

Surface profile analysis for fluidic lens is very tricky. Several different forms of measurement techniques were tested and failed to provide good results. The first type of profilometers tested were contact based profilometers, such as Dektek. The main

problem with contact based profilometer is that the surface of fluidic lens deform when in contact with a tip. This happens even though the force of the tip is very small.

The second type of profilomters is contactless profilometers. The commercially available types are typically interferometers. The most common one is Mirau interferometer. The main limitation with this interferometer is that it has a 27° angle slope limitation. It is possible to stitch the profile of the lens slowly to eventually calculate the surface profile. However, under larger curvature when there is a large slope, the profilometer will not work.

Another often used profilometer in optical testing is the Fizeau interferometer. The working principle of the Fizeau interferometer requires a specific correction lens that has similar curvature compared to lens under test. Fizeau interferometer is a convenient tool for manufacturing lenses; however, in the case with fluidic lens, it is very difficult to find the correction lens since (1) the curvature of fluidic lens is constantly changing, and (2) the actual profile is not truly certain.

Since no commercially available profilometers really work for us, we designed our own proprietary profilometer.

2.3.4.1 Profile Measurement System Design

Since the fluidic lens has curvature on one side only, a transmissive lens profile measurement system can be used. A similar architecture for testing intra-ocular lenses was presented in [5].

The basic idea is to think of optical lenses as optical wavefront modifying components. If we know the input wavefront, then, by measuring the output wavefront, the lens profile that creates the wavefront modifications can be reversely calculated. Since one side of the fluidic lens is known to be flat, there is only one side that needs to be reconstructed. Furthermore, based on our earlier software analysis, the profile of the fluidic lens is most likely elliptical equation, so only 2 parameters are needed.

To measure the output wavefront, Shack-Hartmann Wavefront Sensor (SH-WFS) is used. The SH-WFS is basically composed of a microlens array and a charged coupled device (CCD). Basically, the microlens is designed such that the energy of the wavefront is focused onto a single spot on the CCD. If the wavefront is tilted, the focused spot will deviate from the center position, thus measuring the wavefront slope. The wavefront is then reconstructed numerically from the slopes. One limitation to this mechanism is that the wavefront slope cannot be too large because if the spot deviate too far from the center, it becomes unclear which microlens generated the spot. Due to such limitation, the input wavefront has to match the lens profile to ensure correct reconstruction of the wavefront.

The way to create a good input wavefront is to have a single point source that can generate a wavefront of any curvature, and by moving the point source closer and further away from the fluidic lens, wavefront going into the lens can be controlled to be of any curvature. Three optical components are used to generate a single point source: (1) HeNe Laser, (2) Beam Expander, and (3) Microscope Objective. HeNe laser is used to provide a stable wavefront. Diode lasers were also explored as an alternative option,

but the wavefront profile of diode lasers are too poor for accurate analysis. The laser light has a very narrow beam width. Beam Expander is used to get a better wavefront profile because after beam expansion, only the center portion of the laser will go through the microscope objective entrance pupil. This ensures that only the center, flatter part of the wavefront is used. A diffraction limited high numerical aperture microscope objective is used to focus the wavefront into a single point source. The distance between the microscope objective and the fluidic lens under test is a variable and can be moved such that the wavefront curvature matches the lens power of the fluidic lens. A wavefront relay is used to relay the wavefront from the fluidic lens to the SH-WFS. The main purpose of this relay is to overcome mechanical impossibilities of measuring the wavefront right after the lens.

A system equivalent to the hardware system is built in Code V and ZEMAX. The software then optimizes for the best lens profile that creates the wavefront that matches the wavefront detected by the WFS.

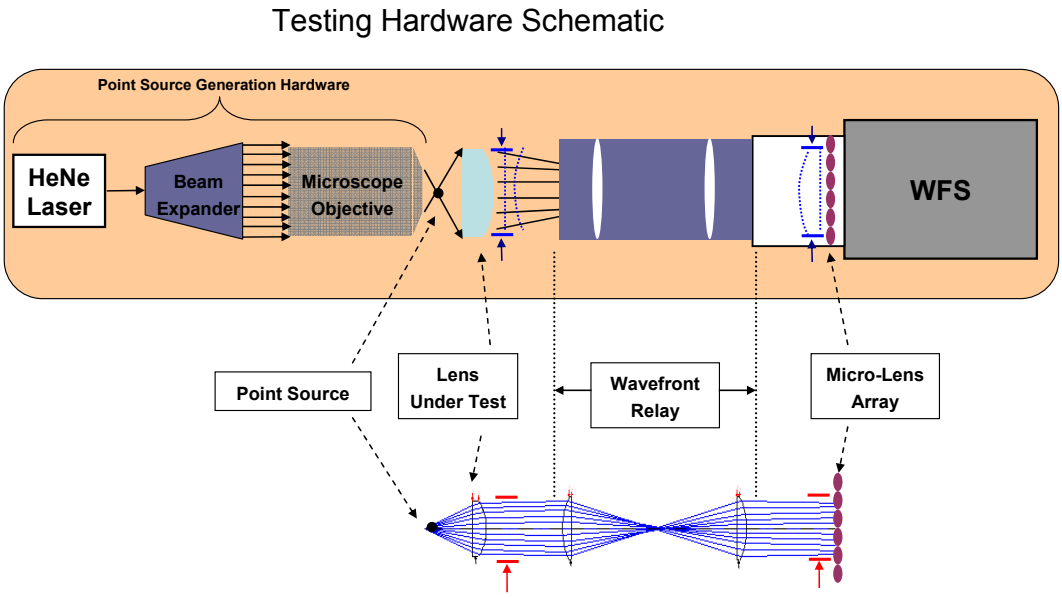

Figure 2.10 Testing Hardware Schematic (a) and its corresponding software structure (b). To create the ideal point source, 3 components: (1) HeNe Laser, (2) Beam Expander, and (3) Microscope Objective are used. The Lens under test, fluidic lens in our case, is then placed behind the point source. By changing the distance between the point source and the lens under test, wavefront with any curvature can be generated. The ideal position to measure how the lens changes the input wavefront is at the vertex of the lens under test. This is mechanically difficult. So a wavefront relay is placed after the lens under test to relay the wavefront to the WFS. To compensate for the aberrations induced by the wavefront relay, optical system including the wavefront relay are included in the ray tracing software for lens profile reconstruction.

2.3.4.2 Profile Measurement Result

Measurement results with the aforementioned optical system are shown in Figure 2.11. The measured data shows the same varying conic constant over curvature trend as the simulated results.

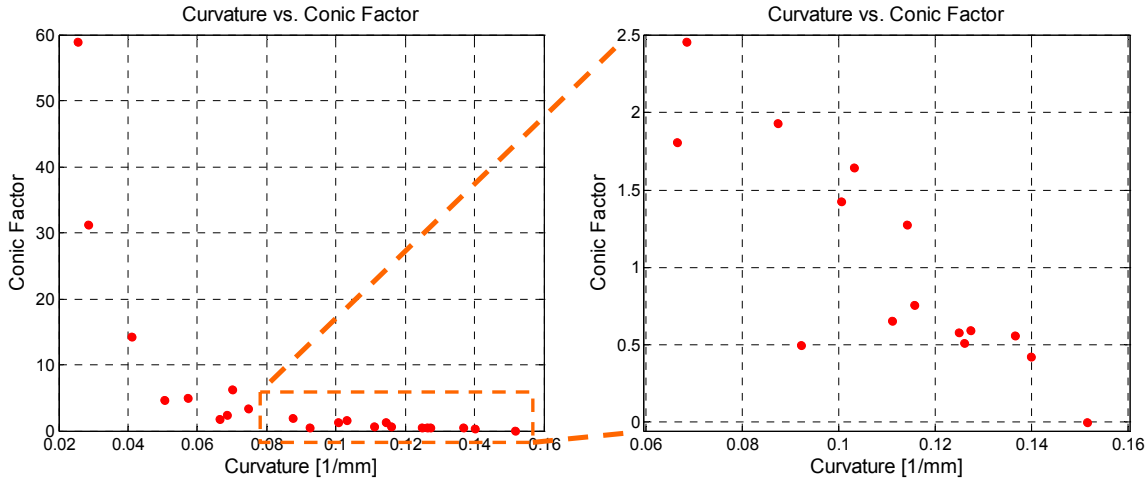

(a) (b)

Figure 2.11 Measured Result. After fabricating a fluidic lens, it is measured with the optical system setup. The measurement results show a relationship between radius of curvature and conic factor similar to the results from simulation.

2.3.4.3 Residual Wavefront Error

The residual wavefront error of the optimization result from Zemax is shown in Fig. 2.11. During the experiment, I explored using different lens size to measure the conic constant. From the measurement data shown in Figure 2.11, when 90% and 80% of the lens coverage shows similar result. However, when 100% of lens is used for

analysis, there is quite a bit of error, particularly at the edge. This shows that there is still some error on the connection edge.

Furthermore, it can be seen from the data that there is still quite a bit of residual wavefront. This is because there are several sources of error in the optical system setup. For instance, the lenses used in the relay system are plano-convex spherical lenses. These lenses introduce spherical aberration into the system. The second potential source of error is that the point source is imperfect, which is very different from the perfect point source modeled in ray tracing software.

The second observation on the residual wavefront error is that it is not rotational symmetric. Several factors could have contributed to this as well. The most likely is that the fabrication process is not perfect. There is still room for improvement, and the most likely reason is at the alignment of the aluminum ring onto the prestretched membrane. Other sources of such irrotational residual wavefront could come from the lateral misalignment of the fluidic lens in the measurement system.

In short, the technology that we developed for measuring the surface profile of the fluidic lens is good and provides valuable feedback as well as insight. However, better equipments and more advanced tools could help improve the understanding of surface profile.

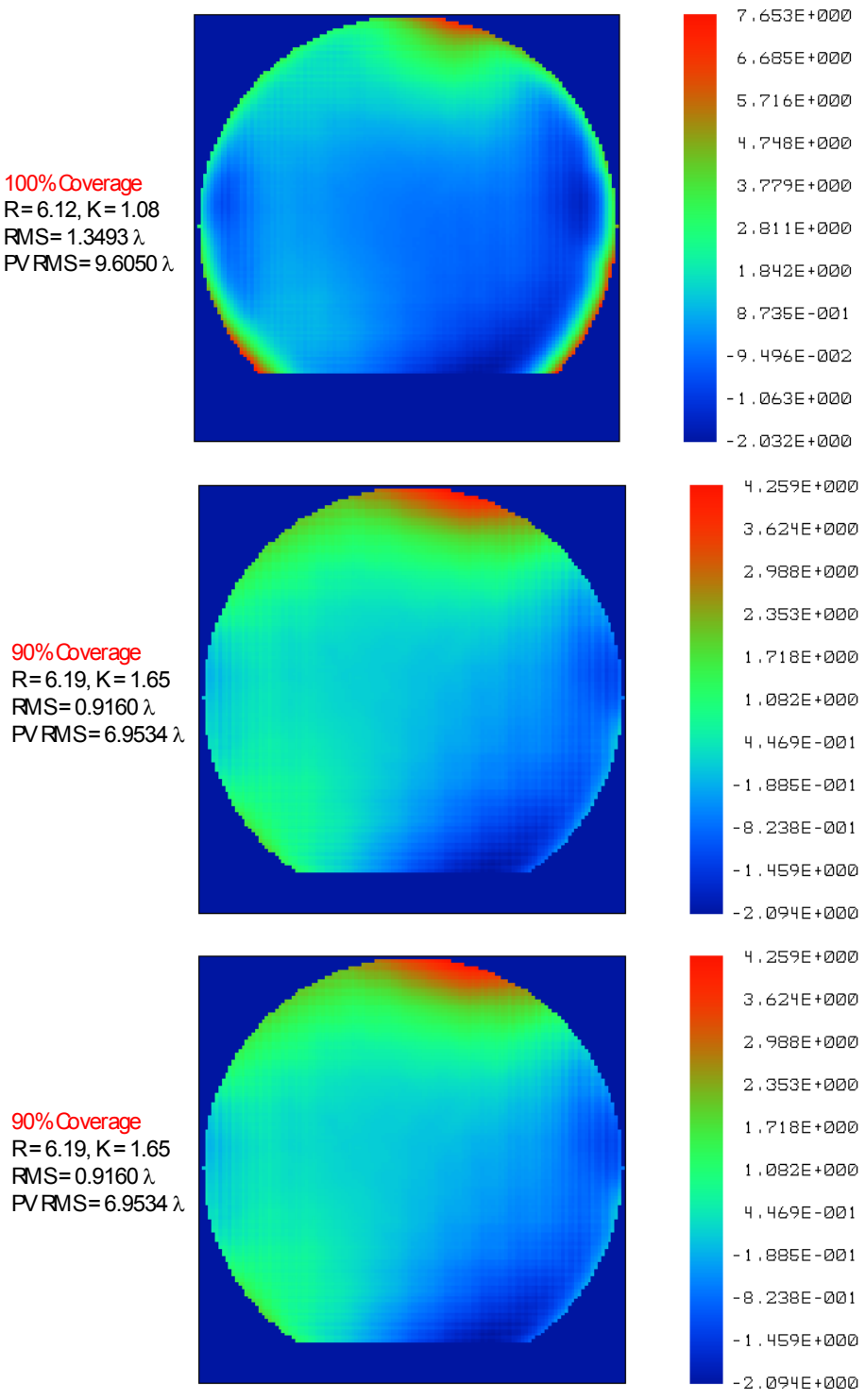

Figure 2.12 Residual wavefront error under different percentage of lens surface coverage.

2.4 Conclusion

In this chapter, we discussed the basic operation of membrane-based fluidic lens. One of the major key technology for improving image quality was improvement in fabrication technology. The key processing technology that correlates to improved image quality are: (1) Prestretch technology and (2) vacuum filling technology.

To get better image quality, the surface profile of the lens was studied. Software analysis with FEM showed that conic constant is a good approximation for the surface profile of membrane-based fluidic lens. Actual hardware measurement shows correlation to our software analysis. However, room for improvement on fabrication as well as better measurement equipment are needed to improve this technology.

References:

[1] A. F. Bower, "Applied Mechanics of Solids," 2008.

[2] Y. C. Fung, *A First Course in Continuum Mechanics, 3rd edition*. Englewood Cliffs, New Jersey 07632: Prentice Hall, 1994.

[3] A. Shabana, *Computational Continuum Mechanics*. New York: Cambridge University Press, 2008.

[4] F. S. Tsai, S. H. Cho, W. Qiao, N. H. Kim, and Y. H. Lo, "Miniaturized unified imaging system using bio-inspired fluidic lens," *Proceedings of SPIE*, 2008.

[5] Rammage, R.R., D.R. Neal, and R.J. Copland, *Application of Shack-Hartmann wavefront sensing technology to transmissive optic metrology.* Proc. SPIE, 2002. **4779**: p. 161-172.

Chapter 2 or portion thereof has been published in ***Proceesings of SPIE*****, vol. 7061, 70610N (2008)**.

Chapter 3

Miniaturized universal imager

The key difference between bio-inspired fluidic lens and regular man-made lenses is in the curvature changing capability. It is possible to form image with fluidic lenses. But what is the key reason for getting good image quality? In this chapter, we demonstrate the capability of fluidic lens. With fluidic lens, we developed miniaturized unified imager that is small (12.5 mm total track) and can switch between a regular

camera, macro mode, super macromode, and microscope mode. Most importantly, we demonstrate that high image quality can be achieved.

3.1 IMAGE QUALITY LIMITATION OF A SINGLE LENS

A single lens imaging system doesn't provide a good image quality because of the large amount of aberration. In a typical optical system, multiple surfaces and lenses have to be utilized to resolve the aberrations. The main function of a single lens is auto-focusing.

As an example, a single fluidic lens system was built to form images of objects at infinity and at 2 cm distance from the lens. The image quality is shown in Figure 3.2. The quality of the image is very poor. There are several reasons for the poor image quality. First of all, there is a very large field curvature. This can be observed from the curve of the focused points in Figure 3.1. Secondly, there is spherical aberration. In a typical optical system design, the power of the entire lens is separated among different surfaces to reduce the aberration. The key intuition in optical design is that less curvature there is on the surface, there will be less insertion angle. With less insertion angle, there will be less 3rd order Siedel aberrations. So the typical technique to reduce aberrations is to introduce more surfaces. In the case of fluidic lens system shown in Figure 3.1, there is only one surface, thus limiting the options in aberration compensation.

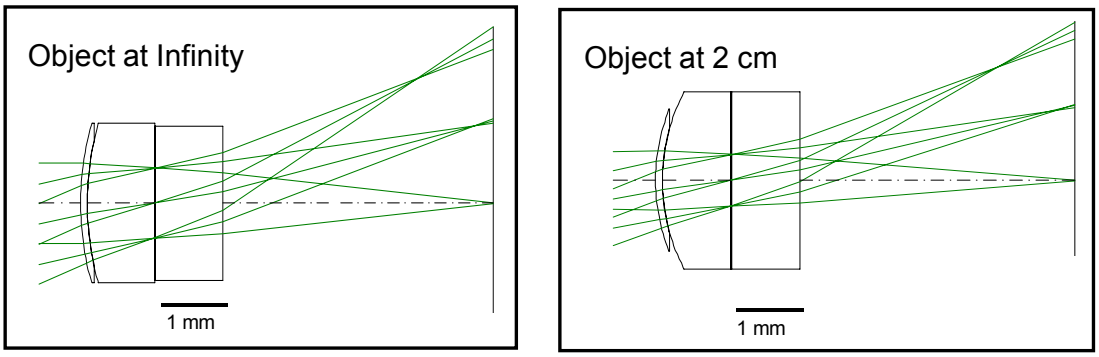

Figure 3.1 Lens view of single fluidic lens. (a) fluidic lens forming an image of an object at infinity; (b) single fluidic lens forming an image of the object at 2 cm distance from the fluidic lens.

Since the key concept if to have multiple surfaces, the logical question to ask is how we can introduce a technology that can compensate for the aberrations. This part of my thesis work involves introducing technology to greatly improve image quality for auto-focusing systems. We call this type of optics miniaturized unified imager.

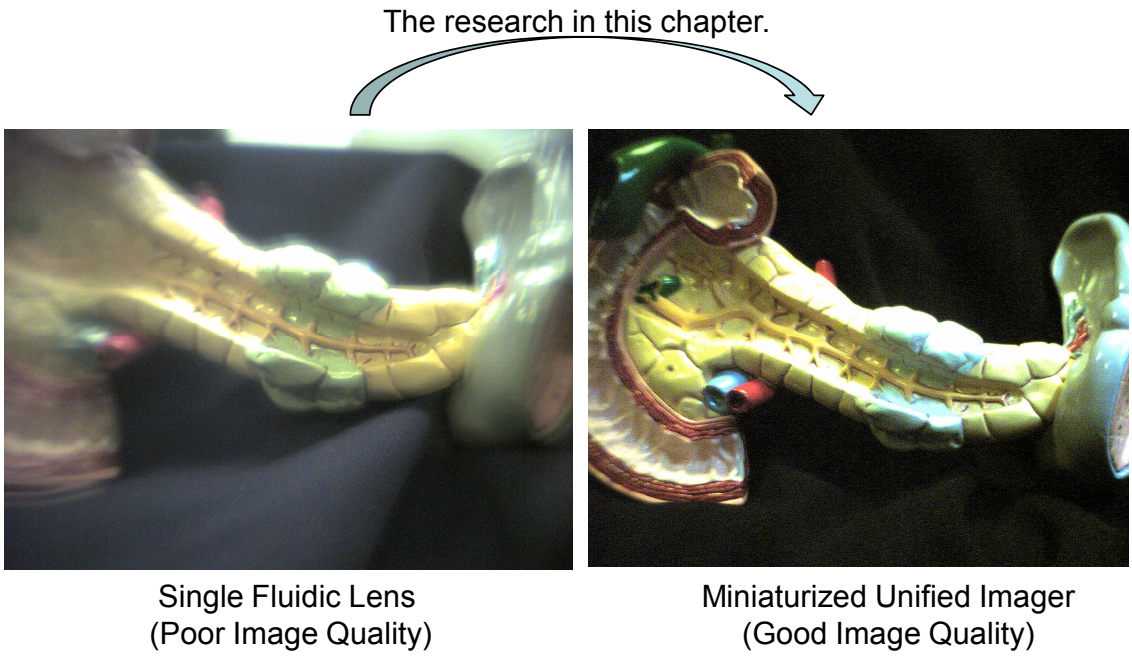

Figure 3.2 Image quality improvement by integrating fluidic lens and fixed lens.

3.2 Miniaturized unified imager design in Code V

By integrating fluidic lens with regular fixed glass/plastic lenses, a miniaturized unified imager with good imaging capability can be designed. The details of the fabrication for fluidic lens and the hardware integration results are documented in this section.

3.2.1 Optical system specification

The first thing to do before starting an optical design is to clarify the design goals. The optical system is described by imager size, total track, object distance etc. The image quality and aberrations are the parameters to optimize. The parameters that can be varied are the number of lenses and lens curvatures. The final goal is to

optimize image quality based on the mechanical limitations of the optical system. The target of the optical system that we are interested in designing is shown in Table 1. Since the target is to design a miniature camera, a sensor with an optical format of 1/4" is selected. To demonstrate the capability of the lens to change from camera mode to microscope mode, the system is zoomed and optimized with two different object distances: 20 mm and 3 meters. The speed of the lens is set at F/2.8.

Due to the mechanical structure of the fluidic lens, special consideration had to be made regarding the edge thickness of the fluidic lens. While the fluidic lens tune, or change curvature, the edge thickness has to be fixed. This is because physically, the membrane has to be fixed somewhere. A realistic edge thickness for the fluidic lens is 1.2 mm. This is usually easily controlled with an edge thickness solve in Code V. However, our design requires a zoomed system, and Code V occasionally corrupts the *.len* file when edge thickness solve is used in zoom systems (bug already reported.). So the work around method is to write a constraint in AUT.

The final design for this lens comprises 3 fixed lenses and 1 fluidic lens and is shown in Figure 2. The fluidic lens is attached in front of the fixed lens. In (a), the object is placed at 3 meter distance while in (b), the object is placed 2 cm away from the lens. The only difference between the two configurations is that the fluidic lens has different curvature. A thin membrane is on the fluidic lens to constrain the optical fluid. This is modeled in Code V, by having 2 surfaces very close and picking up the surface profile. This is why the lens view shows two surfaces very close to each other.

Table 3.1 Optical System Specification

Parameter	Criteria	Code V Command/Constraint
Basic System Parameters		
Full Field of View	30 degrees	Set Full Field to 15 degrees
Wavelength	Visible	656.3 nm, 587.6 nm, 486.1 nm
Optical Format	1/4"	AUT constraint: (Y W2 F4 SI Z1 R1 = 2)
Lens Speed	F/2.8	(SET FNO 2.8)
Mechanical System Parameters		
Object Distance	20mm~infinity	Zoom System. THI S0 3000 20
Back Working Distance	>1 mm	AUT Constraint: CT SI-1 > 1; ET SI-1>1
Curvature on Fixed Lenses	<0.4 >-0.4	AUT Constraint: CUY Sn >0.4 <-0.4
Edge Thickness for Fixed Lenses	>0.8 mm	AUT Constraint: MNE
Center Thickness of Fixed Lenses	>1 mm	AUT Constraint: MNT
Edge Thickness for Fluidic Lens	1.2 mm	AUT Constraint: (CT Sn Z1) - SAGF(n, 1, 0, 2) = 1.2;
Fluidic Lens Curvature Limitation	<0.33 >-0.33	AUT Constraint: CUY
Total Track of the Lens System	<12 mm	AUT Constraint: OAL S1..i < 12
Image Quality Criteria		
Distortion	<2%	Special constraint (shown in next page)
MTF @ 70 lp/mm	>0.3	
MTF @ 30 lp/mm	>0.5	

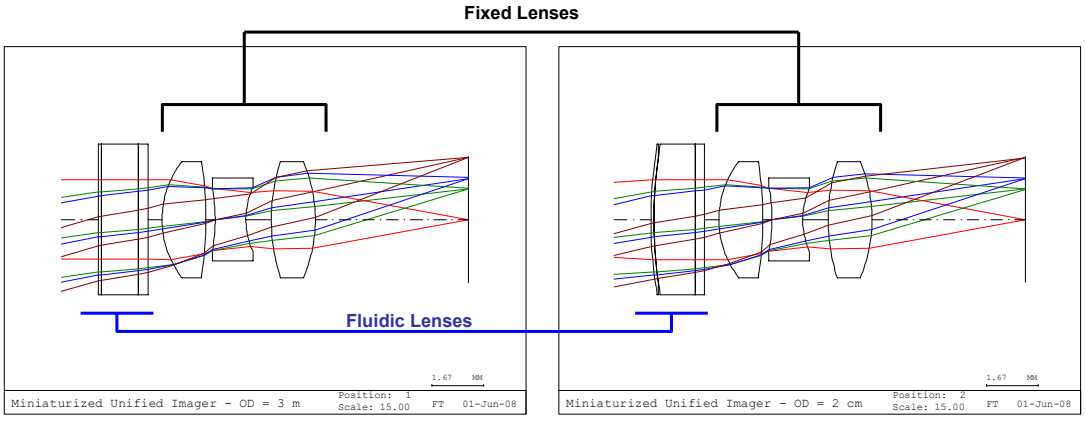

(a) (b)

Figure 3.3 Lens view of example miniaturized unified imager. (a) Object placed at 3 meter distance. (b) Object placed at 2 cm distance. The fluidic lens, first lens in both views, is the only lens that has changed over the different configurations. The fluidic lens has a membrane to constrain the fluid. This is shown as the double surface at the very front of the lens.

3.2.2 Design Procedure

The overall design procedure is to start with a fixed lens system. Optimize the system at a specific object distance. Then add in the fluidic lens and optimize for various distances. The process for designing such a system in Code-V is documented as follows:

3.2.2.1 Fixed lens system setup and preparation

1. A Cooke Triplet is first designed to the specification (1/4" format, 30 degrees full field-of-view)

2. Fields are defined as 1.0, 0.7, 0.5, and 0.0 field.

3. Wavelength is defined as 656.3 nm, 587.6 nm, 486.1 nm.

3.2.2.2 Global optimization with fluidic lens + fixed lens

4. A fluidic lens is added to the Cooke Triplet.

5. The entire system is zoomed into a multi-configuration system. Object distance is zoomed and set to 20 mm and 3000 mm. The curvature and the thickness of the fluidic lens are the only variables zoomed. The other variables are fixed lenses, and shouldn't be zoomed.

6. Since the edge thickness of the fluidic lens cannot change, the edge thickness has to be controlled. However, the ET solve in Code V becomes buggy in a zoomed system (already reported). Hence, it has to be controlled by an optimization constraint. The constraint is: "(CT Sn Z1) - SAGF(n,1,0,2)"

7. Distortion is also controlled by a constraint, "((HCY Si Z1 W2)-(Y Si F4 W2 R1 Z1))/(HCY Si Z1 W2)" This defines distortion from paraxial and real ray.

8. Mechanical constraints are also added.

9. Field is defined in object angle, so an extra constraint is added to control the chief ray of the largest field so that it will hit the 1/4” corner.

10. Global Optimization was run to find the right configuration: glass material, negative or positive power of the lens.

3.2.2.3 Design finalization

11. Glass is replaced by real glasses using the glass fitting macro.

12. Design is re-optimized.

13. Field is changed to real image height and re-optimized locally.

14. AS_BUILT is used for tolerance optimization. This is particularly important for fluidic lens because the conic constant of the fluidic lens is a variable depending on the fabrication situation.

3.2.3 Design performance analysis

Once the optical system is done with the design, the next step is to perform analysis on the image quality.

3.2.3.1 Modulation Transfer Function (MTF)

There are 2 often used methods to characterize image quality: RMS spot size or MTF function. The MTF function provides a more accurate modeling of image quality because it takes into account the effect of the entire point-spread-function (PSF).

In the off-axis image quality analysis of MTF contains tangential and saggital plane modulation function. The difference is due to coma and astigmatism.

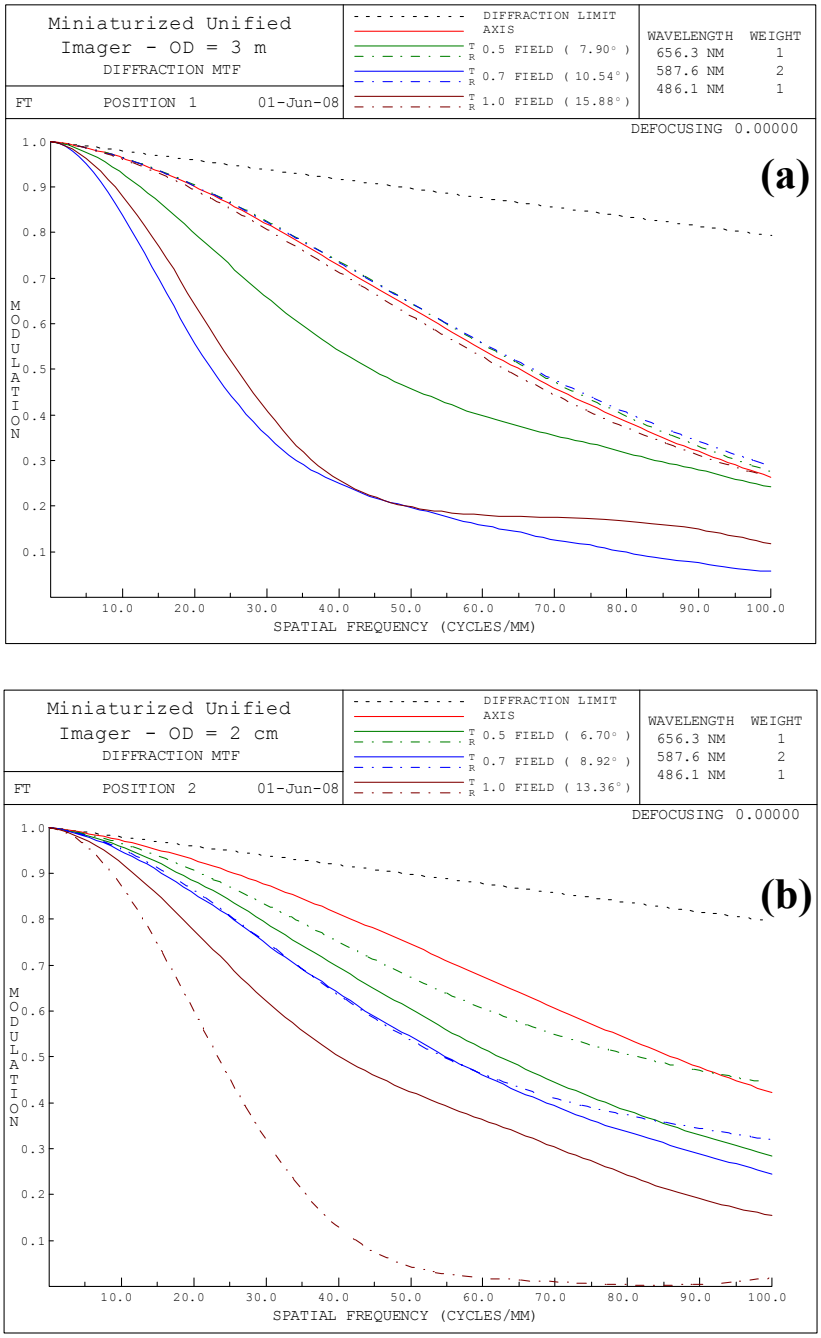

Figure 3.4 Poly-chromatic MTF considering C-d-F (656.3 - 587.6 - 486.1 nm). (a) Object Distance at 3 meters; (b) Object Distance at 2 cm.

3.2.3.2 Field curvature & distortion

Field curvature is an analysis method to understand the source of aberration. In both cases, the field curvature and distortion are relatively small.

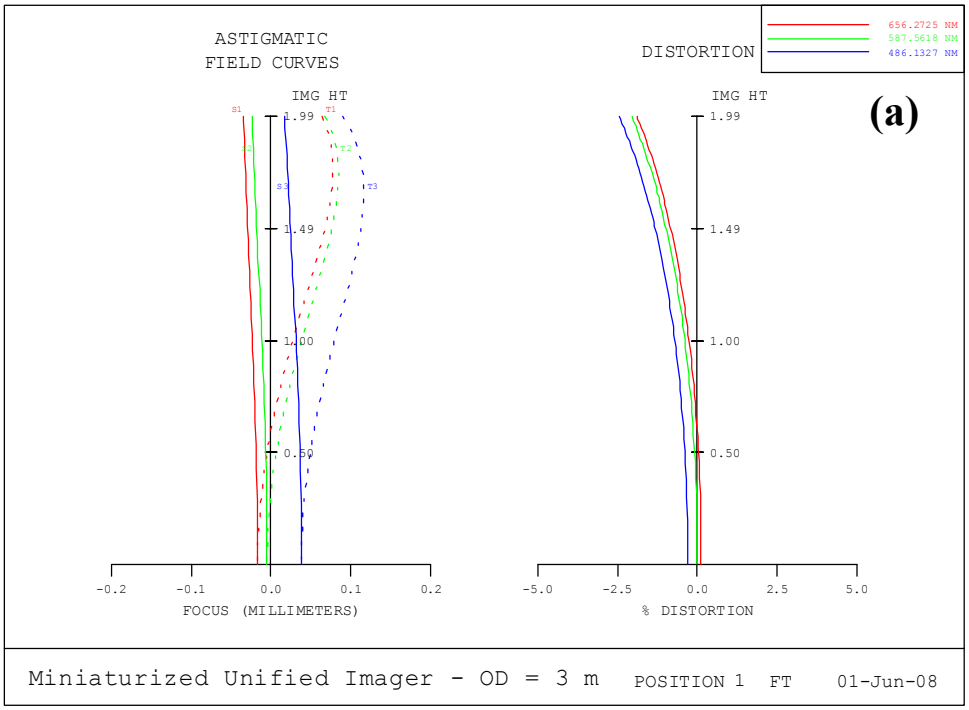

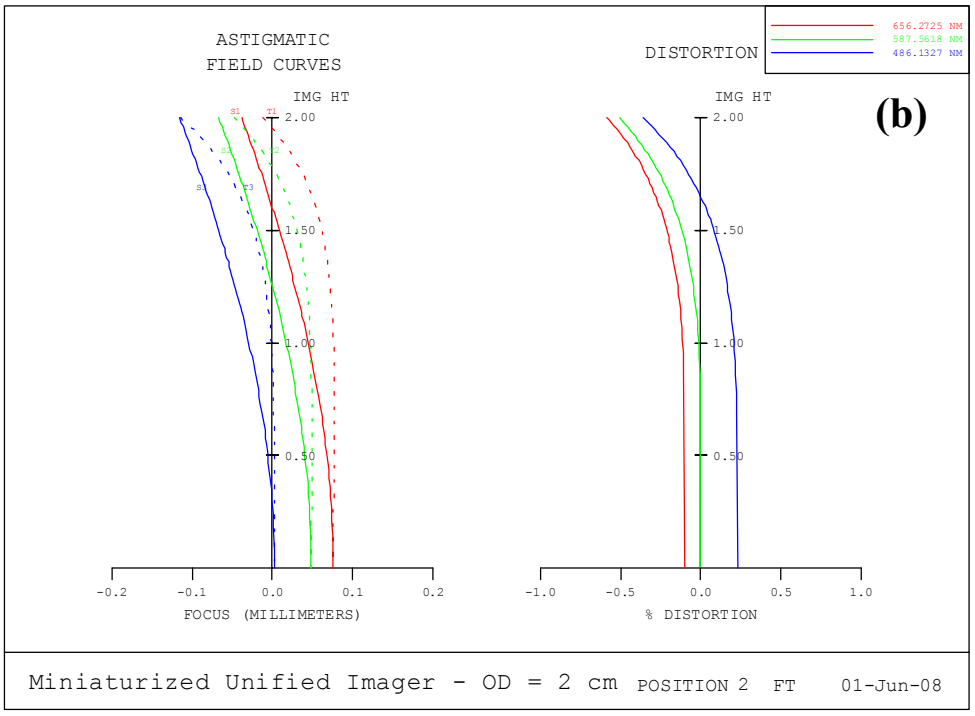

Figure 3.5 Field Curvature results for: (a) Object Distance at 3 m; (b) Object distance at 2 cm.

3.2.3.3 Image simulation

To show the auto-focusing capability of this imager, a high resolution image of a flower is used. Then, image is placed at different object distances, 15 cm and 5 cm, from the camera while the curvature of the fluidic lens is the only parameter changed. This simulates the tuning capability of the camera. The simulation scheme is shown in Figure 3.6 while the simulated images and simulation conditions are shown in Figures 3.7 and 3.8.

The distortion was estimated to be small, and can be seen from the images to be less than 5%.

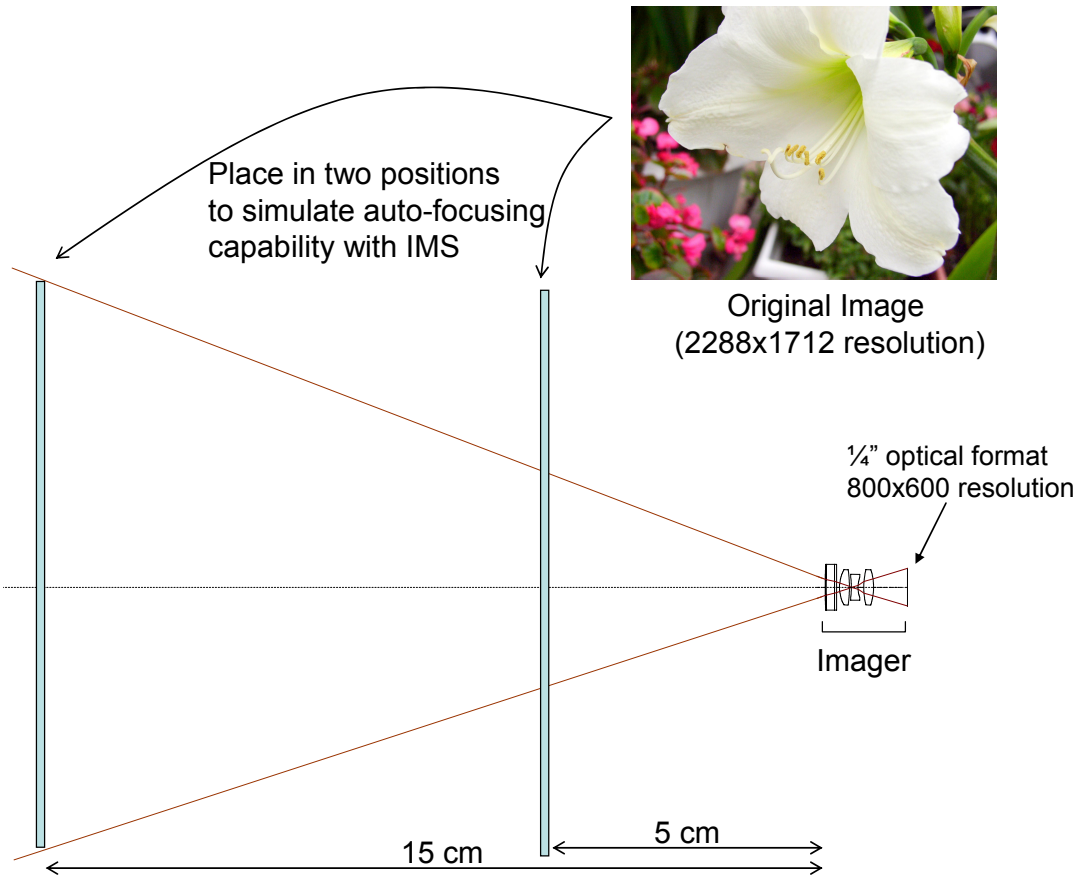

Figure 3.6 Image simulation method in Code-V to demonstrate image quality: place a high quality image in 2 different positions to simulate auto-focusing capability of the fluidic lens.

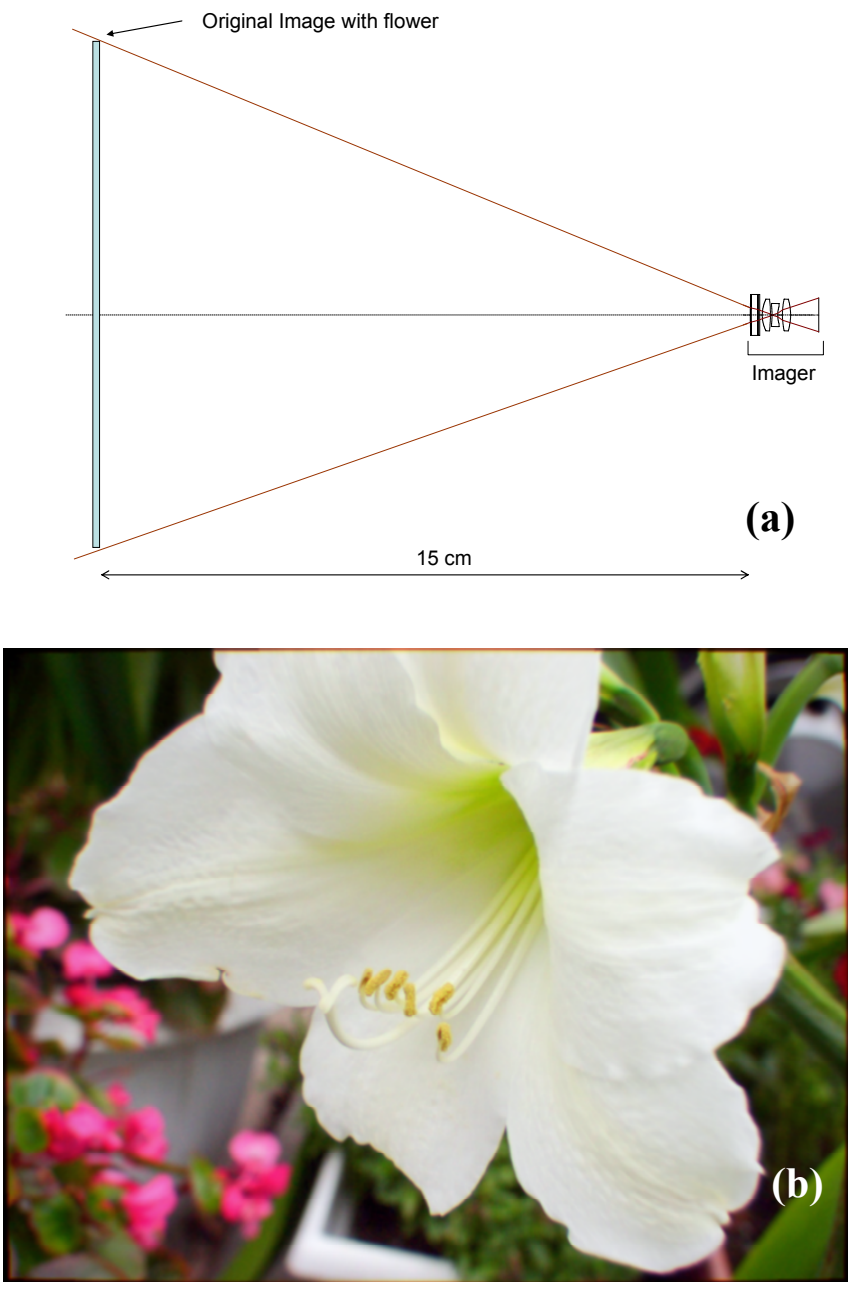

Figure 3.7 Simulated Image. (a) simulation condition (15 cm); (b) simulated image (800x600 resolution). We cannot see the pollen clearly in this image.

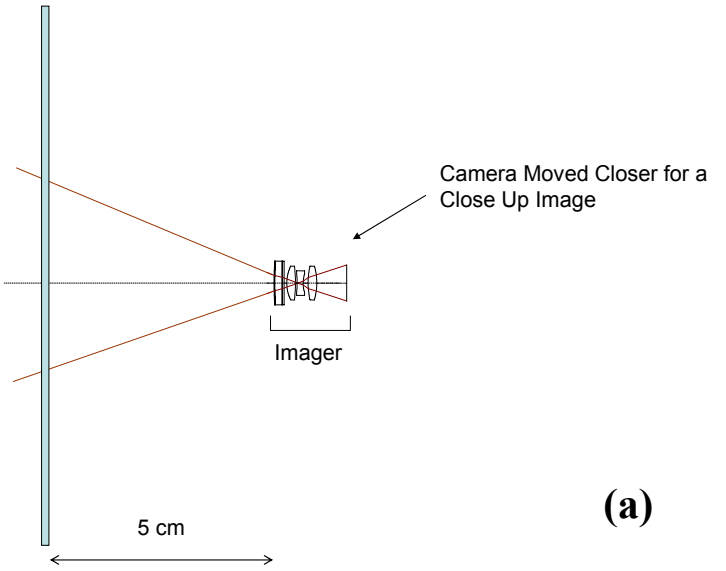

Figure 3.8 Simulated Image. (a) Simulation condition (5 cm); (b) simulated Image (800x600 resolution). With the camera close up, the pollen can now be seen.

3.3 DEMONSTRATION WITH REAL HARDWARE

To demonstrate the image quality of the miniaturized unified imager in hardware, we need to first build a fluidic lens, then integrate the fluidic lens with fixed lens and take various pictures. The process is documented as follows:

3.3.1 Fabrication of fluidic lens with PZT actuator

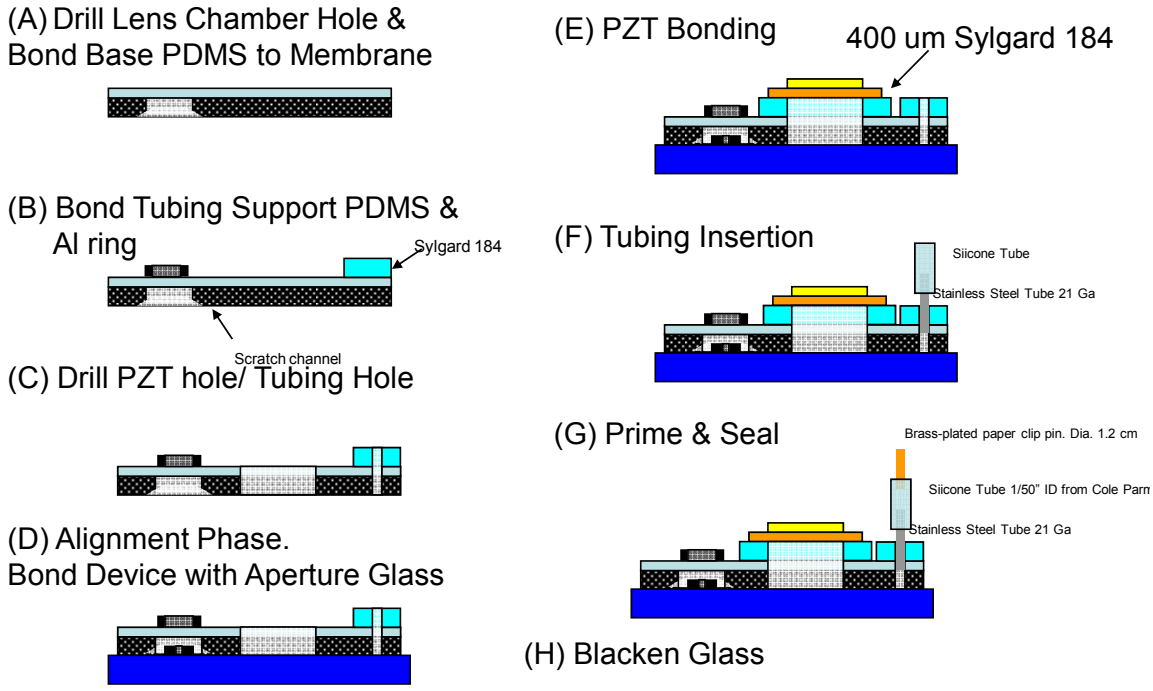

Figure 3.9 Overall procedure for fabricating a fluidic lens with PZT actuator.

A fluidic lens with a flexible membrane and a rigid glass surface to support a convex(concave)-plano lens is fabricated first. The lens chamber and the connecting fluidic channels are lithographically patterned on a silicon wafer with spin-coated Microchem SU-8 photoresist. This silicon wafer is used as a mold after hard bake and coating with Chlorotrimethylsilane. Sylgard 170, a black Polydimethylsiloxane (PDMS)

from Dow Corning, is mixed and poured onto the mold. After heat curing of the PDMS, it is demolded and diced to device size. A circular hole is punched through the PDMS to form the lens chamber. Since Sylgard 170 is opaque, stray light is effectively blocked. To make the lens membrane, transparent PDMS (Gelest 1.41) is spun onto another silicon wafer at 900 rpm to create a 120 μm thick membrane. This membrane is bonded to the top of the black PDMS, as shown in (A) of Figure 3.9. To define the clear aperture (4 mm) of the lens, a carefully machined anodized aluminum ring with an inner diameter of 4 mm is bonded to the membrane above the lens chamber, as shown in Figure 3.9 (B). Notice that on the far right, a thick PDMS block is bonded onto the module for holding the insertion tubing. The original thickness of the black PDMS is typically 1~2 mm; therefore, it is not strong enough to hold tubing. Black PDMS is also much stiffer, making it an unideal material for holding tubing in place. By switching to clear Sylgard PDMS, the elasticity of the material is better, and sealing is improved.

Once the bonding is done, a hole is punched through the entire PDMS holding module to allow bonding of the PZT actuator, as shown in Figure 3.9 (C).

The final step that has to do with optical path is bonding a glass with an optical aperture of approximately 1 mm diameter to the module with membrane. This is a critical alignment step. The detail of how this alignment was done is documented in later sections. The result of this step is shown in Figure 3.9 (D).

The ensuing step, Figure 3.9 (E), is the bonding of PZT actuator to the rest of the module. PZT bonds to Sylgard 184. It also bonds to Gelest. However, because the mechanical property of black PDMS is so stiff and because Gelest is so thing (~100 um),

the PZT doesn't bond stably without an extra layer of Sylgard 184. This layer of Sylgard is made to be very thing to avoid waste of optical fluid material. To ensure good bonding, one can add an adhesion layer of oxide on the PZT as discussed in Chapter 2. However, during the development of this device, we didn't use the oxide adhesion layer.

The final steps include insertion of tubing, vacuum filling and sealing. The details of vacuum filling is already documented in Chapter 2. The device is filled with optical fluid (SL5267, SantoLight), which has index of refraction of 1.67. All materials are carefully selected such that they are compatible with the fluid. Incompatible material could cause early browning of the fluid or etching of the material.

All of the bonding process involving PDMS material is performed with UV/ozone surface activation by placing the PDMS in an UV/ozone cleaner. The process proves to be universally applicable to all materials involved in this work. Finally, the device is filled with optical fluid (index of refraction: 1.67).

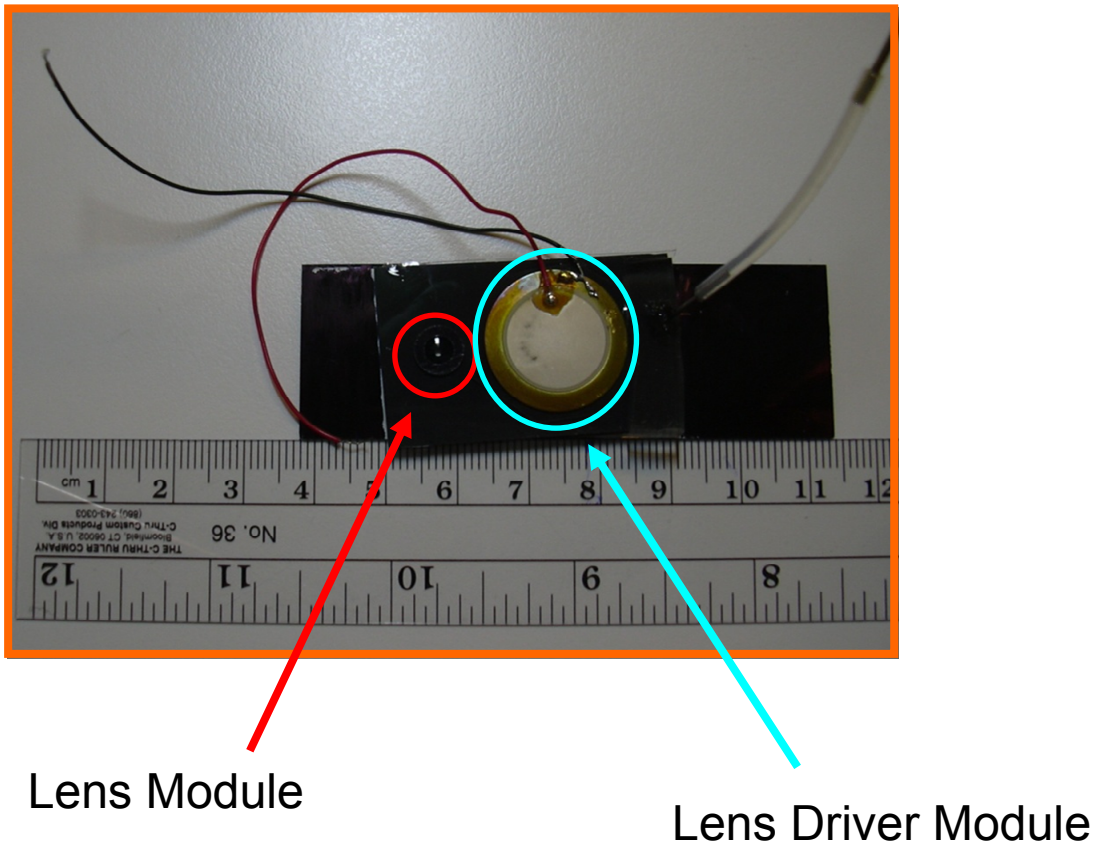

Figure 3.10 Image of fluidic lens device.

3.3.3 Integration of fluidic lens with fixed lens and testing

The fluidic lens is then attached to the aforementioned fixed lens module and a 2 million pixel CMOS (complementary metal oxide semiconductor) image sensor. The pixel size of this sensor is 3.18 μm x 3.18 μm. The fluidic lens is used to change the effective focal length (EFL) of the optical system while the physical spacing between lenses is kept constant. A tuning range as wide as 200 diopters has been demonstrated in our device, thus enabling operation of the device in a full range of camera modes:

normal mode, macro mode, super-macro mode and microscope mode. The entire size of the optical system is about 1 cm^3, with a total track length of about 12.5 mm.

3.3.4 Experimental results

3.3.4.1 Tuning capability demonstrations

Figure 3.11 (a) and (b) show the photographs for objects at 15 meters away and as close as 1 cm away. This is, to our best knowledge, the widest focusing range that has even been achieved with a single camera. The camera's capability of revealing details of an object invisible to human eyes is demonstrated in Figure 3.12 and Figure 3.13. As we move the object (i.e. UCSD emblem) from 14 cm to 1 cm, we can observe the detailed texture of the object in high resolution. In Figure 3.13, we demonstrate that the half-tone of Microsoft mark can be seen when viewed close up.

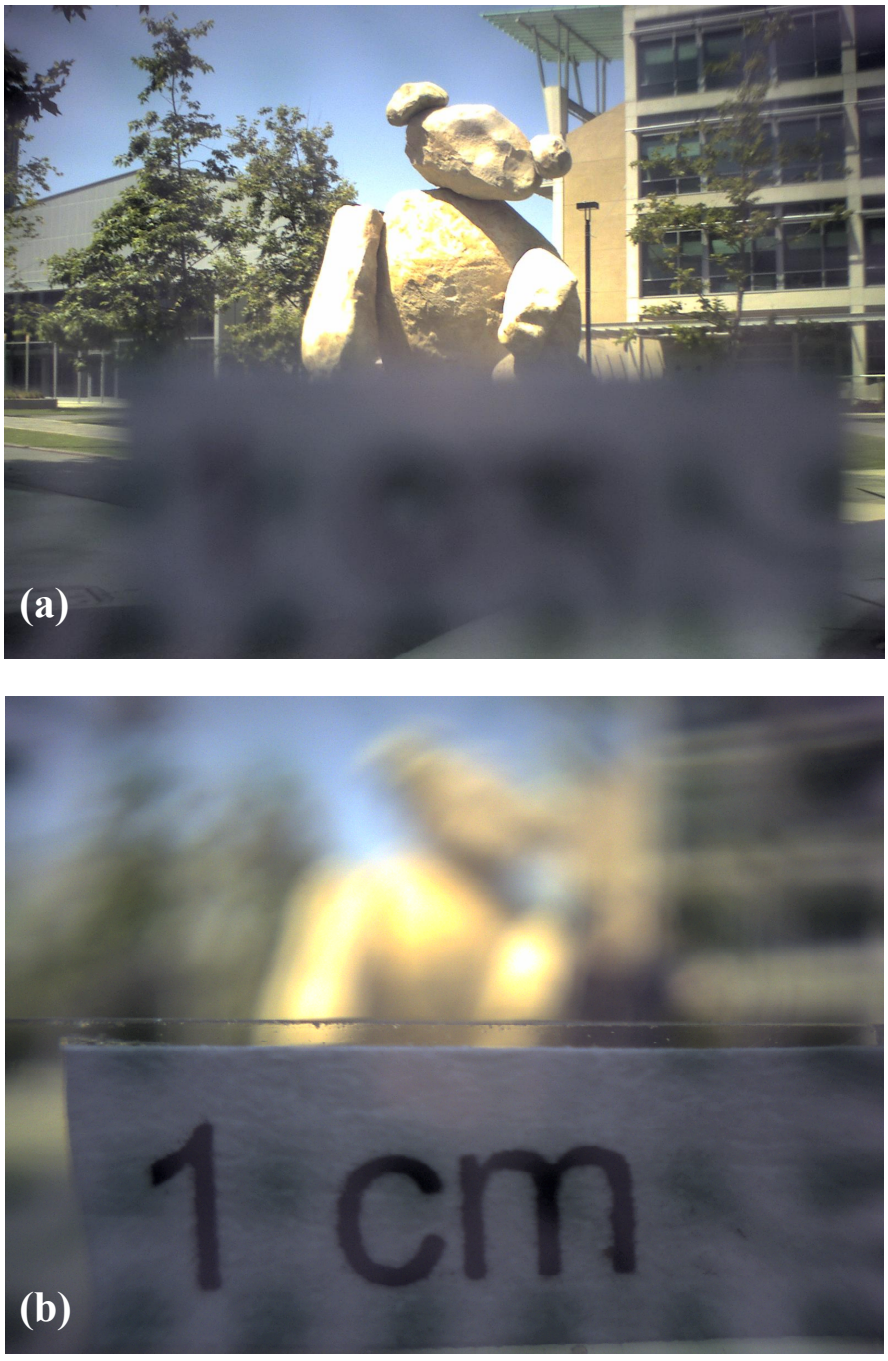

Figure 3.11 (a) Image of a stone bear in UCSD. This stone bear is 15 meters away from the camera. (b) The focus of the fluidic lens is changed to focus on a piece of paper placed 1 cm away from the lens.

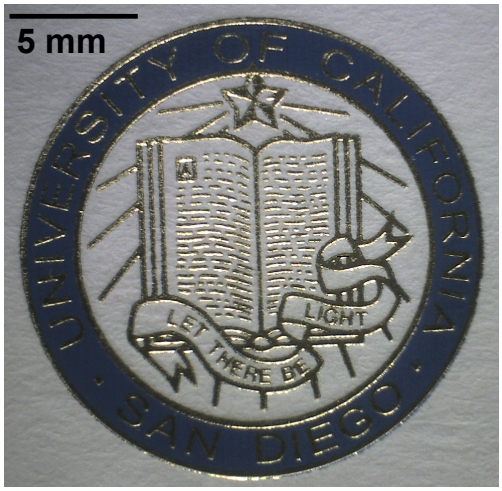

(a) Object distance 14 cm

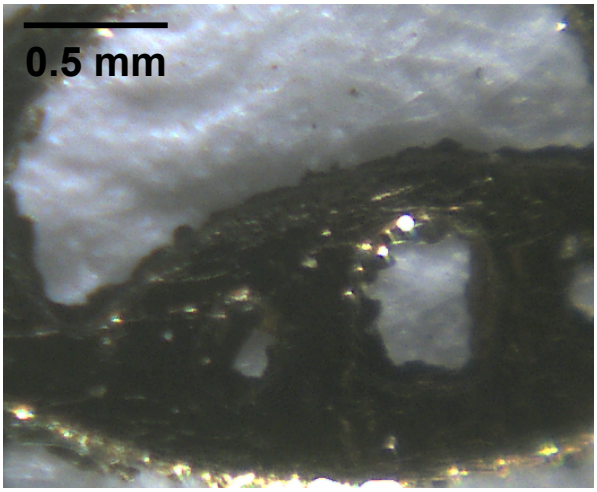

(b) Object distance 1 cm

Figure 3.12 Demonstration of macro-mode and supermacro-mode. (a) UCSD Emblem on a business card. This picture is taken when the card is placed at 14 cm away from the imaging system. (b) The business card is moved towards the imaging device to a distance of about 1 cm. By tuning the focal length of the fluidic lens, we can see the fine texture of the paper.

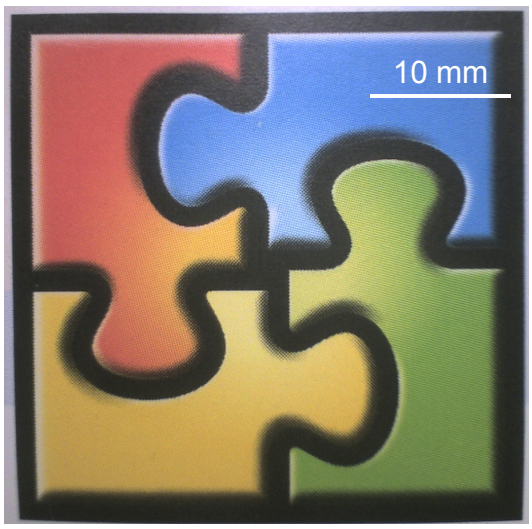

(a) Object Distance 14 cm

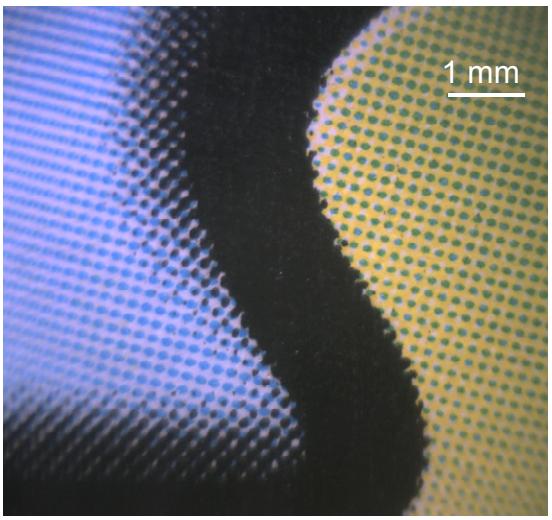

(b) Object Distance 1 cm

Figure 3.13 Demonstration of super macro function of the imager by resolving the print of a Microsoft Office trademark. (a) Picture with the object being 14 cm from the imaging system. (b) Picture with the object being 1 cm from the imaging system. The fine half-toning pattern on the trademark can be clearly resolved.

3.3.4.2 Microscope Function Analysis

One significant feature of the miniaturized unified imager is its capability to see objects very close and turn into a microscope. To scientifically measure the quality of the image, we placed Edmund Optics USAF target in front of the fluidic lens and tuned it to be in focus. This is the way to measure the resolution of the features. In this experiment, we demonstrate that the miniaturized unified imager has less than 3 um resolution.

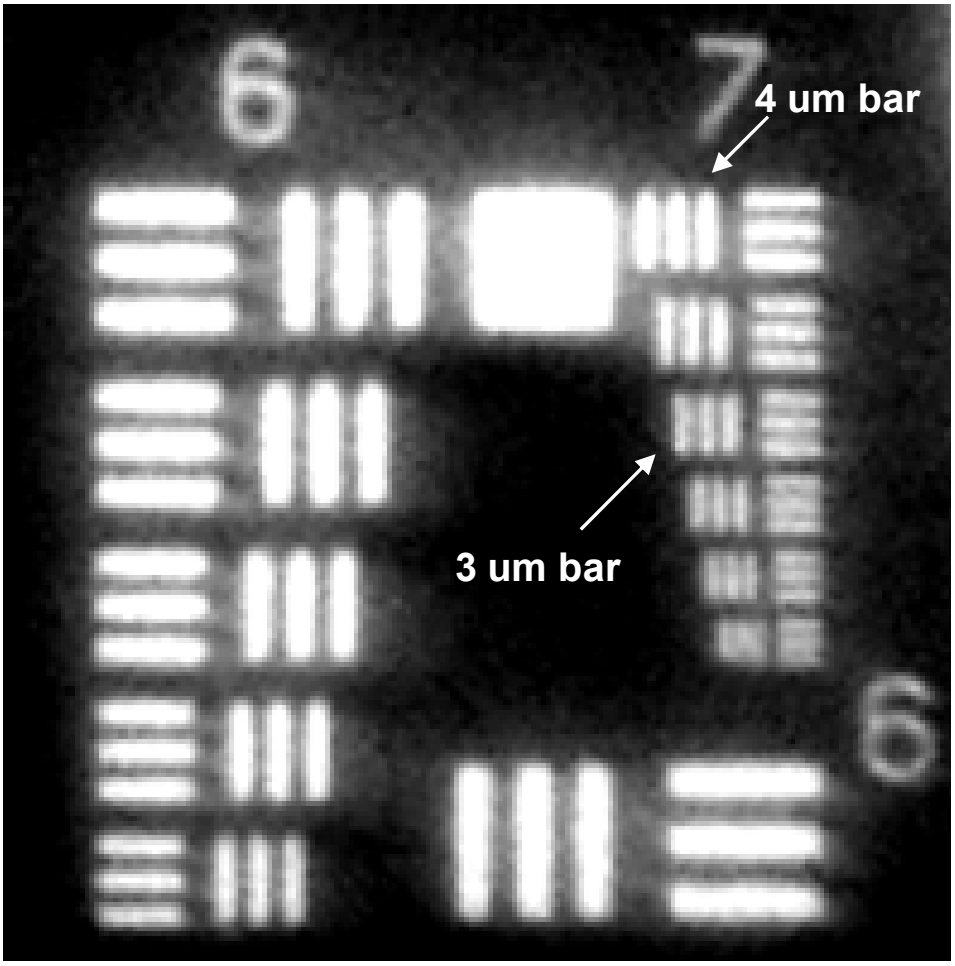

Figure 3.14 The same Edmund Optics USAF target taken with our universal imaging device. Features as small as 3 μm can be resolved from our device.

3.3.4.3 Bio-photonic Applications

Having quantified the resolution limit, the next step is to demonstrate the function of the microscope with different biological samples. The first sample that we acquired is mouse heart tissue sample from Dr. Ian Lien, UCSD Bioengineering Department. Part of his research is on the study of cardiovascular disease. He selected

mouse as a sample because the genes for mouse is similar to genes for human. Therefore, he can perform knockout genes to study possible cardiovascular disease. From his work, he can study histology, which involves structure integrity, and pathology, which involves disease, hypertrophy, etc.

The slide is prepared by cryo-section technique: that is to freeze the heart sample and then cut with a sharp blade. The thickness of each slide is around 8 um. The section shown in Figure 3.15 is the left ventricle, which is the largest chamber used to pump blood out.

In Figure 3.15, we are able to see muscle fiber and muscle cells. The orientation of the muscle fiber can also be identified, which is very important since it determines how the muscles contract and how blood is pumped out. Dr. Ian Lien was able to identify with our image that the heart of this particular mouse is healthy since there are no atrophy or hypertrophy.

As a quick note, the holes between the cardiac muscles are artifacts for sectioning. During the freezing and cutting procedure, some pieces shrink and fold.

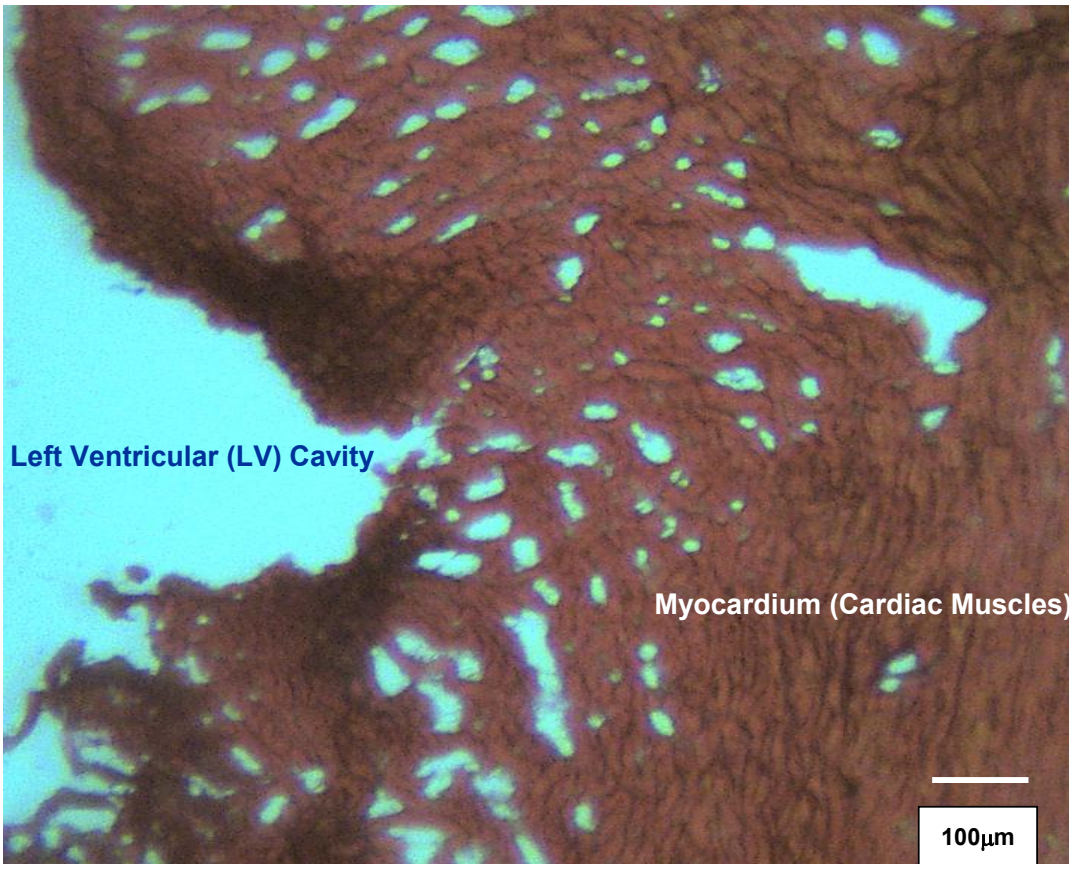

Figure 3.15 Mouse heart taken with the universal imager under microscope mode. The mouse heart sample was first frozen and then sliced to 100 um thickness with a slicing machine. The red part on the right are the cardiac muscles, and the orientation of the fibers can be seen on the image. This orientation shows the direction of movement for the heart muscles.

3.4 Conclusion

In this chapter, we discuss how to integrate one fluidic lens in to the optical system. The fabrication of a fluidic lens integrated with a miniature actuator such as the PZT.

With fluidic lens, I demonstrated a good image quality miniaturized unified imager with wide tuning range. This camera can operate as a regular camera, micro-mode, and as a microscope. This is not possible with a traditional regular optical device.

This chapter or portion thereof has been published in ***Optics Letters*, Vol 33, Iss. 3, pp. 291-293 (2009)**.

Chapter 4

Bio-inspired fluidic zoom lens for minimally invasive surgery

4.1 Introduction to minimally invasive surgery

Classically, surgical access to the abdominal cavity has been accomplished through large incisions through the abdominal wall. Such "open" procedures allow direct visualization and manipulation of the abdominal organs, but produce considerable postoperative pain and significant scars. In contrast, minimally invasive surgery (MIS)

requires much smaller incisions (~1cm or less) [1], resulting in less pain [2], faster recovery times [3], fewer wound infections [4], and minimal scarring. Also known as laparoscopic surgery, the critical technology enabling MIS is the video laparoscope, a long (30-45cm), thin (5-15 mm diameter) rigid cylinder containing rod lenses, coupled proximally to a video camera. It acquires real-time images from inside the abdomen for display on operating room monitors, obviating the need for large incisions to visualize the abdominal contents.

A typical laparoscopic surgery is performed using 3-5 small "keyhole" incisions through which plastic sheaths called trocars are inserted, creating transabdominal ports for the laparoscope and surgical instrumentation, as shown in Figures 4.1(a) and 4.1(b). The abdomen is then insufflated with CO2 gas, causing the abdominal wall to balloon outward, exposing the underlying abdominal organs to the laparoscope, as seen in Figure 4.1(b). Under laparoscopic visualization, surgeons introduce long, thin tools through the ports and into the gas filled intraabdominal space to carry out the operation. Commonly performed laparoscopic procedures include cholecystectomy (gallbladder removal), hernia repair, appendectomy (appendix removal), colectomy (large bowel excision), nephrectomy (kidney removal), and bariatric (weight loss) procedures.

Recent innovations in MIS minimize the total number of skin incisions required during a procedure. Cholecystectomy and appendectomy have both been performed using just a single incision, through which the laparoscope and surgical instruments simultaneously access the abdominal cavity [5, 6]. Another important advancement in MIS is natural orifice surgery, in which access to the abdomen cavity occurs through the

wall of either the stomach (via the mouth), the vagina, or the colon (via the anus). This potentially eliminates the need for any external incisions. To date, transvaginal appendectomy, transvaginal cholecystectomy, and transgastric appendectomy have been *partially* successfully performed. [7]

Current video laparoscopes are not ideal for several reasons. First, they lack optical zoom; therefore continuous manual operation to obtain desired views is required. "Zoom" is simulated by moving the device towards or away from the point of interest. This generally necessitates a second individual to operate the laparoscope so that the surgeon can use both hands for surgical instruments. Furthermore, laparoscopes also lack the capability to perform autofocus; therefore, they are designed to have very long depth-of-focus, and strong illumination (~20,000 lux) is required. The strong illumination is provided from an external light source, and delivered to the laparoscope through a bulky optical bundle. Challenges faced during single incision and natural orifice surgery demonstrate limitations of current video laparoscopes [8]. In both, the laparoscope and instruments share a single, crowded access site. The limited space results in physical and visual interference between the laparoscope and instruments inside the body, and interference between camera operator and surgeon outside the body.

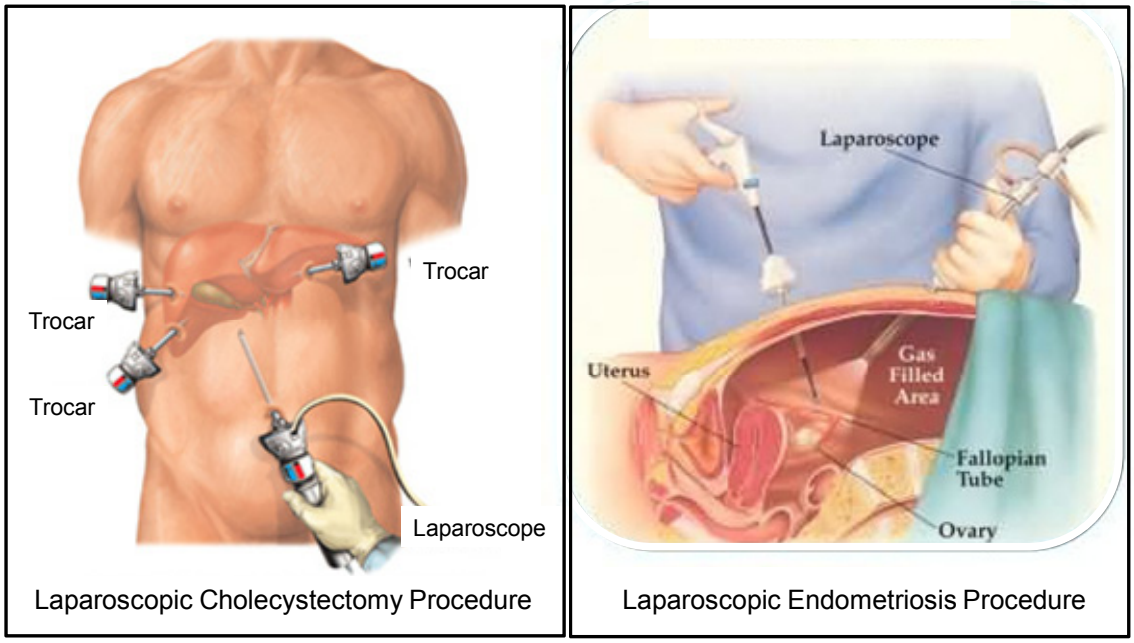

Figure 4.1 Laparoscopic surgery. Transabdominal ports are established by insertion of trocars through small skin incisions. Insufflation of the abdominal cavity with CO2 creates an operative space and provides exposure of the abdominal organs by lifting the anterior abdominal wall. The laparoscope and surgical instruments are then introduced into the abdominal cavity through the trocars. [9, 10]

Improving the feasibility of cutting-edge MIS procedures demands a new approach to the vision system. We propose that the ideal vision system is one that can be mounted onto the internal surface of the abdominal wall, has optical zoom and autofocus capability, and does not require strong external lighting. A conceptual drawing of such a technology is shown in Figure 2. In order to be passed into the abdomen for mounting, the camera must be small enough to pass through a small incision. Zoom capability is essential since surgeons need the ability to see wide views of organs to provide spatial orientation and anatomical context, as well as close up

views when operating on the tiny substructures of organs. An advanced surgical camera as shown in Figure 4.2 is still difficult to design with traditional optical lens technology. However, our bio-inspired fluidic lens is perfect for this application.

Utilizing bio-inspired fluidic lens, we designed a small camera with 17 mm total track and 4 mm diameter clear aperture, making it suitable to be insert through a small incision. Even with its small size, this camera can achieve more than 4X optical zoom. With optical zoom, the miniaturized bio-inspired laparoscopic zoom camera can be mounted onto the abdominal wall during a surgical operation, as shown in Figure 2. The camera can also operate in very low light conditions (~1,500 lux), which eliminate the need for strong external lighting. Overall, with bio-inspired fluidic lens, we were able to design a powerful camera system that meets the criteria to advance MIS technology.

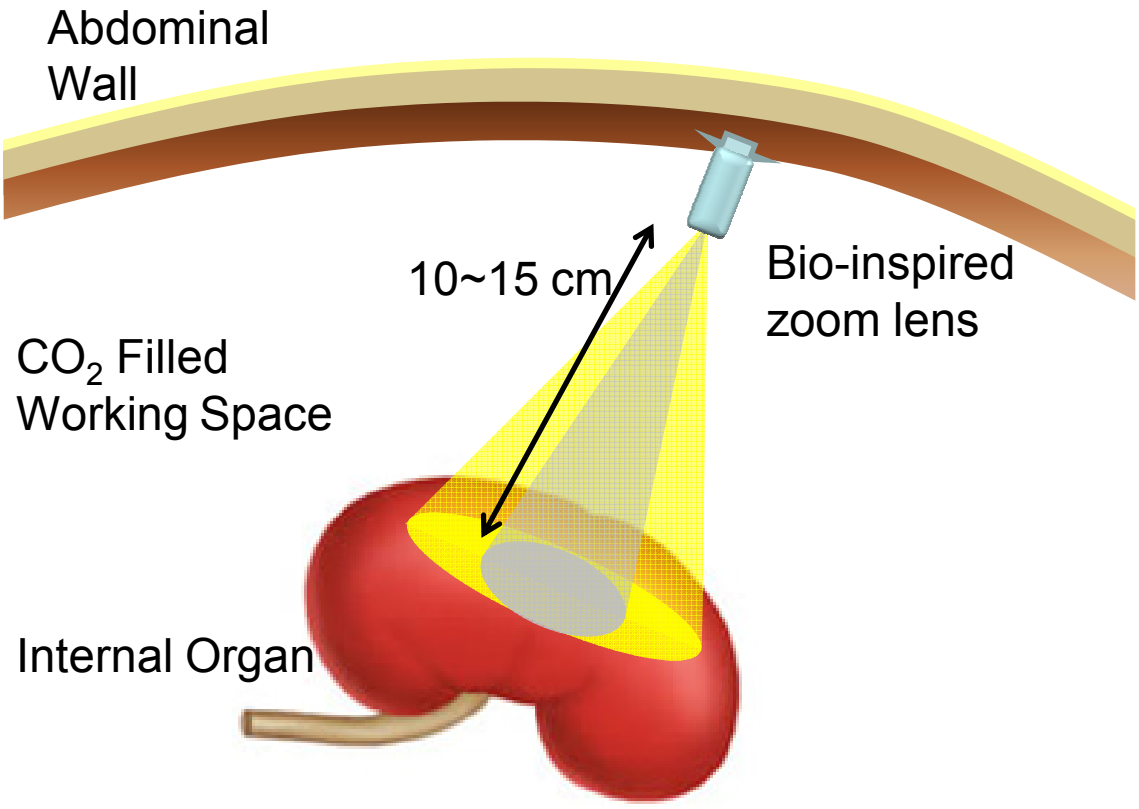

Figure 4.2 Conceptual idea for the operation of advanced laparoscopic camera for MIS. The adnominal cavity is filled with CO2 gas, creating a 10~15 cm working distance. The laparoscopic camera needs to have optical zoom and need to be able to view in low light condition to eliminate the need for strong external lighting.

4.2 Optical Zoom Lens Design Theory

In an optical system, the effective focal length (EFL) and the image sensor format (e.g. optical format) determine the field-of-view. The change in field-of-view creates the optical zoom effect. Since the optical format of an optical system cannot change, EFL is the parameter to control to change zoom. In order to achieve continuous zoom, a zoom system usually need at least 2 lenses, or sets of aberration controlled

lenses, to control the EFL and the back focal length (BFL). The BFL determines the distance between the image plane and the optical lenses. Controlling BFL ensures that the image stays in focus. The factors contributing to the EFL and the BFL of a 2 lens optical system are shown in the following equations:

$$EFL = \frac{f_1 f_2}{f_1 + f_2 - d} \tag{4.1}$$

$$BFL = \frac{EFL \cdot (f_1 - d)}{f_1} \tag{4.2}$$

where f_1 and f_2 are the focal length of the respective lenses and d is the distance between the lenses. Basically, *EFL* and *BFL* are being controlled through the focal length of individual lenses and the distance between them.

In an optical system built with traditional optical lenses, the only parameter that is tunable is the distance between the lenses and the sensor, which are the parameters d and *BFL*. The movement of the lenses are mounted and moved by a specially designed CAM module where the nonlinear motion of d and *BFL* precisely controlled. The precise nonlinear control of the lens positioning also makes the optical design phase much more challenging since multiple points have to be analyzed and simulated during design phase.

If the optical system is designed with bio-inspired fluidic lens, the tunable parameters are now the curvatures of the 2 lenses. With 2 varying parameters, it is sufficient to tune *EFL* and maintain *BFL*. There is no need to change between the lenses. This eliminates the need for a delicately designed mechanical module to control the location of the lenses. [11]

4.3 Designing Basic Fluidic Zoom Lens

The design of a fluidic zoom lens involves optical simulation through ray tracing software. First, two lenses are set up in the lens design, then the system is optimized by using default merit function to control spot size and by setting the mechanical and optical function constraints. Instead of trying to optimize for all fields, only the on-axis field is optimized to get the highest image quality. The reason is because there are no extra lenses to compromise for the image quality.

4.3.1 ZEMAX Design of Zoom Lens

To demonstrate that a zoom lens is feasible with 2 bio-inspired fluidic lens, such a system was designed and simulated in ZEMAX. The ray tracing and performance analysis result are shown in Figures 4.3 and 4.4, respectively. Due to the large tuning range of the fluidic lens, the total track of the zoom lens can be made to be very short at 17 mm and still have 4X optical zoom. The wide tuning range of the back lens allows for a real-time zooming and auto-focusing algorithm to take place.

A closer look at Figure 4.3, one can observe that the bio-inspired fluidic lens optical system is switching between 2 different optical configurations when zooming in and zooming out. When zoomed in, Figure 4.3 (a), the front lens is functioning as a convex lens and the back lens is working as a concave lens. This is the telephoto configuration which has short total track length and long EFL. This type of configuration is widely used in telescopes. Conversely, when zoomed out, Figure 4.3 (b), the front lens is now a concave front lens and a convex back lens can be created.

This is a reversed-telephoto system which is a longer system with shorter EFL. This type of configuration is widely used in fish-eye lenses, such as the lens on doors. The configuration changing capability of the bio-inspired fluidic lens allows for large zooming ratio even when the module has such a short total track.

To analyze the performance of the image quality, polychromatic diffraction modulation transfer function (MTF) of each configuration is simulated and is shown in Figure 4.4 (a) and (b). This MTF curve considers wavelengths most often considered C-d-F (656.3-578.6-486.1 nm) for visible wavelengths. The performance of the optical system is quantified with the CMOS sensor in mind. The target CMOS sensor is 1/3" optical sensor with a pixel size of 3.18 um x 3.18 um. The result shows that image quality is sufficient for a 1/3" optical format sensor.

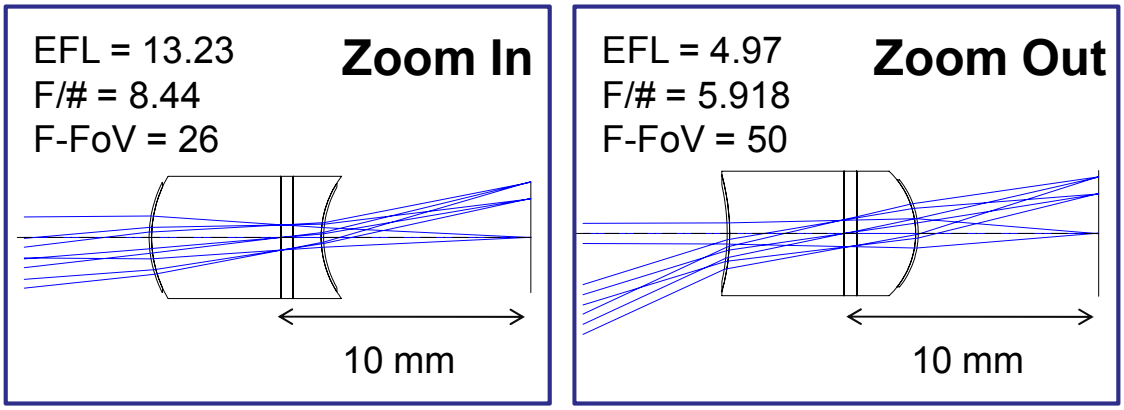

Figure 4.3 Two fluidic lenses are sufficient to create optical zoom. By tuning the curvature of the front and back lens, the optical system can switch between a telephoto system (a) and a reverse-telephoto system (a). The configuration changing capability allows for large zoom ratio with short total track. The effective focal length (EFL) and the diagonal full field of view (FFoV) are shown on the upper left of the lens plot.

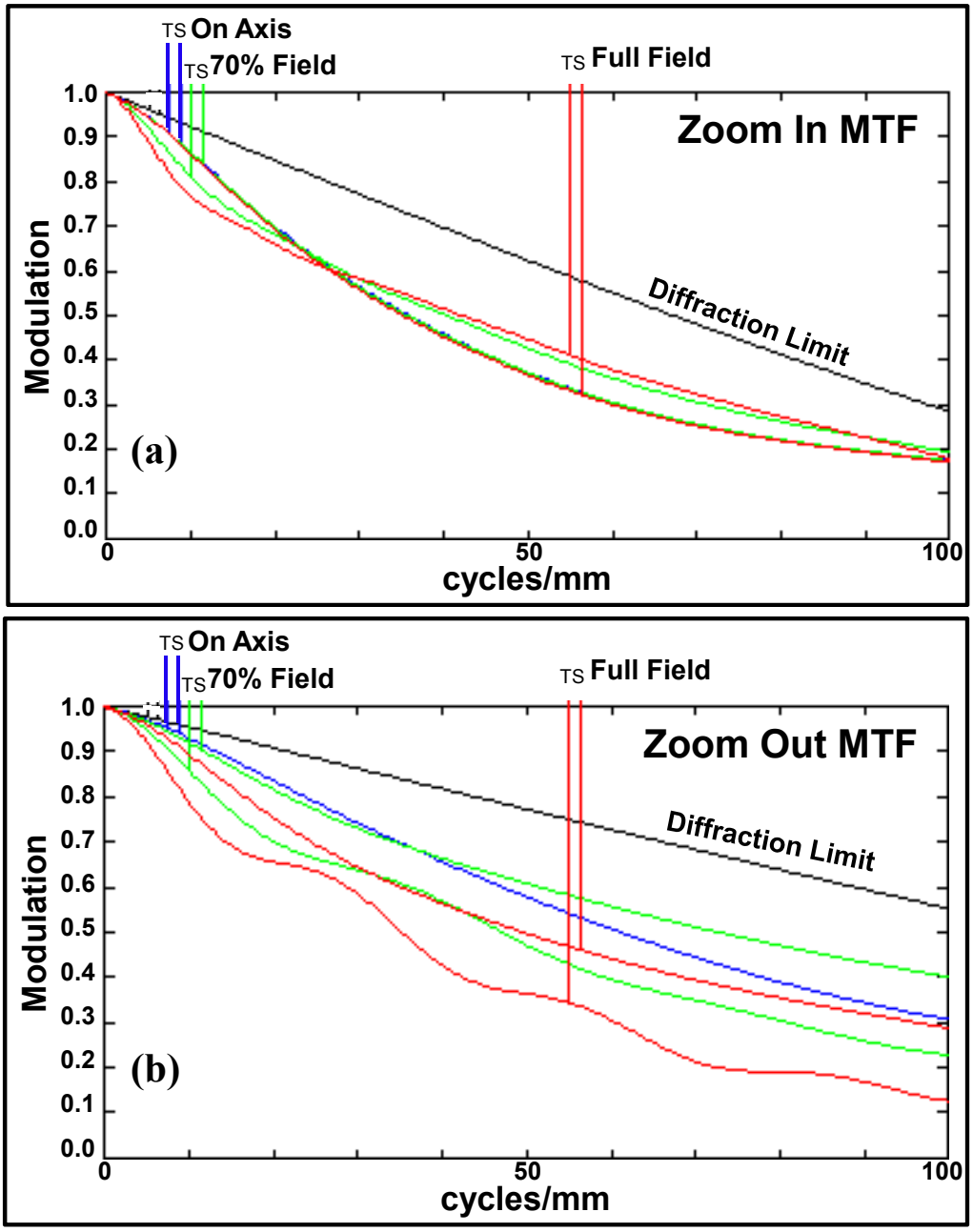

Figure 4.4 The performance of the optical system is characterized by the polychromatic diffraction MTF plots considering C-d-F (656.3-578.6-486.1 nm) wavelengths for miniaturized fluidic zoom lens. The object distance is 12 cm. The MTF of on-axis field, 70% field and full field are shown. The tangential and sagittal MTF for each field are

also shown and labeled with ‘T’ and ‘S’. (a) MTF for Zoom-in, corresponding to the configuration in Figure 3(a); and (b) MTF for Zoom-out, corresponding to the configuration in Figure 4(b).

4.3.2 FABRICATION ISSUES

After the design of the ZEMAX, we machined the parts in hardware. To ensure matching of the material properties, we used Delrin as the lens body. The first design was based on the best possible image quality under 3 different zoom conditions, zoomed out, middle zoom, and zoomed in. During optimization, only the center portion is optimized. This is because with only 2 lenses, there is no way to control the aberration off-axis.

Fabrication of the device involves SolidWorks design and machining of the actual module in a machine shop. The rings are designed to be pressed fit such that it will automatically be aligned to the system.

During the design phase, the first version of the design was designed with the lens, and center glass and the back glass as shown in Figure 4.6 (a). However, after actual fabrication, we noticed that the extra relief in the hardware blocks the curvature of the back lens. This blocking limits the zoom ratio of the fluidic lens optics. We dub the first design UCSD_O1. Upon realization of the issues in zoom ratio, we moved the back lens back for 1 mm. Before actual fabrication of the new hardware, we ran RMS (root-mean-square) spot size analysis to compare image quality and zoom ratio. The result is shown Table 4.1.

Based on ZEMAX simulation result, the image quality of the two designs are comparable. Actual hardware shows similar image quality. The zoom ratio shows drastic improvement for UCSD_O2, thanking to the extra space. For UCSD_O1, the optical zoom (field-of-view) is ~4X for 1/3 inch optical format. For UCSD_O2, the optical zoom (field-of-view) is 5.7X for 1/4 inch optical format. A more detailed analysis of the zoom ratio is documented in later section.

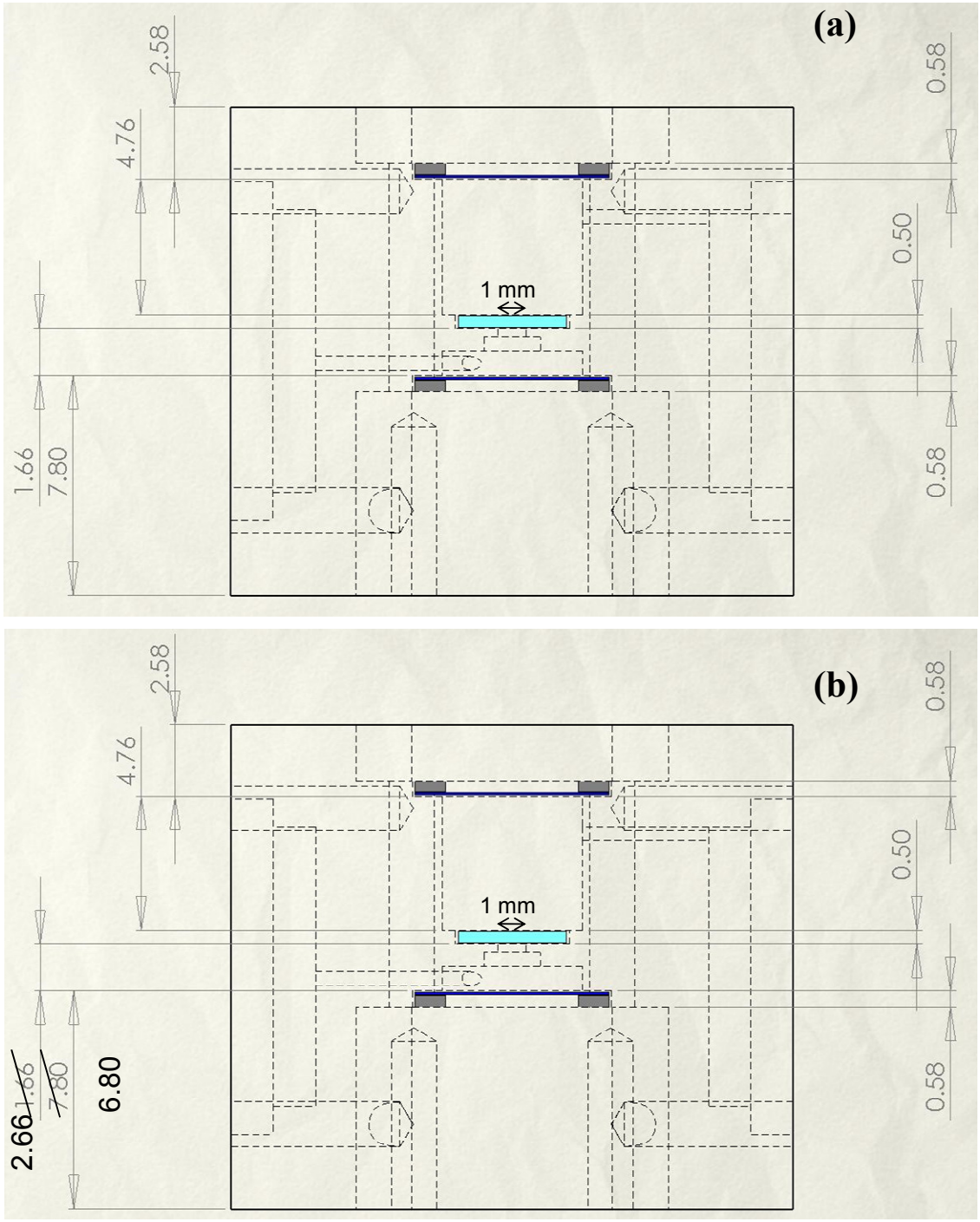

Figure 4.5 Mechanical Dimension of the fabricated fluidic lens structure. The original design (a) and (b) modified design to avoid mechanical blocking.

4.3.3 ENGINEERING ROOM TESTING

Different test targets were designed to test image quality of optical systems. We mainly focus on image quality, resolution and feature resolution. Subject test is the ultimate test of an optical system, so objects of interest are taken to demonstrate the image quality.

4.3.3.1 ISO CHART RESOLUTION TEST

ISO 12233 is a standard target that can test the resolution of electronic still picture cameras. To test the image quality of fluidic zoom lens, we placed the target at difference distances to demonstrate the capability. With the target at different distances, the lens will have to zoom to different ratios. Based on our analysis, the optics has 600 line pairs/picture height. This translates to ~10 um spot size since we are on a 1/3" optical sensor.

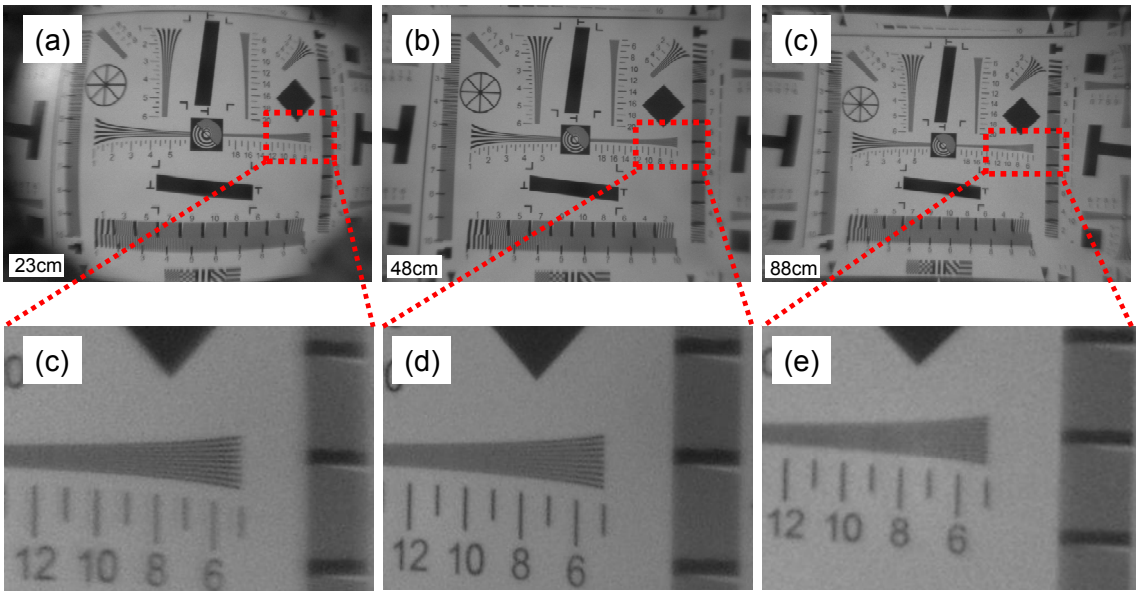

Figure 4.6 Images of the ISO resolution chart. (a), (b), and (c) are taken at a distance of 23 cm, 48 cm, and 88 cm distance from the camera. The distances simulates the zoom function. (d), (e) and (f) are the blow up view of the images in (a), (b), and (c). The figures show that the camera has 600 lp/PH throughout all zoom.

4.3.3.2 USAF TARGET

ISO resolution chart provides a good analysis on the performance of the optical system. The second question that is very important is to know the smallest feature that the optical system can see. For the laparoscopic camera, this will determine if cells can be seen. Based on the experiment, we demonstrate that the fluidic zoom lens can see features down to 30 um when the target is placed at 6 cm distance, which is the distance relevant to operation. This kind of feature resolution promises clear resolution of small features during operation.

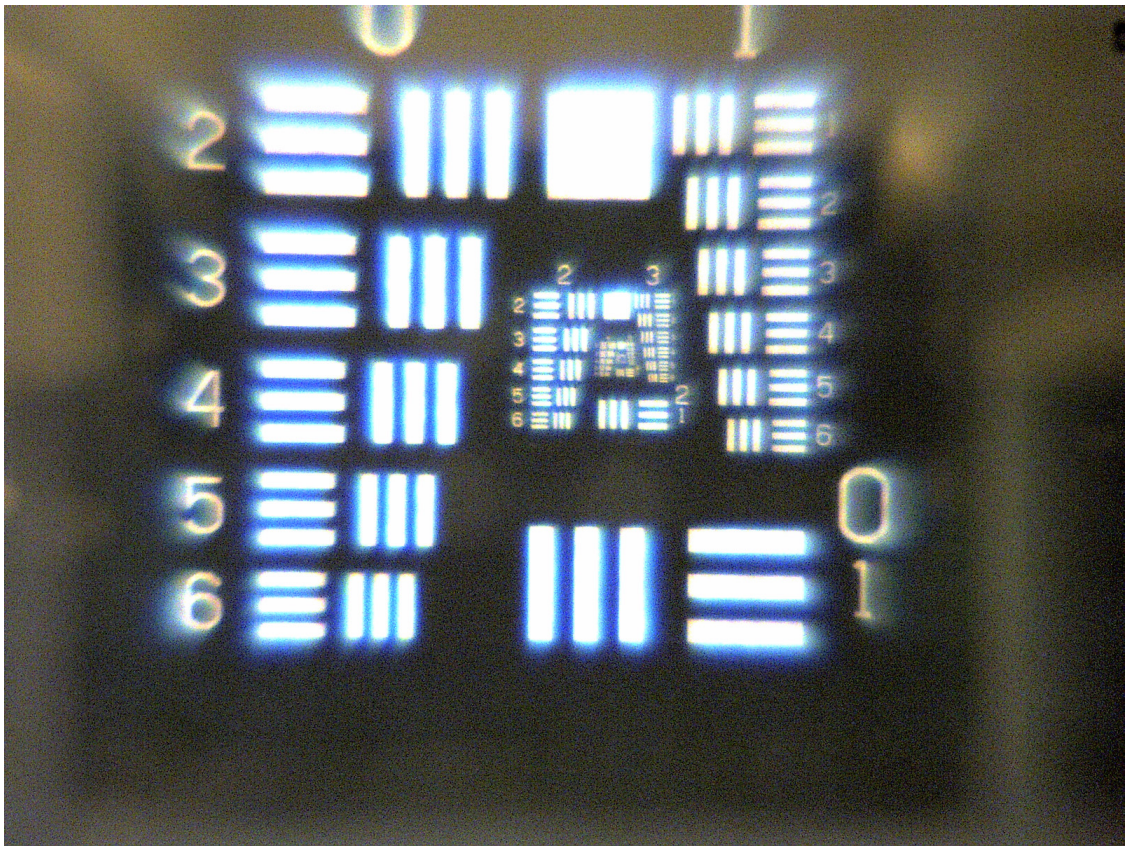

Figure 4.7 Edmund optics 1951 USAF target placed at 6 cm distance.

4.3.3.4 ZOOM RATIO AND DISTORTION ANALYSIS

Since this is a zoom camera, it is important to characterize the zoom ratio. Note that there are 2 versions of the zoom camera available. The first version is UCSD_O1. This is the version that has a mechanical limitation on the back lens. To mitigate this problem, we moved the back lens back 1 mm. This design is UCSD_O2. The performance of the 2 systems was analyzed in ZEMAX. Both provided similar optical performance.

To analyze the zoom ratio, we only used UCSD_O2 to measure it. Measurement method is by taking images of squares at extreme zoom in and extreme zoom out. To analyze the optical zoom ratio from EFL, the size of the square at the center is compared in the two images. The result shows that the zoom ratio is 4.3962.

For laparoscopic applications, the surgeons are more worried about the actual field of view where distortion comes into play. The more view that the surgeons can see, the better it is for the surgeons as well. Therefore, the field of view zoom ratio is also very useful. This can be done by calculating the number of squares (cubes). Based on the extreme zoomed in and zoomed out images, the optical zoom for field of view is 5.7x. Note that this is at roughly 70% field.

The main reason for the difference in optical zoom for EFL and field of view is due to distortion. In a typical zoom lens design, the distortion will not change much because the lens configuration is basically the same. For instance, a telephoto system stays as a telephoto system throughout the entire zoom. This is very different for the fluidic lens zoom lens. In a fluidic zoom lens system, the configuration changes. When zoomed out the optical configuration is a reversed-telephoto configuration. When in, the optical configuration is a telephoto configuration.

The distortion change can be calculated for 70% field. In the case for zoomed out, the barrel distortion at 70% field is 27.92%. The image prepared for analyzing distortion is not detailed enough to calculate the distortion for zoomed in. However, based on experience, when the distortion is less than 5%, the human eye doesn't detect it.

An educated guess for the amount of pincushion distortion during zoomed in is roughly 5%.

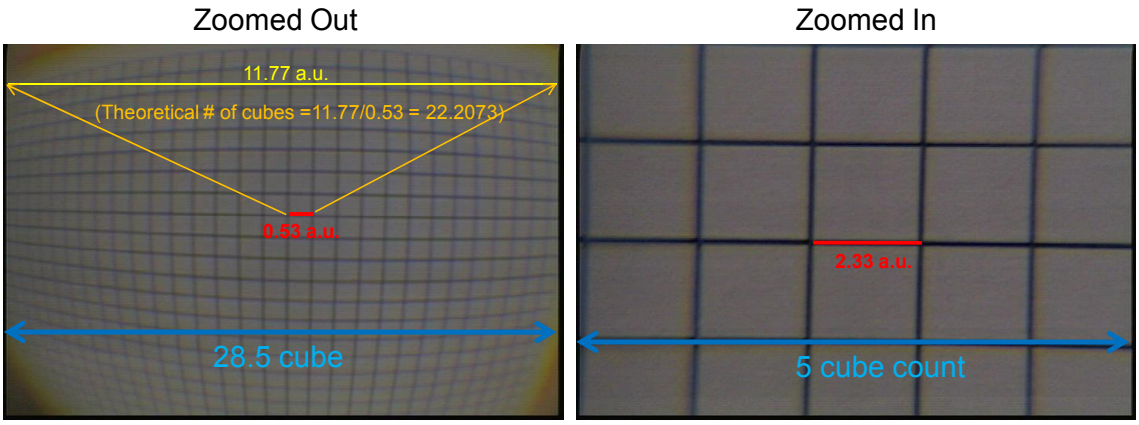

1. Optical Zoom (EFL) = Zoomed out cube length / zoomed in cube length
= 2.33/0.53 = **4.3962** (estimated from paraxial)

2. Optical Zoom (Horizontal F.O.V.) = Zoomed out cubes/zoomed in cubes
= 28.5 (cubes) /5 (cubes)= **5.7**

3. Zoomed Out Distortion @ Horizontal (~70% field)
= (Actual Horizontal Cubes - Theoretical # of cubes) / Theoretical # of cubes
= (28.5-22.2073)/22.2073*100% = **27.92%**

Figure 4.8 Zoom analysis through cube comparison.

4.3.3.6 REAL LIFE-SIZE HUMAN ANATOMY TEST

To test the surgical camera in an engineering experimental environment, a real life size anatomy is placed at 15 cm distance from the bio-inspired fluidic lens. Since the amount of lighting is of particular interest, a lux meter (LX-101A, LT Lutron) is used to measure the amount of light that reached the stomach. The measurement was 1500 lux. The camera then zoomed in and out to take images Figure 4.9(a) and 4.9(b). When zoomed out the entire organ can be seen. When zoomed in, the cracks on the anatomy from over 30 years of use can be clearly seen.

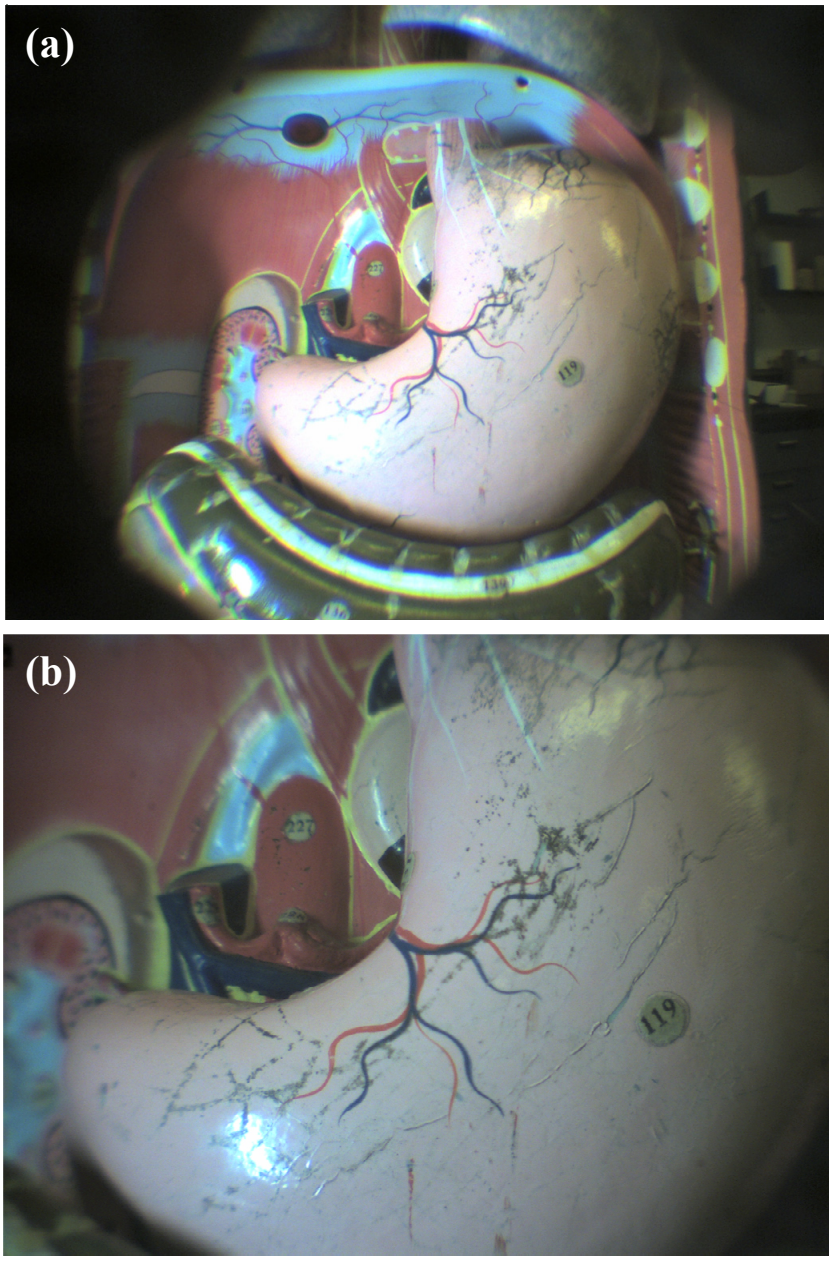

Figure 4.9 Zoomed out (a) and zoomed in (b) photograph of the stomach from a human size anatomy taken with bio-inspired fluidic zoom lens. The stomach is 10 cm wide and is illuminated at 1500 lux. The camera is placed at 15 cm distance from the stomach.

4.3.3.3 Near infra-red test

The human eye cannot see infrared, but the CMOS sensor can detect that wavelength. Furthermore, most of the parts inside the human body is So there is interest in understanding how well the camera performs in infrared. It is also worth noting that the all pixels in the CMOS sensor can detect near infrared.

To demonstrate and test the functionality of the camera under infra-red wavelength, high-output infrared LED (276-143, RadioShack) is used as the illumination light source. This LED emits at a peak wavelength of 940 nm. Since the human eye cannot see 940 nm, the room is completely dark.

In our experiments, we took several different images of different objects with room light on and room light off. To demonstrate the resolution limit, Edmund Optics USAF 1951 target is placed at 5 cm distance from fluidic zoom lens camera under room lighting (regular visible lighting) and 940 nm illumination from the LED, as shown in Figure 4.10. Based on the image quality, the fluidic lens system has similar performance under infrared (at least under 940 nm, which is widely used for security camera) and under regular room lighting. One question that is worth exploring is whether the fluidic lens system needs to refocus during this illumination light source switching process. This is possible due to chromatic aberrations. Unfortunately, at the time of the experiments, the fluidic lens slowly losses its original pressure over time and curvature changes. So it was not possible to identify whether refocusing was needed for different wavelengths.

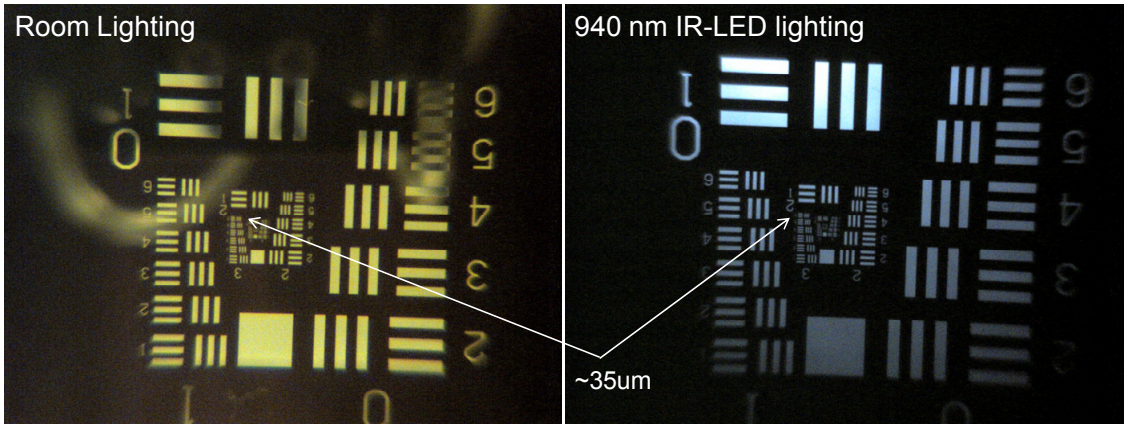

Figure 4.10 Comparison of feature resolution with USAF target under regular visible lighting (room lighting) and 940 nm IR-LED lighting. USAF target is placed at 5 cm distance from the camera. The infrared LED is placed at the back of the USAF target, therefore illuminate dfrom the back. If the LED is placed in the front, the reflection coming from the USAF target is too strong. Feature resolution is similar for both conditions.

Another experiment is on identifying whether veins and blood vessels can be seen under 940 nm lighting. A human had was placed in front of the camera under 940 nm infrared light illumination. Because the room is completely dark, so the only lighting source is the 940 nm infrared lighting. The experiment result demonstrates that the human veins are visible under this lighting condition. This is because the original color of the vein is bluish. The image are shown in Figure 4.11. This is the image of the human hand. The left image is the palm connecting to the little finger. The image on the right is the knuckle. Overall, the visible vein demonstrates that the there are potential biomedical applications for the fluidic zoom camera operating in infrared wavelengths. Also of note is that the images are black and white again because the

room lighting is not on. There are no light of other wavelength except for 940 nm; hence, no color.

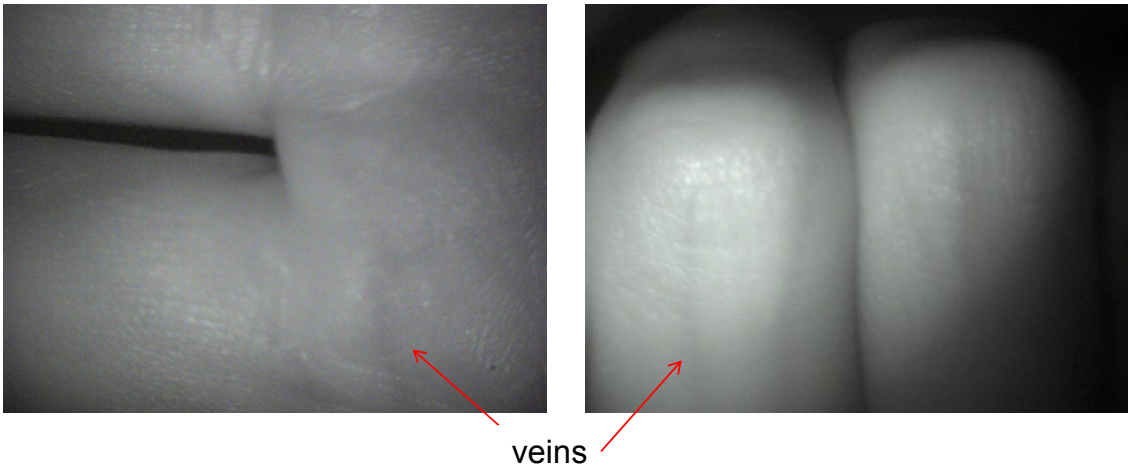

Figure 4.11 Demonstration that the human vein can be seen with 940 nm infrared lighting. This shows that there are potential biomedical applications for the fluidic zoom lens working in this illumination regime.

4.3.4 Surgical room test

Following the *in vitro* testing, the bio-inspired fluidic surgical camera was tested on a live pig in an operating room. The pig was placed under general anesthesia with its abdomen incised, and the camera was inserted into the abdominal cavity. Still images and videos were captured on a laptop computer connected to the camera by universal serial bus (USB). The illumination level was set to be 1500 lux for the experiment. Pictures were captured by the bio-inspired laparoscopic zoom camera at a distance of 10 cm from the organs. The zoom-in and zoom-out images are shown in Figure 4.11 (a) and (b). Excellent, high-definition image quality was observed at all levels of zoom. When zoomed out, the entire surgical field was within the field-of–view and the whole

organ can be seen. When zoomed in, the details of blood vessels were visible to facilitate precision surgical operation. In comparison with commercial laparoscopes, images were also obtained with a Stryker 10mm laparoscope at the same illumination level (i.e. 1500 lux) used for the bio-inspired laparosocpic zoom camera. Figure 4.11 (c) shows the image taken from our camera and Figure 4.11 (d) is the image taken from the state-of-the-art Stryker's laparoscope. For aforementioned reasons (i.e. large F-number), the commercial laparoscope was unable to function under low light conditions. Also, the distance between the camera and the stomach for bio-inspired fluidic zoom lens was 12 cm while the laparoscope was only 4 cm. Hence, bio-inspired fluidic zoom provides more working space for the surgical tools to operate on the surgical site without interference.

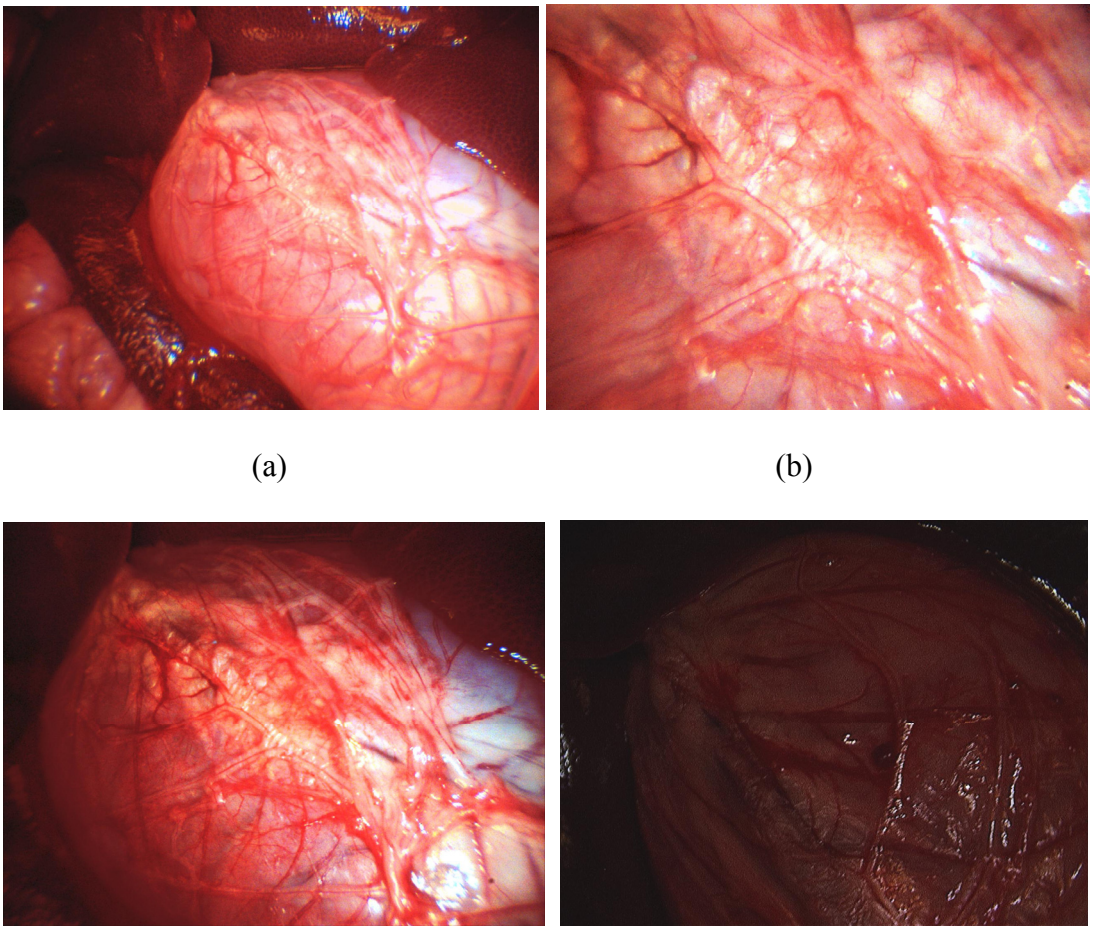

(a) (b)

(c) (d)

Figure 4.12 Images from experiment in the surgical room. (a), (b), and (c) are images taken with the bio-inspired laparoscopic zoom camera when placed at 12 cm distance from the stomach, but with the lens set at different zoom ratios. The lighting is provided from the LED and is measured to be 1500 lux. At zoom out (a), the entire stomach can be seen. At zoom in (b), the fine details of the vessels can be seen. (d) is the image taken from 10 mm laparoscope under the same LED lighting conditions. To match the field of view of (c), the laparoscope has to be at 4 cm distance from the surface of the stomach.

4.4 Advanced fast NIR surgical zoom camera design

One of the major limitations of a simple 2 lens system is that it cannot control the aberrations. In the original case, the image quality, the speed, and the illumination condition was suitable for surgical applications. The main factor for the low light condition is contributed by the sensitivity of the CMOS sensor. To further reduce the requirement for illumination, one can work with the optics and make it faster and create a larger entrance pupil. To attain such a target, extra lenses are needed to compensate for the aberrations.

Similar to the original simple 2 lens design, two fluidic lenses are still used to provide optical zoom and auto-focusing as derived in the optical zoom theory earlier. Additional fixed lenses are introduced between the fluidic lenses to correct astigmatism and other aberrations. The curvatures of the fluidic lenses change in a similar fashion to the previous design to achieve telephoto and reversed telephoto systems. However, by placing fixed lenses between the fluidic lenses, aberrations can be minimized. The designed optical system is shown in Figure 4.13.

In the designed optical system, 4 glass lenses, 2 in front of the stop and 2 behind the stop, are inserted. Such a quasi-symmetric design yields good quality images, and the effect of symmetry is particularly obvious for the middle-zoom position in Figure 4.14 (b). When the symmetry of the entire system is attained as in Figure 4.14 (b), the highest image quality is obtained. As the system moves away from the symmetry point, as in Figures 4.14 (a) and (c), image quality starts to degrade. The optimization

program of the ray tracing software makes a graceful degradation of the image quality from its optimal position to assure HDTV quality images from zoom-in to zoom-out positions.

It is also worth mentioning that the doublet right before the image sensor is used to bend the rays to reduce the incident ray angle to the imager. This is important for the design to meet the chief-ray angle requirement for CMOS image sensors. To reduce the size of the device, we make the membranes of both fluidic lenses face the aperture stop. Since the clear aperture is typically smaller when closer to the stop, a smaller fluidic lens can be used with less vignetting, resulting in a better relative illumination. The design is a very fast optical system (F/2.8-4.45), producing excellent sensitivity with limited lighting.

The lenses in between the fluidic lenses are important in providing better image quality. Those lenses mostly created virtual images of the fluidic lens when seen from the stop. In other words, if the rays are traced from the stop, the fluidic lenses are moved further away from the stop due to those extra lenses. Based on earlier equation, when the distance between the two power changing lenses increase, the total power of the system will also change faster. So the extra lenses in the middle create a much larger effective distance between the 2 fluidic lens. This allows for a much shorter total track of the actual fluidic zoom lens.

The total track length of the design is 22 mm. The maximum diameter among all (fluidic and fixed) lenses is less than 5 mm, making the device easy to insert via a small incision for laparoscopic surgery or a natural orifice for NOTES.

To evaluate the optical zoom system, ZEMAX Geometric Bitmap Image Analysis is performed at an object distance of 15 cm (zoom-in) and 6.5 cm (zoom-out). Looking at Figure 4.15, the images demonstrates much better image quality throughout all fields. This is different from the image quality of a simple 2 fluidic lens zoom camera where no extra fixed lenses are added in.

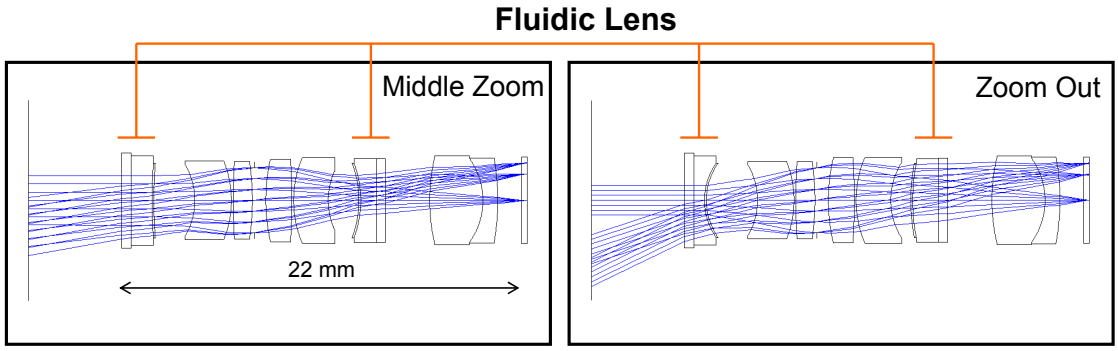

(a) (b)

Figure 4.13 Advanced surgical camera lens view. Two fluidic lenses are used to create a telephoto and reversed telephoto system. Fixed lenses are added between the fluidic lenses to reduce aberrations. The total track length is 22 mm and the maximal lens diameter is less than 5 mm, suitable for camera insertion. The optical system is designed for a 1/4" optical format image sensor.

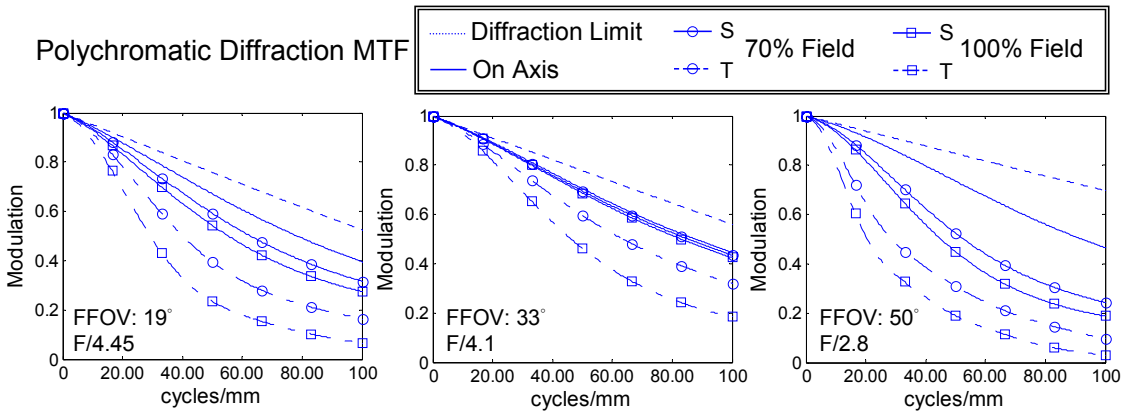

(a) (b) (c)

Figure 4.14 Polychromatic MTF plot considering 0.8, 0.85, and 0.9 μm wavelengths for various zoom conditions. The plots are based on calculations from ZEMAX. Diffraction limit is shown in dotted line in each curve. The on-axis field is shown as a solid line. The 70% and 100% field are separated by round and square markers. The tangential and saggital MTF of each field is shown by a dotted line and solid line, respectively. The difference between the tangential and sagittal MTF for each field indicates astigmatism. The image quality for the middle zoom position (b) is the best. The image quality slowly drops off as the zoom position deviates from the middle zoom position. The EFL for the different views are: (a) 11.8 mm, (b) 10.65 mm, and (c) 4.46 mm.

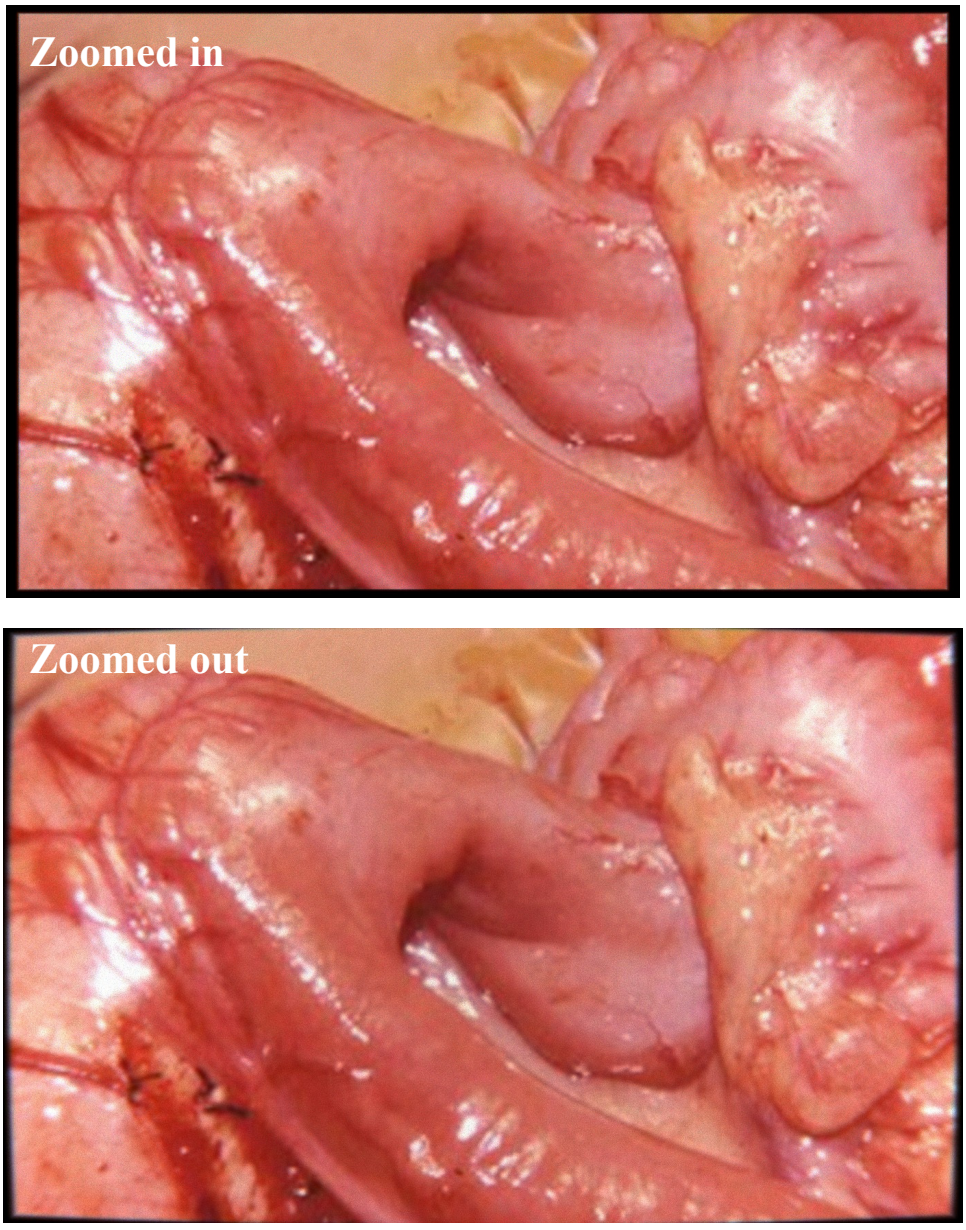

Figure 4.15 ZEMAX Geometric Bitmap Image Analysis demonstrating the image quality of the camera system when zoomed in and zoomed out. The edges show much better image quality demonstrating that image quality is improved by adding in extra lenses.

4.5 Conclusion

In this chapter, we talked about the design and a major application for fluidic zoom lens. To create optical zoom, the total power of the optical system has to change, this means that 2 lenses are needed.

With fluidic lens, a very small zoom lens was made. The optical zoom is very large, etc. The total track of the optical system is 20 mm and the optical zoom is over 4x. Another important feature is that the working distance of this zoom camera can be as short as 2 cm to infinity. This is not possible with fixed lens zoom cameras, even when they are miniaturized. This is the world's smallest zoom camera with largest optical zoom. The working distance of this camera is also better than any other commercial miniature zoom cameras.

In the end of this chapter, I discussed the design of an advanced version of bio-inspired fluidic zoom lens where fixed lenses are added in to improve image quality and increase the speed of the lens system. With fixed lenses, the zoom camera can be as fast as F/2.8. More importantly the camera has good image quality throughout all fields. To demonstrate the continuous image quality through out the entire field, I ran ZEMAX image analysis to demonstrate the image quality through out all fields.

References:

[1] R. McCloy, et al., "Is smaller necessarily better? A systematic review comparing the effects of minilaparoscopic and conventional laparoscopic cholecystectomy on patient outcomes," *Surgical Endoscopy*, 22(12), pp. 2541-53, 2008.

[2] K.L. Chan, W.C. Hui, and P.K. Tam, "Prospective randomized single-center, single-blind comparison of laparoscopic vs open repair of pediatric inguinal hernia," *Surgical Endoscopy*, 19(7), pp. 927-32, 2005.

[3] H.S. Tilney, et al. "Laparoscopic vs open subtotal colectomy for benign and malignant disease," *Colorectal Disease*, 8(5), pp. 441-50, 2007.

[4] J. E. Varela, S. E. Wilson, and N. T. Nguyen, "Laparoscopic surgery significantly reduces surgical-site infections compared with open surgery," *Surgical Endoscopy*, published online, 2009.

[5] E.R. Podolsky, et al. "Single port access (SPA) cholecystectomy: a complete transumbilical approach," *Journal of Laparoendoscopic and Advanced Surgical Techniques*, 19(7), pp. 219-222, 2009.

[6] K.E. Roberts, "True single-port appendectomy: first experience with the "puppeteer technique"." *Surgical Endoscopy*, 23(8), pp. 1825-30, 2009.

[7] S. Horgan, et al., "Natural orifice surgery: initial clinical experience," *Surgical Endoscopy*, 23(7), pp. 1512-1518, 2009.

[8] Y. Mintz Y, et al., "NOTES: a review of the technical problems encountered and their solutions," *Journal of Laparoendoscopic and Advanced Surgical Technique,* 18(4), pp. 583-7, 2008.

[9] www.laparoscopicsurgeryinfo.com/procedure.htm

[10] http://www.fertilityalabama.com/fertility-tests-laparoscopy.html

[11] W. J. Smith, *Modern Optical Engineering*, 4 ed: McGraw-Hill Professional, 2007.

This chapter or portion thereof has been published in ***Proceesings of SPIE*****, vol. 7061, 70610N (2008)**. This chapter or portion thereof has also been submitted for publication in the following manuscript: Frank S. Tsai, Daniel Johnson, Cameron S. Francis, Sung Hwan Cho, Wen Qiao, Ashkan Arianpour, Yu-Hwa Lo, "Fluidic lens laparoscopic zoom camera for minimally invasive surgery."

Chapter 5

First gallbladder removal surgery with Surgicam

5.1 First gallbladder removal with bio-inspired fluidic lens

The first ever gallbladder removal surgery was performed on 10/16/2009. This is the first demonstration of the surgery with bio-inspired fluidic lens. In earlier chapters, I have discussed the potential of using bio-inspired fluidic lens in minimally invasive surgery. With a super small zoom lens, the camera can be mounted on the

abdominal wall and the number of trocars can be reduced. In this chapter, I will document the gallbladder removal sugery.

Almost all gallbladder removal surgery, or cholecystomy, is performed with laparoscopy. Cholecystomy is also the highest volume in abdominal surgeries. Therefore, we choose to demonstrate gallbladder removal as the surgery to demonstrate the functionality and the capacity of Surgicam.

Figure 5.1 Stryker Laparoscope. This is a rigid laparoscope that doesn't provide the functionality required for next generation laparoscopy.

5.2 Surgicam system design and description

Surgicam is a complete laparoscopic camera including bio-inspired fluidic lens, actuators, electronic circuit boards, etc. The laparoscopic camera is intended to be inserted into the body for surgery. There are 2 major sections: optics section and the electronics section. The optics section has (1) bio-inspired fluidic lens, (2) LED lighting, and (3) actuator for fluidic lens. The fluidic lens and the actuators are enclosed in a box made out of Delrin, which is a black Teflon material that greatly reduces the material interactions with the optical fluid. LED is place on the side of the lens body. This is mainly for ease of placement. A ring LED is our target design.

The electronics board has 4 major functions: (1) CMOS sensor for sensing; (2) control circuit for actuators; (3) control for lighting; and (4) transmission to external boards. The current version of surgicam that was used for surgery uses a 640x480 CMOS sensor. The limiting factor for this entire system is mainly because of transmission. The video signal coming out of the 640x480 sensor is PACS format. This transmission format can be easily adjusted to become wireless transmission by adding a simple video transmitter. For the purpose of transmission, 640x480 sensor is good, but the image quality is some what compromised.

The image of the entire constructed surgicam that is used in the surgery is shown in Figure 5.1. The schematic of the imaging optics section, along with the actuators are shown in Figure 5.2. The layout of the electronics board is shown in Figure 5.3. From Figure 5.2, the actuator is in fact the largest device in the system. This is because we are

currently using the E-Cell from Med-e-cell. The original design of the E-cell was for other applications, therefore, the size was much larger than what we needed. With some engineering design work, the size of the actuator can be shrinked down tremendously. The other larger component is the electronic circuit board. Theis board is already 6 layers, and the footprint is already very tight. Although there are also several circuit components that can be taken out, the most likely method to shrink down the board is by geometric arrangement of the boards. All in all, it is still possible to reduce the size of the boards.

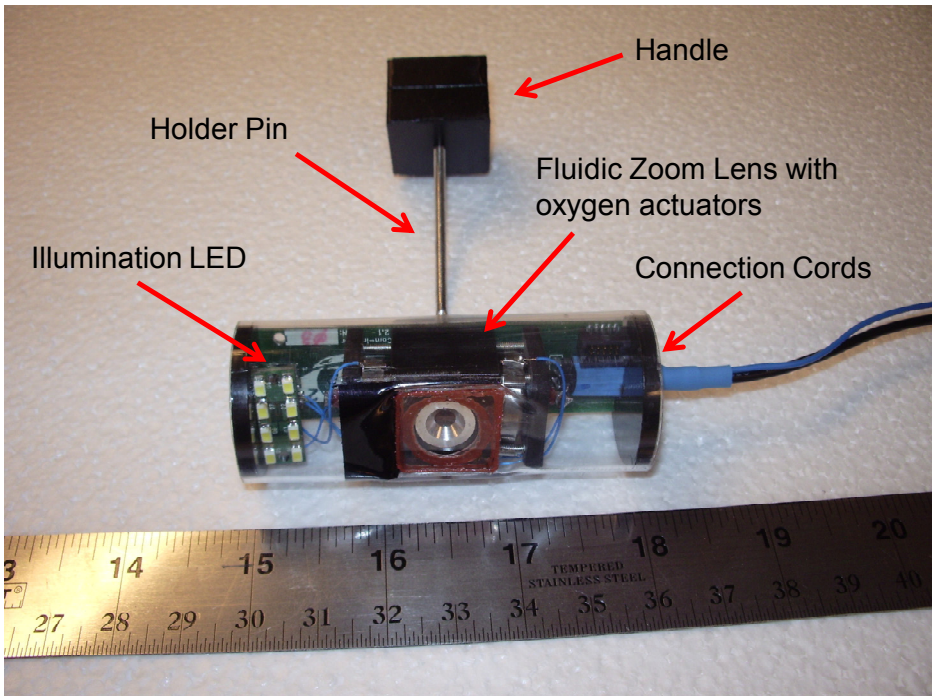

Figure 5.2 Image of Surgicam camera section. The optics of Sugicam is much faster than a regular laparoscope, thus allowing for internal LED illumination. This greatly reduces the size requirements.

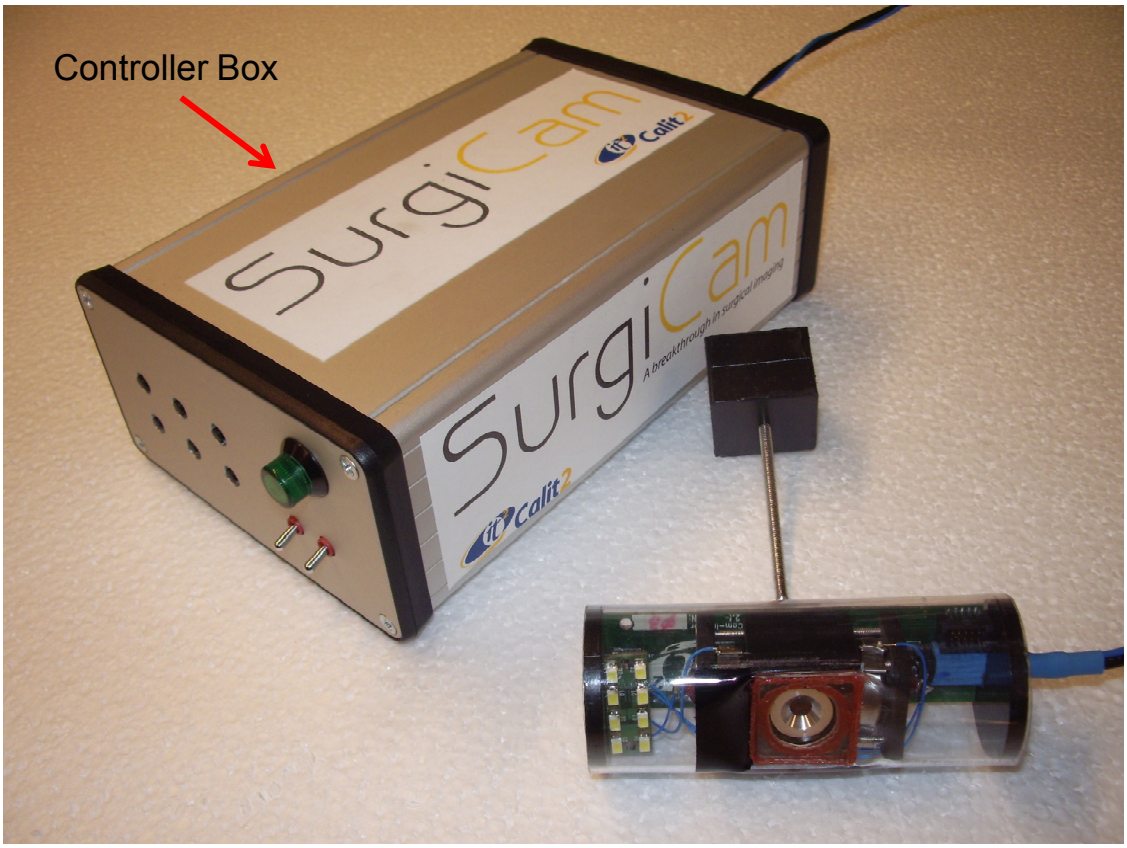

Figure 5.3 Image of Surgicam camera with the controller box.

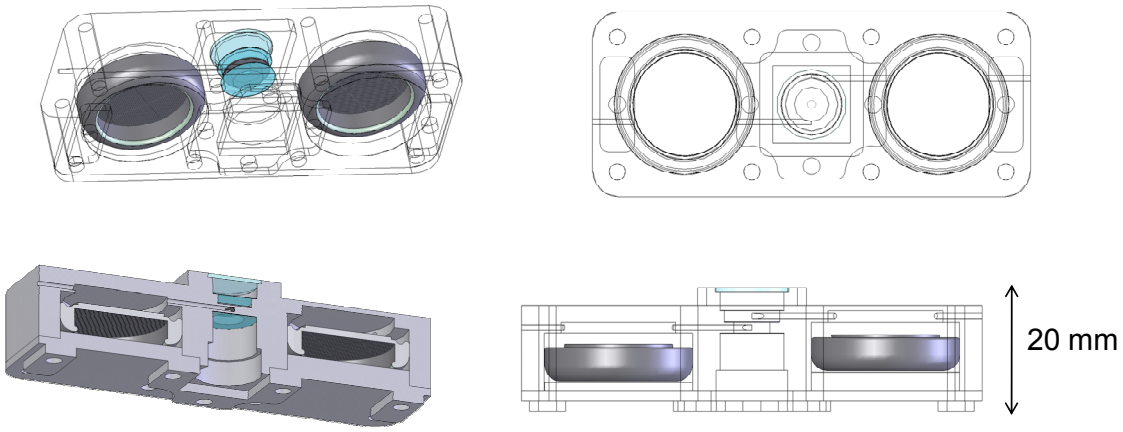

Figure 5.4 Schematic of surgicam imaging optics section

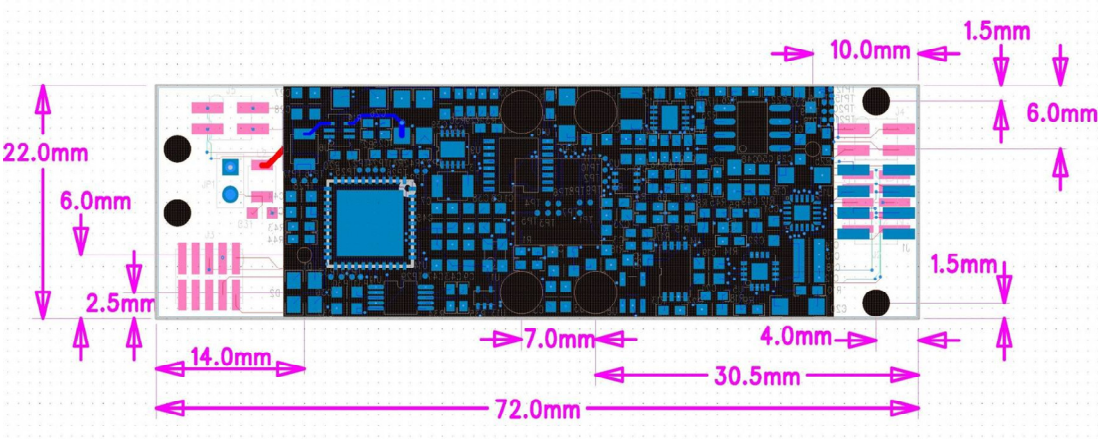

Figure 5.5 Layout of electronics board

5.3 Surgical Procedure

5.3.1 Preparation and insertion of Surgicam

The current version of Surgicam is tube that is 25 mm in diameter and roughly 10 cm long. The limiting factor for the size is due to the electronics board and actuator design. Both of these can be reduced tremendously with reasonable amount of engineering work. Although the size of the Surgicam can be reduced, its current sized limits the way that it is inserted into the pig body.

At the day of experimental surgery, the surgeons first studied the camera careful to determine how to use it during surgery, Figure 5.6. Once the surgeons have got a feel for the camera, the camera was inserted into the experimental pig body. First, ~8 cm vertical abdominal skin incision was made in the midline and extended through the abdominal wall and peritoneum using electrocautery, Figure 5.7. Through this incision, the camera was introduced into the abdominal cavity. With the abdominal wall retracted away from the internal organs, the camera was fixed to the inner surface of the abdominal wall by advancing the fixation pin back through the abdominal wall, and screwing the handle down to the skin at the site of penetration to keep the camera steady. After the insertion of the first camera, a second camera, contralateral to the first camera, was introduced and fixed to the abdominal wall in the same manner.

The incision was then sutured closed and the first trocar was pushed introduced through the abdominal wall following the traditional approach. Using this trocar, a working space, and pneumoperitoneum, was established by CO2 insufflation.

With the pig prepared for surgery, real-time video feed from inside the abdomen is displayed on an external monitors for the surgeons to see. We placed our monitor on the original laparoscope tower as seen in Figure 5.8.

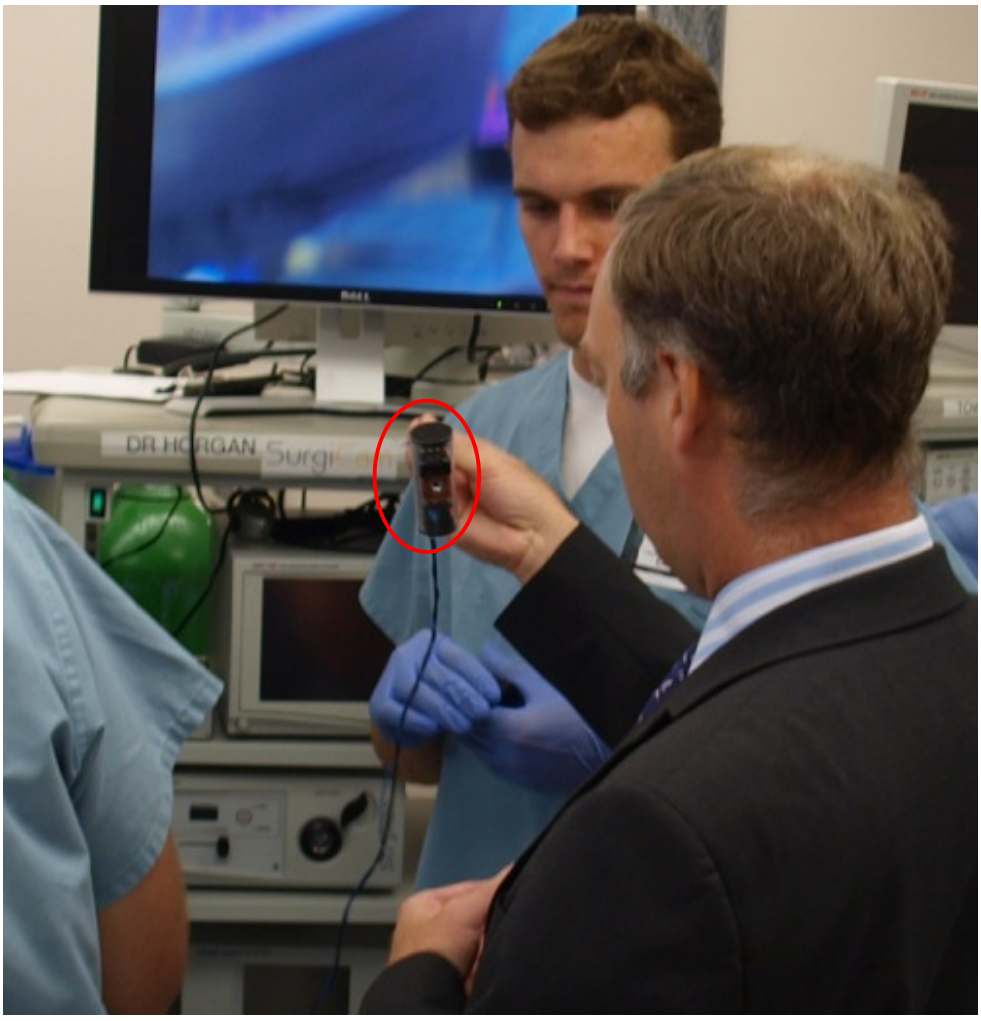

Figure 5.6 Surgeons studying the surgicam module. Dr. Horgan, surgeon, is holding the surgicam in his hands to understand the structure of the new. Daniel Johnson, mechanical engineer, is explaining the mechanical structure of Surgicam to Dr. Horgan.

Figure 5.7 Preparation for the incision of Surgicam into the surgical pig.

Figure 5.8 Real-time image acqcuired from inside the abdominal with Surgicam. Here, the Sugicam is looking at the mesentary of the large intestine. The image quality is shown on the monitor and the color is corrected to the level where surgeons are used to. Also, the only external component of the surgicam module is the small controller box that is circled in red. This is a major reduction of size from the multiple components in the laparoscope tower.

5.3.2 Flipping the liver

First, the liver is reflected for easy access to the gallbladder.

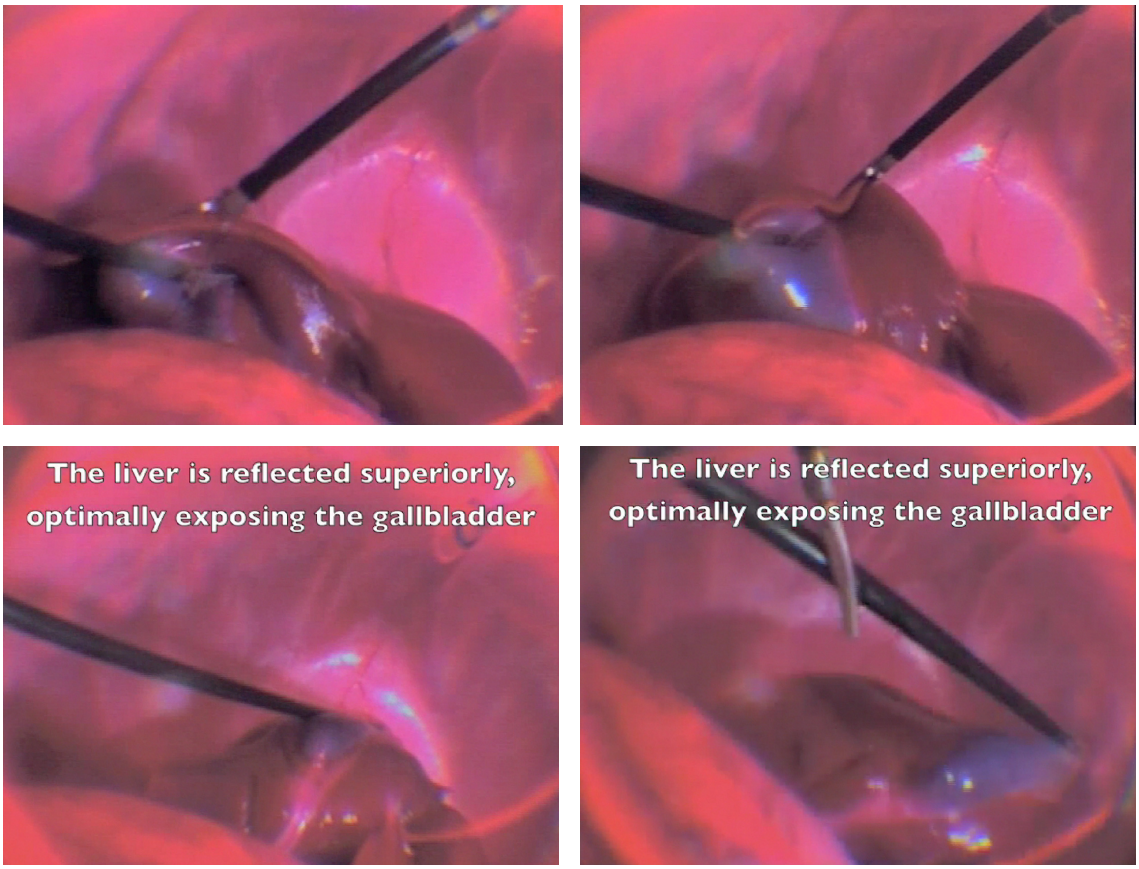

Figure 5.9 Reflecting the liver to expose gallbladder.

5.3.3 Dissecting the Gallbladder with harmonic scalpel

Once the liver is in superior position and the gallbladder is exposed, a harmonic scalpel is used to dissect the gallbladder.

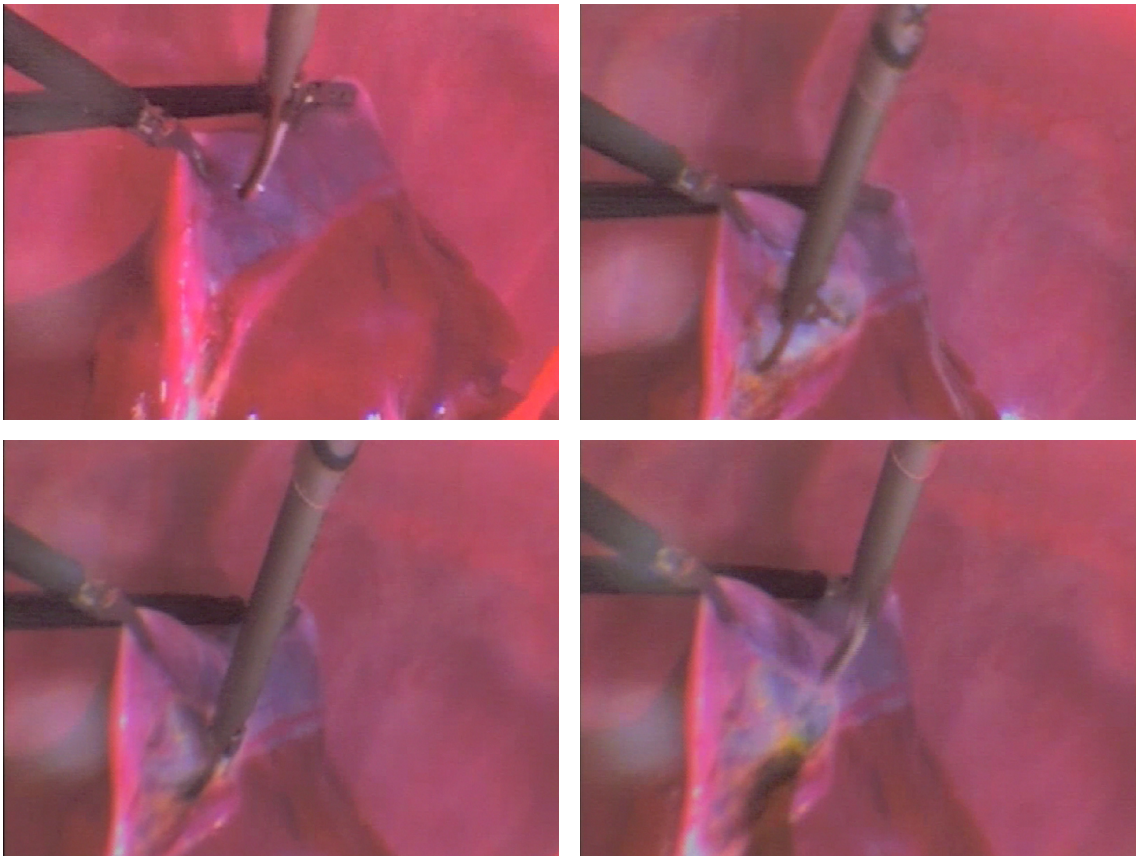

Figure 5.10 Dissecting the gallbladder and associated ducts with the harmonic scalpel.

5.3.4 Clipping the artery

The artery was clipped to avoid bleeding.

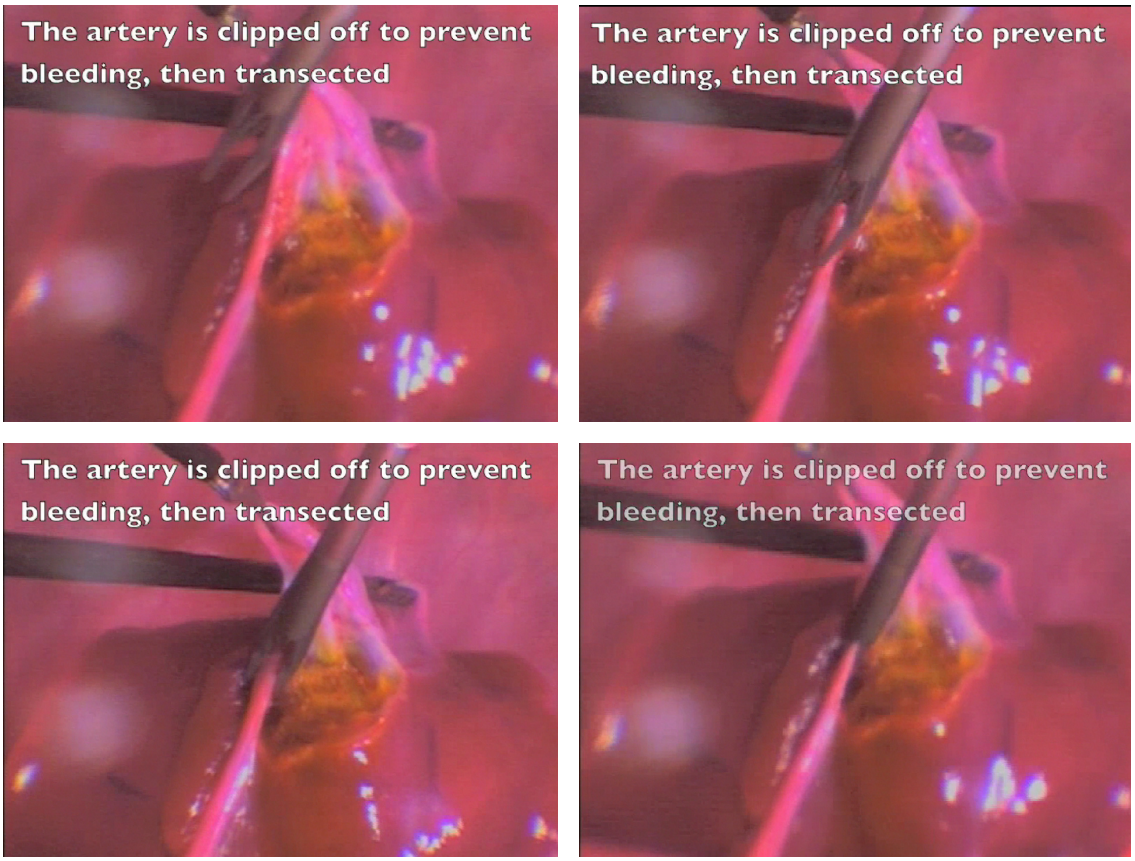

Figure 5.11 Clipping of artery.

5.3.5 Continued dissection of gallbladder

After clipping of the artery, the dissection continues with the harmonic scalpel.

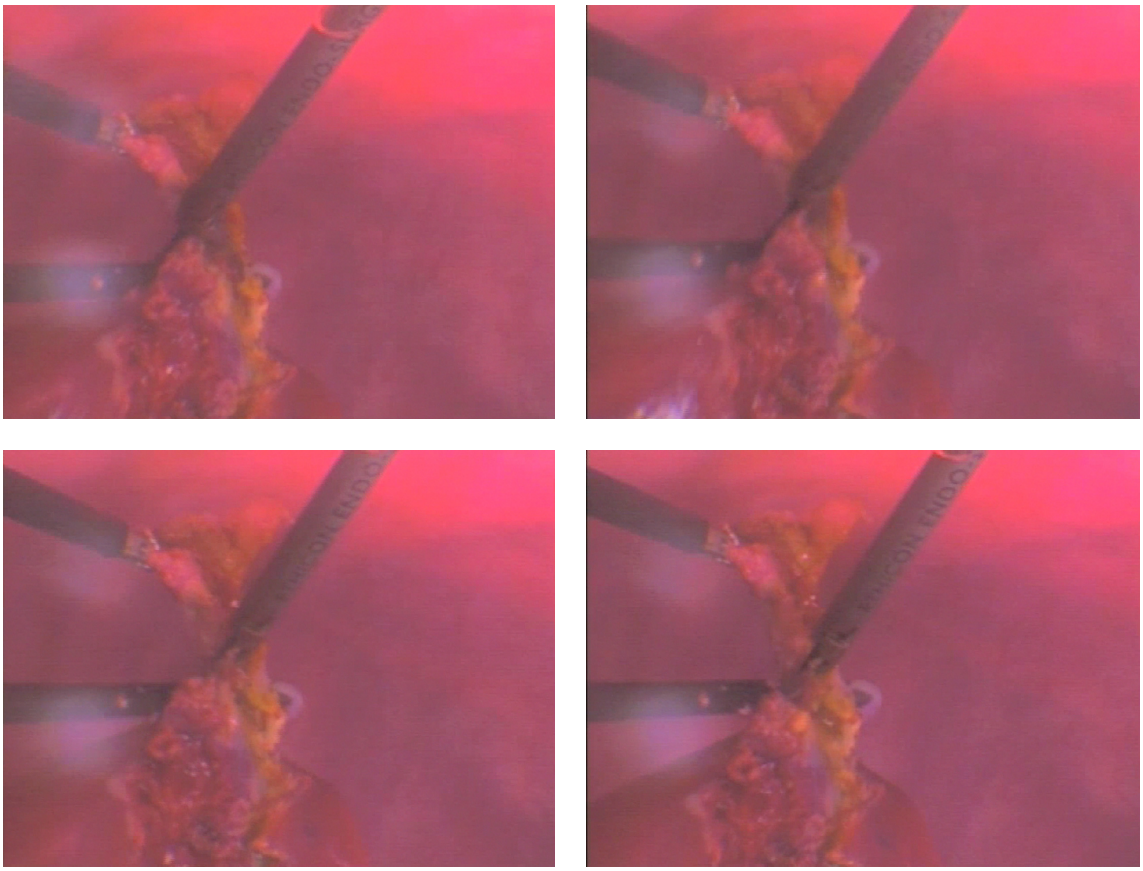

Figure 5.12 Continued dissection of the gallbladder.

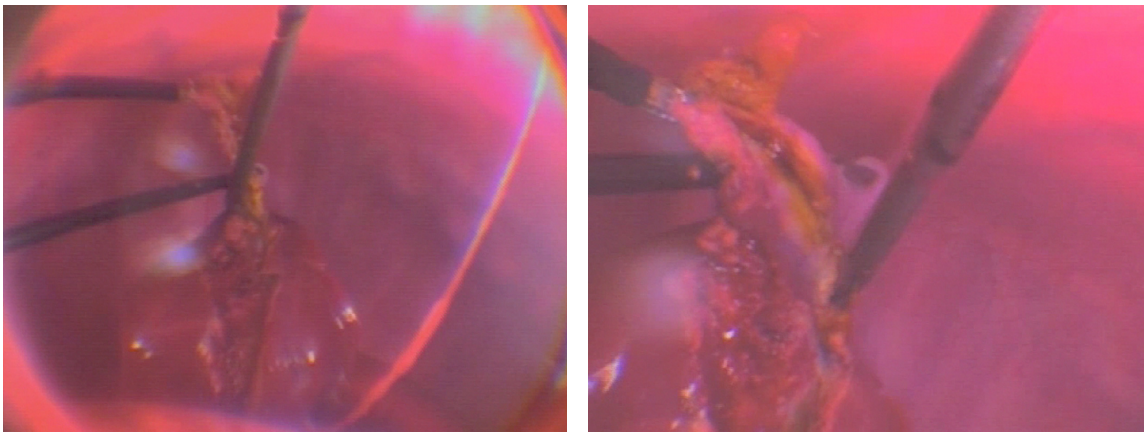

Figure 5.13 Demonstration of zoom function during surgery. When zoomed out, the entire organ can be seen. When zoomed in, details can be seen to facilitate operation.

5.3.6 Final cutting between the liver and the gallbladder

The final cut is made with a scissor. The bottom right image shown in Figure 5.13 shows the liver falling down separted from the gallbladder.

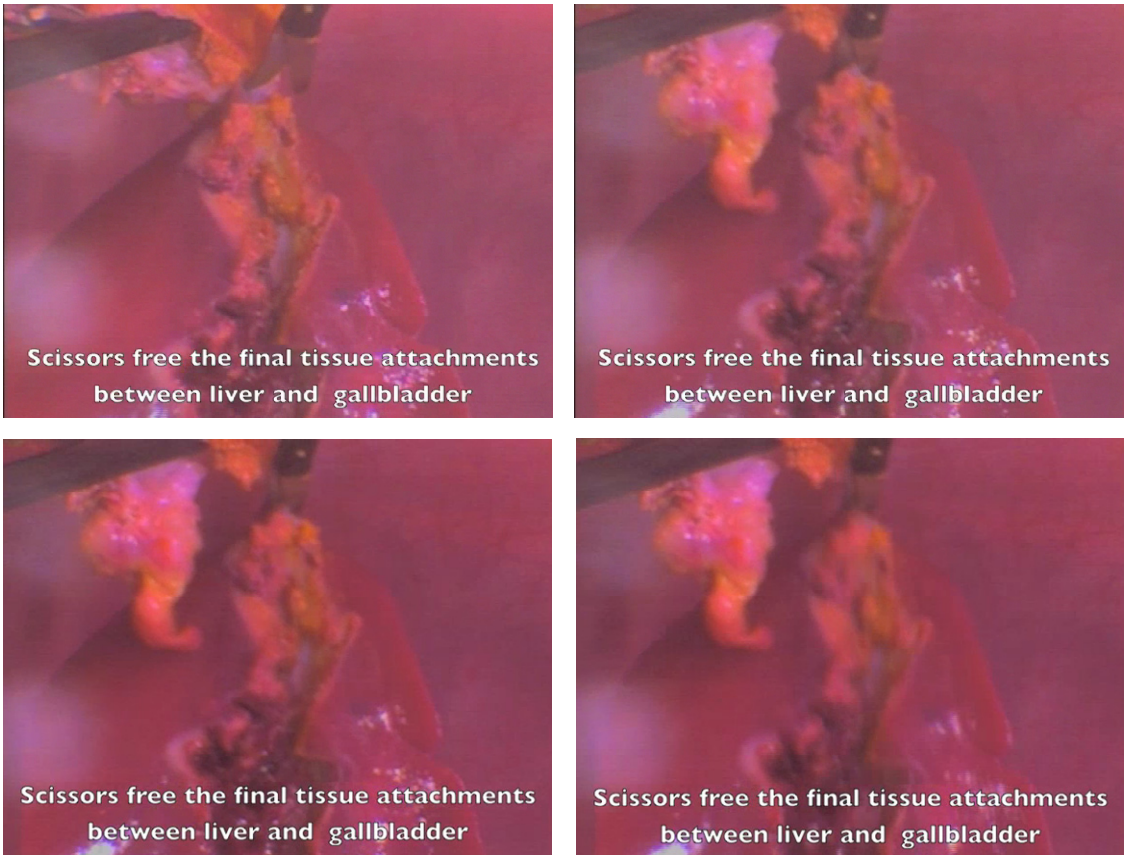

Figure 5.14 Final cut with a scissor.

5.3.6 Gallbladder ready for removal

After cutting, the gallbladder is ready for removal from the abdomen.

Figure 5.15 Resected gallbladder ready for removal.

5.4 Lessons learned from surgery

After the first cholecystomy with fluidic lens, the surgeons were very happy with the functionality and the performance of surgicam. Holding the laparoscope camera on the abdominal wall turns out to be very convenient for the surgeons because the work space is created. The camera can be controlled from outside of the abdominal wall, fascilitating the usage and the panaromic view of the camera.

With a complete surgical procedure, several things were learned about the problem between the engineering field and medical field. Here are some of the lessons that we learned that we can improve on the engineering side through the surgical procedure. The most important lesson is that the internal body is very humid. After leaving the camera body inside the human body for some time, fog starts to build up on the camera. This can be solved by either some mechanical engineering work. The other lesson that was learned is that the LED lighting has to be aligned very well with the imaging optics. The main reason for this is because inside the body cavity, the camera could be pushed around. Occassionally, the lighting section could be buried under an organ. Therefore, aligning the optics with the illumination section will greatly help the entire system. Finally, one thing that was learned and was quickly fixed during the surgery was that color is very important. The surgeons are used to the images with a specific color with images from the laparoscope. The colors help surgeons identify the location of different parts of the body.

Overall, the surgery demonstrates that bio-inspired fluidic lens is the key technology to a powerful next generation laparoscope. The image quality and the functionality provided from fluidic lens provide a new dimension for the laparoscope. Through the surgery, we learned that there is still a decent amount of technology improvement needed. But most of those improvements are needed in the support structure, such as the actuator, the electronics, etc. Most of those are achieveable with sufficient amount of resource. But the most important thing is still, fluidic lens provides the key functionality needed for the next generation minimally invasive surgery.

Chapter 6

Summary and future work

6.1 Summary

Bio-inspired fluidic lens is a new type of optical lens device that can change curvature just like the crystalline lens in human eyes. This is a major breakthrough from current standard optical lenses. The capability to change the curvature of the lens device in position ensures a very large tuning range in a very small limited space.

With bio-inspired fluidic lens, we have demonstrated several optical systems that can be built with it. To begin with, I have demonstrated a miniaturized unified imager htat can work as a camera, work in micromode, and work as a microscope. Merging of all these functions with traditional optical lenses is unheard of. I have also demonstrated a 2 fluidic zoom lens system. With the ultra-wide tuning range of the fluidic lens, I was able to design the current smallest camera with the widest optical zoom. One of the most important applications for it is the surgical camera where a successful surgery was carried out to remove the gallbladder from a surgical pig.

Aside from carrying the technology into biomedical applications, my major contribution in the technical side is in improving image quality. On the device processing end, one of my contribution was in introducing vacuum filling technology to fill the fluid chamber with optical fluid. The original method of filling up the fluid chamber include using two syringes, one to fill with fluid and one to suck out the air. The challenge of this technique is in the preservation of the membrane and the difficulty of removing bubbles. With vacuum filling technology, residual bubbles in the fluid chamber were greatly reduced. The second major contribution that I made to the processing end was to improve membrane quality. To do so, I have developed the prestretch technology. There are 2 key factors in the prestretch technology. First, there is the vacuum cup prestretch technology. Utilizing the vacuum cup, the membrane was evenly stretched by air pressure. This ensures symmetry during prestretch. The second key technology enabling prestretch is a very special adhesive layer that I found – SiO2. With this special layer, I was able to bond PDMS to different materials. Since the

bonding here are chemical bonds, the fine prestretch introduced in the vacuum cup was well preserved. This kind of prestretching technique and bonding technique out-performs other techniques such as clamping, which slips, and applying pressure sensitive adhesives (PSAs).

The second major contribution that I made to image quality was including optical system techniques to improve image quality. There are 2 different approaches here. First, the introduction of the fixed lens into fluidic lens system improves the overall aberration of the system. Basically, the fixed lenses provide the image quality and the fluidic lens provides the large and tremendous amount of tuning capability that is not feasible with fixed lens. The first system that I demonstrated is the miniaturized unified imager. This system contains only one fluidic lens. The second fluidic optical system that I improved was the zoom lens. In this case 2 lenses are used. I have explored the utiltizing both only fluidic lenses and fixed lens integrated with fluidic lenses. When fixed lenses are utilized, the overall image quality is improved, particularly the field is greatly improved. Also, the speed of the optical system is greatly improved. F/2.8 systems with good image quality can be made with fluidic/fixed lens integration. On the other hand, the cost of making purely fluidic lens is much cheaper. This is because any fixed lens is very expensive due to the small size (< 4 mm diameter). With only 2 fluidic lens, with good processing technology as well as good optical system design skills, we were able to demonstrate a miniature optical system (< 20 mm total track) with very wide optical zoom (>4x) while still having good image quality.

Finally, I have also explored several applications for utilizing fluidic lens in biomedical applications. The parts that I have demonstrated already are utilizing fluidic lens for laparoscopic applications and as a microscope for research applications. Some other works that I have also explored includes application of fluidic lens for application such as in a retinal camera and heart applications.

With improved image quality, new applications for fluidic lens will definitely come up and new opportunities will be available. The small size and high functionality will provide new applications that are unthought of in the surgical domain and in different domains.

6.2 Potential Future Bio-medical Applications

There are several potential applications in the biomedical field for bio-inspired fluidic lens. As mentioned earlier in Chapter 1, some applications such as dermatology, denstistry, laryngoscopy, retinal diagnosis, intraocular lens, digital pathology, etc. We focus on demonstrating one important application, the minimally invasive surgery, in this dissertation. I have explored some applications.

6.2.1 Fundus Camera for Diabetic Retinopathy

6.2.1.1 Introduction to Diabetic Retinopathy

There are 2 main categories of diabetes. Type 1 usually occurs during childhood or adolescence; and type 2, which is the most common form of the disease, usually occurs after age 45. As the fifth-deadliest disease in United States, there is no cure for

diabetes. The microvascular complications of diabetes, including diabetic retinopathy, account for a major proportion of disease-associated morbidity. This is because excess amount of sugar in the blood damages microblood vessels. For both type 1 and type 2 diabetes, one of a frequent complication is vision impairment. The main cause of blindness in people with diabetes is diabetic retinopathy (DR). Within 20 years of diagnosis, almost all patients diagnosed with type 1 diabetes will develop diabetic retinopathy. Even more drastic, more than 20% of people with type 2 diabetes already have retinopathy when they are first diagnosed with diabetes, and almost all will eventually develop some degree of retinopathy.

DR is defined by the presence of retinal microvascular lesions. There are 2 stages of DR. The initial stage is the onset of DR, and is called non-porliferative DR (NPDR). At this stage, there are damages to the blood vessels, but new vessels hasn't been formed. At the next stage of DR, porilferative DR (PDR), new blood vessels are formed. At this point, the chance of loss of vision is very high, and laser therapy is needed. A potential threat for patients with PDR is the detachment of retina.

During the NDPR stages, the clinical features are microaneurysms, retinal hemorrhages, hard exudates, cotton wool spots, intraretinal microvascular abnormalities, and venous beading [1]. These can be observed with a fundus camera. Later, at the PDR stage, the growth of abnormal new blood vessels and increased vascular permeability (which frequently lead to pre-retinal and vitreous hemorrhage, retinal detachment, iris neovascularisation and neovascular glaucoma) can also be observed under fundus camera [1]. Another major cause of visual loss is macular edema (fluid

build-up around the area of the retina that provides detailed central vision), which may occur in both NPDR and PDR [1].

The identification of the stage of the DR is done through a standard procedure. Basically, fundus photos are scored by trained doctors using the Airlie House Classification System. Current fundus photos are taken with expensive fundus cameras. Patients have to come into see the ophthalmologists to take fundus photos and the photos have to be sent to specialized doctors. We propose using bio-inspired fluidic lens to develop a portable fundus camera to fascilitate this diagnosis procedure.

6.2.1.1 Bio-inspired fludic zoom lens for diabetic retinopathy

To demonstrate the feasibility of using bio-inspired fluidic lens for retinal camera, I studied the system using optical ray tracing tool, ZEMAX, to simulate the optical system and image quality. I used Liou and Brennan's eye model for the eye optics, including the cornea, intraocular lens, pupil, and retina, being the curved surface at the end of the modeled eye [13]. The simplest bio-inspired imaging system consisting of only two fluidic lenses and an optical aperture is employed without including the illumination optics (see Figure 6.1). The diameter of the pupil is assumed to be 6 mm. The rays emanating from different positions of the curved retina travel through the eye lenses and the fluidic tunable lenses to form a retina image on the CMOS sensor. The sensor in this simulation has a diagonal of 6.4 mm, corresponding to 1/3" optical format.

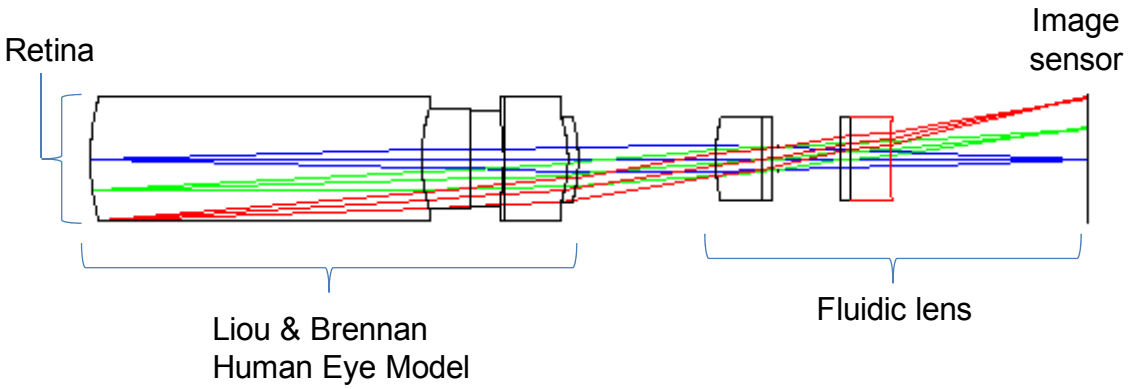

Figure 6.1 Simulation of a design of a bio-inspired fluidic retinal camera.

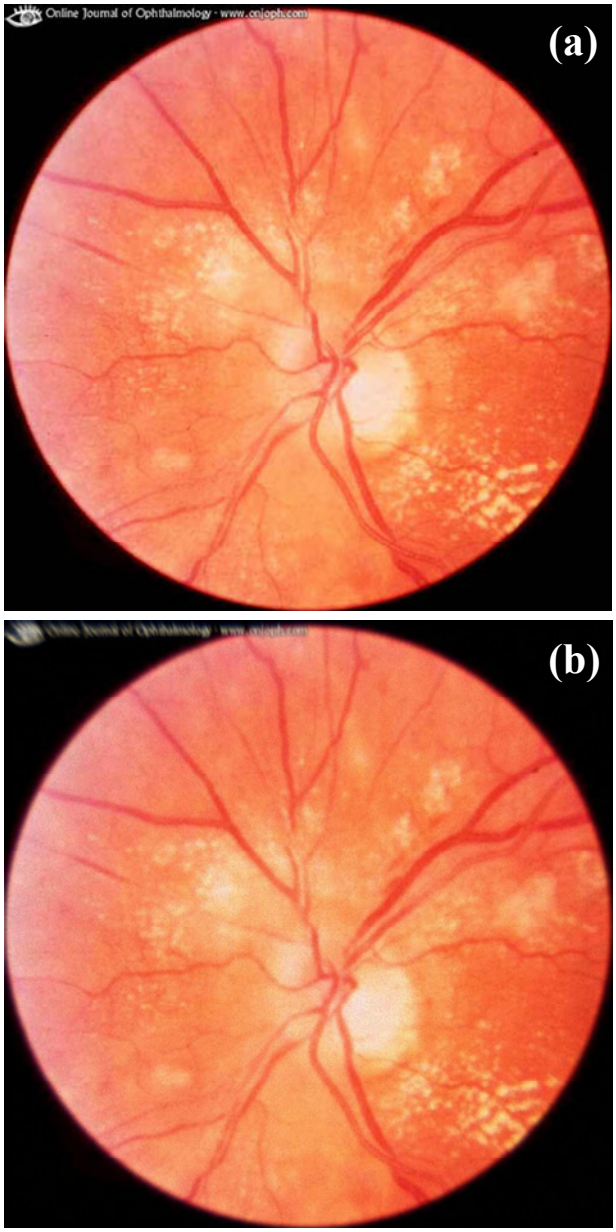

Figure 6.2 (a) is the photograph of a retina. The image was taken by a commercial retinal camera. This image is numerically positioned on the curved surface at the position of the retina in Figure 6.1. The simulated ray-traced retina image obtained from the setup of Figure 6.1 is shown in Figure 6.2(b). Comparing the simulated retina

image (Figure 6.2(b)) and the original image (Figure 6.2(a)), we found that all important features revealing the conditions of retina are well preserved.

The key benefit the bio-inspired retinal camera is that it can automatically adjust for the accommodation of the human eye. Furthermore, different people in the family with different near-sightedness or far-sightedness can all use the same bio-inspired retinal camera. This is because the bio-inspired fluidic lens can accommodate for different lenses. This is very different from a regular fundus camera where specialized accommodating lenses have to be used for different people. Finally, the two lens system allows for adjustable field-of-view. This can adjust for different pupil size of a patient during measurement and between different patients. This allows for less moving components (an adjustable iris) and greatly simplifies optical system design.

Overall, bio-inspired fluidic retinal camera is a promising technology to assist patients with diabetic retinalpathy.

6.2.2 Heart Surgery

Another potential application for bio-inspired fluidic lens is in heart surgery. A camera that can zoom in and out of the heart area can greatly assist the surgical procedure. Figure 6.3 demonstrates the potential for the bio-inspired fluidic zoom lens to work as a surgircal camera for heart surgery. A human-sized anatomy is placed in front of the bio-inspired fluidic zoom lens. The camera demonstrates the capability to zoom out to see the entire chest section, and then zoom in to see the details of the

vessels for detail operation. The extra space between the camera and the heart during operation creates extra workspace for the surgeons.

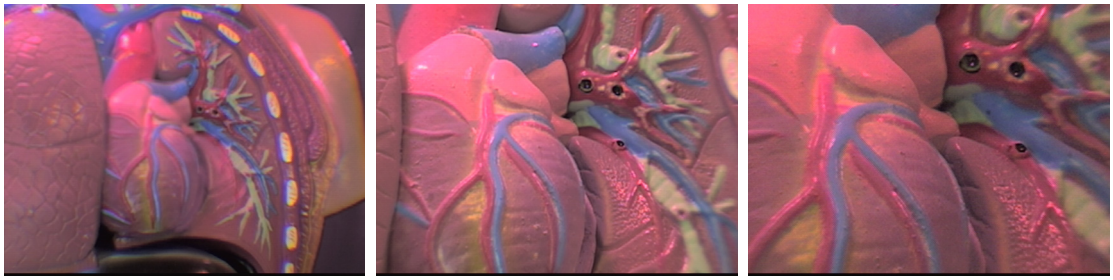

Figure 6.3 Demonstration of zoom on the human anatomy for heart surgery.

6.3 Conclusion

Bio-inspired fluidic lens is a new type of optical device that can provide new applications and functionalities never seen before. The key features in bio-inspired fluidic lens include smaller size, ultra-wide tuning range, and good image quality. In this dissertation, I demonstrated the miniature unified imager, which is a camera that can function as a regular camera and a microscope. This is made possible with bio-inspired fluidic lens. The image quality is very good, and I have demonstrated it with biomedical applications.

The second key system that I demonstrated is the bio-inspired fluidic zoom lens, which is the smallest camera with the largest optical zoom. This is also made possible with bio-inspired fluidic zoom lens.

Finally, a successful gallbladder removal surgery was demonstrated with bio-inspired fluidic zoom lens.

I have also explored some potential future applications for bio-inspired fluidic zoom lens, such as retinal camera, dental applications, as well as heart surgery.

I believe that bio-inspired fluidic lens is a key technology that has major impact on optical system design, and new applications and functions from the optical system new functions to support advanced research in the bio-medical society. As initial demonstration, I have demonstrated the function in surgical camera.

References:

[1] Clinical practice guidelines for the management of diabetic retinopathy. 1 ed., Canberra, Editor. 1997, National Health and Medical Research Council.

[2] H. L. Liou and N. A. Brennan, "Anatomically accurate, finite model eye for optical modeling," Journal of the Optical Society of America a-Optics Image Science and Vision, vol. 14, pp. 1684-1695, 1997.